University of Alberta

Toughness of Polymers under Various Fracture Conditions

by

Hyock-Ju Kwon ©

A thesis submitted to the Faculty of Graduate Studies and Research in partial fulfillment of the requirements for the degree of *Doctor of Philosophy*

Department of Mechanical Engineering

Edmonton, Alberta

Fall, 2007

Library and
Archives Canada

Published Heritage
Branch

395 Wellington Street
Ottawa ON K1A 0N4
Canada

Bibliothèque et
Archives Canada

Direction du
Patrimoine de l'édition

395, rue Wellington
Ottawa ON K1A 0N4
Canada

Your file Votre référence
ISBN: 978-0-494-33003-6
Our file Notre référence
ISBN: 978-0-494-33003-6

NOTICE:
The author has granted a non-exclusive license allowing Library and Archives Canada to reproduce, publish, archive, preserve, conserve, communicate to the public by telecommunication or on the Internet, loan, distribute and sell theses worldwide, for commercial or non-commercial purposes, in microform, paper, electronic and/or any other formats.

The author retains copyright ownership and moral rights in this thesis. Neither the thesis nor substantial extracts from it may be printed or otherwise reproduced without the author's permission.

AVIS:
L'auteur a accordé une licence non exclusive permettant à la Bibliothèque et Archives Canada de reproduire, publier, archiver, sauvegarder, conserver, transmettre au public par télécommunication ou par l'Internet, prêter, distribuer et vendre des thèses partout dans le monde, à des fins commerciales ou autres, sur support microforme, papier, électronique et/ou autres formats.

L'auteur conserve la propriété du droit d'auteur et des droits moraux qui protège cette thèse. Ni la thèse ni des extraits substantiels de celle-ci ne doivent être imprimés ou autrement reproduits sans son autorisation.

In compliance with the Canadian Privacy Act some supporting forms may have been removed from this thesis.

While these forms may be included in the document page count, their removal does not represent any loss of content from the thesis.

Conformément à la loi canadienne sur la protection de la vie privée, quelques formulaires secondaires ont été enlevés de cette thèse.

Bien que ces formulaires aient inclus dans la pagination, il n'y aura aucun contenu manquant.

Canada

Abstract

Fracture toughness and deformation behaviour of ductile polymers were investigated under various conditions and fracture modes. New methodologies to encourage the fracture modes that are hard to be generated in the past have been developed.

The thesis proposes test methodology to evaluate the fracture toughness of highly ductile polymers such as high-density polyethylene (HDPE). The first method is based on essential work of fracture (EWF) concept to measure toughness in plane-strain condition, which is about one order of magnitude smaller than the plane-stress counterpart. A new work-partitioning principle was developed to generate thickness-independent EWF values.

The thesis also discusses deformation and fracture of polymers involving stable necking. The study shows that crack growth of double-edge-notched tensile (DENT) test on HDPE can be divided into 2 stages. The EWF values for each stage were determined. The study concludes that the EWF value for stable necking varies with the deformation behaviour.

Another new method developed is to evaluate the toughness of polymers in shear fracture. The method was firstly applied to poly(acrylonitrile-butadiene-styrene) (ABS). The measured shear fracture toughness was then compared with that in the tensile mode. The results suggest that the ratio of shear to tensile fracture toughness is about 2.5. Validity of the new shear test was further evaluated using HDPE. For HDPE, shear fracture toughness could be determined by double extrapolation of specific work of fracture to zero ligament length and zero ligament thickness.

The last part of the thesis explores the yielding behaviour of HDPE using FEM. The study shows that the traditional way to determine the yield stress is not appropriate for the stable necking. Instead, an iterative process is proposed to determine the effective yield stress, based on which the loading level and the deformation behaviour can be simulated accurately. The simulation also considered anisotropic yielding in the stable necking process, which was verified by the simulation of DENT test. The study showed that anisotropic work-hardening occurred in the necking process. An empirical parameter, shear stress ratio, was implemented in anisotropic yield function, which successfully reproduced the load-displacement curves of DENT test in the FEM simulation.

Acknowledgements

I am particularly indebted to my supervisor, Dr. P.-Y. Ben Jar for his guidance and financial support throughout this study.

I also wish to thank Mr. Bernie Faulkner and Mr. Albert Yuen who offered me excellent technical help and valuable discussions.

Appreciation is extended to members of the Durable Materials Research Lab: Mr. Chengye Fan, Mr. Yemi Setiadi and Ms. Tik Dik for their friendship and the provision of a pleasant environment.

Special thanks go out to NSERC, Queen Elizabeth II scholarship and Andrew Stewart Memorial Prize for the financial support throughout the study.

Finally, my gratitude must be given to my wife, H. E. Chun, for her supporting me and believing in me throughout the study, as well as my life.

TABLE OF CONTENTS

Chapter 1 Introduction 1

1.1 Background 1
1.2 Objective 2
1.3 Essential Work of Fracture 3
1.4 Materials 7
1.5 Thesis Overview 8
Figures 11
Tables 12
References 13

Chapter 2 Toughness of High-Density Polyethylene in Plane-Strain Fracture 16

2.1 Introduction 16
2.2 EWF Concept 19
2.3 Experiments 23
2.4 Results and Discussion 23
2.5 Conclusions 27
Figures 28
References 31

Chapter 3 New Work Partitioning Approach to the Measurement of Plane-Strain Fracture Toughness of High-Density Polyethylene based on the Concept of Essential Work of Fracture 34

3.1 Introduction 34
3.2 Brief Review of EWF Method 37
3.3 Experiments 41
3.4 Results and Discussion 41
3.5 Conclusions 45
Figures 46
References 52

Chapter 4 On the Application of Essential Work of Fracture Concept to Toughness Characterization of High-Density Polyethylene Introduction **56**

4.1 Introduction 56
4.2 Experimental Details 58
4.3 Stress-Strain Relationship from the UT Test 61
4.4 Deformation Behaviour in the DENT Test 65
4.5 Energy Consumption in the DENT Test and the EWF Values 72
4.6 Conclusions 78
Figures 80
References 91

Chapter 5 Shear Fracture Toughness of Polymers in Shear Mode **94**

5.1 Introduction 94
5.2 Theoretical Analysis 96
  5.2.1 Review of fracture analysis using classical LEFM 96
  5.2.2 Review of essential work of fracture (EWF) 98
  5.2.3 Velocity discontinuity in plastic deformation zone 99
  5.2.4 The proposed EWF analysis for mode II fracture 100
5.3 Experimental Study 103
  5.3.1 Material 103
  5.3.2 Mode I fracture toughness 103
  5.3.3 Mode II fracture toughness 104
  5.3.4 Fractography 105
5.4 Results and Discussion 105
  5.4.1 Mode I fracture toughness 105
  5.4.2 Iosipescu test on specimens without grooves 107
  5.4.3 Iosipescu test on specimens with grooves 110
  5.4.4 Discussion 117
5.5 Conclusions 118
Figures 120
References 132

Chapter 6 Toughness of High-Density Polyethylene in Shear Fracture 135

6.1 Introduction 135
6.2 Literature Review 136
6.3 Experimental Details 140
6.4 Results 141
6.5 Deduction of Mode II Fracture Toughness 145
6.6 Conclusions 151
Figures 152
References 160

Chapter 7 On the Application of FEM to the Deformation of High-Density Polyethylene 163

7.1 Introduction 163
7.2 Literature Review 166
 7.2.1 Large deformation of materials and its constitutive equations 166
 7.2.2 Numerical simulation on cold drawing of semi-crystalline polymers 168
7.3 Uni-axial Tensile Test 170
 7.3.1 Determination of yield stress based on the traditional approach 170
 7.3.2 Numerical simulation based on the traditional approach 172
 7.3.3 Uni-axial tensile tests 175
 7.3.4 Stress distribution inside the specimen 176
 7.3.5 Determining effective yield stress-strain curve 178
7.4 Double-Edge-Notched Tensile Test 179
 7.4.1 Numerical simulation of the DENT specimen 180
 7.4.2 Yield Function 182
 7.4.3 Simulation scheme for DENT test 184
7.5 Conclusions 186
Figures 187
Tables 200
References 201

Chapter 8 Conclusions and Recommendations 206

Main Conclusions 206
Recommendations 209

Appendix A. Test Details **212**

A-1. Uniaxial Tensile (UT) Test 212
A-2. Double-Edge-Notched-Tensile (DENT) Test 214

Appendix B. Finite Element Modeling **217**

B-1. Simulation of UT Test 217
B-2. Simulation of DENT Test 220

Curriculum vitae **224**

List of Tables

Table 1-1. The map showing the degree of exploration on the deformation behaviour of the materials having different ductility: ■, explored extensively; ▨, explored moderately; □, explored rarely; ●, explored in this study. 13

Table 1-2. Material properties of ABS and HDPE (*: published.) 13

Table 7-1. Constants in Eq. (7.3) before necking. 201

Table 7-2. Constants in Eq. (7.3) after necking. 201

Table 7-3. Load drop ratio (DR) from the simulation. 201

Table 7-4. Load drop ratio (DR) from the experiment. 201

List of Figures

Fig. 1-1 Double-edge-notched (DEN) specimen. 13

Fig. 1-2 Schematic illustration of HDPE. 13

Fig. 2-1 Double-edge-notched tensile (DENT) specimen. 28

Fig. 2-2 Schematic plot of the specific work of fracture (w_f) versus ligament length (L_o), adopted from ref. [6, 7]. The plot suggests the existence of transition from plane-stress to mixed plane-stress and plane-strain conditions, which has been used in the past to determine EWF value in the plane-strain condition. 28

Fig. 2-3 Specific work of fracture of HDPE as a function of ligament length: "O" for specimens in the rolling direction and "△" for specimens in the transverse direction. 29

Fig. 2-4 Photographs of fracture behaviours in: (a) plane-stress region, (b) transition region, and (c) plane-strain region of Fig. 3. Photos were taken to show the variation of specimen thickness. Length of the white bar in each photograph corresponds to 1mm. 30

Fig. 3-1 Double-edge-notched tensile (DENT) specimen. 46

Fig. 3-2 Partitioning of the total work of fracture into work for (a) fracture initiation (W_i) and fracture growth (W_g) [7, 8], and (b) yielding (W_y) and necking and tearing (W_n) [11, 26, 30]. 46

Fig. 3-3 DENT test results from 12.5mm-thick specimens: (a) Representative load-displacement curves with different ligament lengths, taken from specimens in the transverse direction, and (b) specific work of fracture based on the total work of fracture, plotted as a function of ligament length in the rolling (O) and the transverse (△) directions. 47

Fig. 3-4 Front and side views of 12.5mm-thick specimens after fracture, with (a) $L_0 = 32$ mm, (b) $L_0 = 10$ mm, and (c) $L_0 = 3$ mm. 48

Fig. 3-5 Energy partitioning of the DENT test results for 12.5mm-thick specimens: (a) Typical load-displacement curve in the plane-strain region, from a specimen in the transverse direction with $L_0 = 6$mm, and (b) specific work of fracture, w_D, based on W_D in (a), plotted as a function of ligament length, L_0. 49

Fig. 3-6 DENT test results for 6.25mm-thick specimens: (a) Typical load-displacement curve in the plane-strain region, from a specimen in the transverse direction with $L_0 = 3.5$ mm, (b) specific work of fracture (w_D), as a function of ligament length (L_0) based on W_D calculated up to Δ_n in (a), and (c) w_D as a function of L_0 based on W_D calculated up to Δ'_n in (a). 51

Fig. 3-7 Plots of specific work of fracture, w_y, based on W_y in Fig. 2(b), as a function of ligament length L_0 for specimens of 6.25 *mm* thick, in the rolling (—) and the transverse (- - -) directions. 51

Fig. 4-1 Double-edge-notched tensile (DENT) specimen. 80

Fig. 4-2 Typical UT test results for HDPE: (a) load versus time, (b) true stress-strain curve, and (c) nominal stress-strain curve. 81

Fig. 4-3 DENT test results: (a) Typical load-displacement curves for specimens in the transverse direction (ligament length is indicated on each curve), and (b) specific work of fracture as a function of the ligament length (○ for specimens in the rolling direction and △ for specimens in the transverse direction). 82

Fig. 4-4 Top, front and side views of a fractured DENT specimen, $L_0 = 27$ mm. Length of the white bar corresponds to 1mm. 83

Fig. 4-5 Development of FPZ in the DENT test from point A of Fig. 3(a) to the final fracture. 84

Fig. 4-6 Deformation of a DENT specimen at point B of Fig. 3(a): (a) front view and (b) side view. Length of the white bar in each photograph corresponds to 1mm. 85

Fig. 4-7 Plots of ligament length reduction versus time from two DENT tests with $L_0 = 30$ mm. 85

Fig. 4-8 Variation of Δ_n / Δ_f (△) and Δ_y / Δ_f (◆) of DENT specimens in (a) the rolling direction and (b) the transverse direction. 86

Fig. 4-9 Angle at the tip (α) of a growing crack in the DENT test: (a) α in the neck inception stage, and (b) α in the neck propagation stage, and (c) a schematic illustration of the relationship of α with displacement Δ and ligament length L. Length of the white bar in each photograph corresponds to 1 mm. 87

Fig. 4-10 Partitioning of the total work of fracture: (a) for fracture initiation (W_i) and fracture (W_f) [3,8], (b) for yielding (W_y) and necking and tearing (W_n) [4,23,24], and (c) for the neck inception stage (W_{ni}) and the neck propagation stage (W_{np}). 88

Fig. 4-11 Partitioned specific work of fracture as a function of the ligament length: (a) for specimens in the rolling direction, and (b) for specimens in the transverse direction. 89

Fig. 4-12 The variation of η (defined as L_p / L_0) in the rolling (○) and the transverse (△) directions. 90

Fig. 5-1 Normalized variation of $K_1(\theta)$ (———) and $K_2(\theta)$ (– – –) with respect to θ: (a) under mode I (tensile) loading, and (b) under mode II (shear) loading. 120

Fig. 5-2 Double-edge-notched (DEN) tensile specimen for mode I fracture. 120

Fig. 5-3 Velocity discontinuity. 121

Fig. 5-4 Double-edge-notched (DEN) shear specimen for mode II fracture. 121

Fig. 5-5 Test set-up and specimens used in this study: (a) Iosipescu device and the specimen without grooves, and (b) the specimen with grooves. 122

Fig. 5-6 Plot of specific work of fracture in mode I (w_f^I) as a function of ligament length. 122

Fig. 5-7 Plot of specific work of fracture in mode I (w_f) as a function of ligament length with different thickness: ○, 6mm; ✸, 5mm; ▲, 4mm; ■, 3mm; ◆, 2mm. 123

Fig. 5-8 Crack propagation during the Iosipescu test on specimens without the grooves: (a) first crack generation, (b) second crack generation, and (c) formation of a cylinder during the crack growth, and (d) SEM micrograph taken from the fracture surface indicated by an arrow in (c). 124

Fig. 5-9 Typical load-displacement curve from the Iosipescu test of ABS specimens without grooves 125

Fig. 5-10 Plot of specific work of fracture from Iosipescu test specimens without grooves. 125

Fig. 5-11 Iosipescu test on the grooved specimens, showing (a) an array of cracks generated in the whole ligament section, and (b) the velocity discontinuity along the groove. 126

Fig. 5-12 A typical load-displacement curve from the Iosipescu test of the grooved specimens. 126

Fig. 5-13 Plots of the specific work of fracture (w_f) against ligament length: (a) from the total area under the curve, (b) by excluding the area covered by the curve after point D in Fig. 5-12. Groove thickness is 4 mm (■), 3 mm (✸), and 2 mm (◆). 127

Fig. 5-14 (a) SEM micrograph of fractured surface from a specimen with groove thickness of 4 mm, (b) cross-sectional view along A-A in (a) for a specimen with groove thickness of 4 mm, (c) cross-sectional view for a specimen with groove thickness of 2 mm, and (d) magnified image from the circle B in (a). 128

Fig. 5-15 Penetration depth of each of the first pair of cracks against (a) ligament length, and (b) groove thickness........129

Fig. 5-16 Plot of the fracture displacement (Δ_f) as a function of groove thickness, using specimens of the same ligament length (5 mm), with the grooves and notches machined by a cutter of 60° in angle and 25 mm in thickness. 129

Fig. 5-17 Plot of the specific work of fracture (w_f) as a function of groove thickness, using specimens of the same ligament length (5 mm), with the grooves and notches machined by a cutter of 60° in angle and 25 mm in thickness........130

Fig. 5-18 Plot of the specific work of fracture (w_f) as a function of the groove thickness, using specimens of the same ligament length (5 mm) with the grooves and notches machined by a cutter of 45° in angle and 20 mm in thickness 130

Fig. 5-19 Schematic representation of shear fracture process of ABS: (a) voids formation, (b) void rotation and crack emanation, and (c) side view of the surface topology. 131

Fig. 6-1 Description of the DEN specimens used in the study. 152

Fig. 6-2 Crack propagation during the Iosipescu test, for a HDPE specimen without side grooves........152

Fig. 6-3 Crack propagation during the Iosipescu test, for a HDPE specimen with side grooves. 153

Fig. 6-4 Typical plots of normalized load versus displacement from the Iosipescu tests of HDPE specimens: (a) without the side grooves (having the original thickness of 6.25 *mm*), and (b) with the side grooves and ligament thickness of 4 *mm*. 154

Fig. 6-5 Specific work of fracture as a function of ligament length: (a) from specimens without the side grooves (having the original thickness of 6.25 *mm*), and (b) from specimens with the side grooves and ligament thickness of 3 *mm*. 155

Fig. 6-6 Depiction of the bending motion of the right half of the DEN specimen during the Iosipescu test. 156

Fig. 6-7 Plots of the "further displacement": (a) experimentally measured values versus the ligament length for specimens of different ligament thickness, and (b) the extrapolated values from (a) at zero ligament length versus ligament thickness. 157

Fig. 6-8 Plots of the specific work of fracture (w_f) from specimens machined using a mill cutter of 60°: (a) experimentally measured values versus ligament length based on the total energy consumption (ligament thicknesses: 4 *mm* (●), 3.5 *mm* (▲), 3 *mm* (■), and 2.5 *mm* (♦)), and (b) the extrapolated values from (a) at zero ligament length versus ligament thickness. 158

Fig. 6-9 Plots of the specific work of fracture (w_f) from specimens machined using a mill cutter of 90°: (a) experimentally measured values versus ligament length based on the total energy consumption (ligament thicknesses: 4 *mm* (●), 3.5 *mm* (▲), and 3 *mm* (■)), and (b) the extrapolated values at zero ligament length from (a) versus ligament thickness. 159

Fig. 7-1 Typical UT test results for HDPE: (a) Nominal stress-elongation curve, and (b) true stress-strain curve: test data (———) and trend curve from Eq. (7.2) with $n = 1.8$ (– – –). 187

Fig. 7-2 Results of the FEM numerical simulation of UT test: (a) the undeformed model and deformed model at elongation of 50 mm, (b) load-elongation curve, and (c) true stress-strain curve: solid line (———) from test data and "○" from the FEM simulation with $n = 1.8$. 189

Fig. 7-3 UT test results: the plots of (a) axial strain, (b) axial stress and (c) stress-strain curves at the distance of 2 mm (– – –), 4 mm (–·–·), 6 mm (- - - -), 8 mm (–··–) and 10 mm (———) from the neck initiation section. The arrows in the plots indicate the direction of the increase of the distance from the neck initiation section 190

Fig. 7-4 Stress distribution at (a) axial strain of 0.26: at the neck initiation section; and (b) at 3mm away, in the thickness and width directions. 191

Fig. 7-5 Stress distribution at (a) axial strain of 0.5: at the neck initiation section; and (b) at 3mm away, in the thickness and width directions. 192

Fig. 7-6 Stress distribution at (a) axial strain of 0.75: at the neck initiation section; and (b) at 3mm away, in the thickness and width directions. 193

Fig. 7-7 S2 stress determined experimentally (———) and by FEM simulation (■) after one iteration. Data presented by (○) represent the effective yield stress function as input to the FEM model to determine S2 (■). 194

Fig. 7-8 (a) Load - elongation and (b) axial strain - elongation curves, from the experiment (———), and the FEM simulation after one iteration (◆). 195

Fig. 7-9 The FEM model of DENT specimen with $L_0 = 20\ mm$ 196

Fig. 7-10 The deformation behaviour of DENT specimen after 40% of the half ligament length was debonded. 196

Fig. 7-11 Load-displacement curve for the DENT specimen with $L_0 = 20\ mm$, from the test (———) and FEM simulation (◊). 197

Fig. 7-12 Comparison of experimental curve of normalized load vs. displacement (solid line) with those determined from the FEM simulations with various R_s values. 197

Fig. 7-13 Comparison of experimental curves (solid lines) with the FEM simulation for DENT tests with different ligament lengths (L_0):, $24\,mm$ (◊), $20\,mm$ (○), and $16\,mm$ (□). 198

Fig. 7-14 FEM model of DENT specimen after fracture (simulated using $R_s = 0.67$). The original half ligament length = 10 mm. 199

List of Abbreviations and Symbols

ABS	poly(acrylonitrile-butadiene-styrene)
b	the width of the deformation band where velocity discontinuity occurs
CTOA	crack tip opening angle
DEN	double-edge-notched
DENT	double-edge-notched tensile
$d\varepsilon$	strain increment
du	displacement increment
E	Young's modulus
EWF	essential work of fracture
f	yield function
FPZ	fracture process zone identified with the region that necks ahead of crack tip
h	height of the plastic deformation zone
H	length of the specimen
HDPE	high density polyethylene
J_2	second stress invariant
J_{IC}	critical J value at crack initiation
K	strength coefficient
K_I	stress intensity factor in mode I
K_{II}	stress intensity factor in mode II
K_C^I	critical stress intensity factor in mode I
K_C^{II}	critical stress intensity factor in mode II
k	material constant in exponential stress function
k'	material constant in exponential stress function insensitive to strain rate
kN	Kilonewton
L_i	ligament length failed in the neck inception stage
L_p	ligament length failed in the neck propagation stage

M	material constant in exponential stress function
m	exponent of strain rate in exponential stress function
MPa	Megapascal
N	work-hardening coefficient in Holomon equation
n	work-hardening exponent in exponential stress function
L_o	original ligament length of DENT specimen
RCP	rapid crack propagation
R_{ij}	stress ratio, i.e. the ratio of the non-zero stress component at anisotropic yielding to the equivalent stress component in the case of isotropic yielding
R_S	shear stress ratio, i.e. the ratio of the on-zero shear stress component at anisotropic yielding to the shear stress component at isotropic yielding
r_p	size of the plastic zone ahead of the crack tip
S1	transverse normal stress in the width direction
S2	axial stress
S3	transverse normal stress in the thickness direction
S12	shear stress acting on the plane normal to 1 axis in the direction of 2 axis
S23	shear stress acting on the plane normal to 2 axis in the direction of 3 axis
Se	effective stress
SAN	poly(styrene-acrylonitrile)
SEN	single-edge-notched
t	thickness of the specimen during the test
t_o	original thickness of the specimen
W_{ni}	work for the neck inception stage
W_{np}	work for the neck propagation stage
UT	uni-axial tensile
v_n	normal component of the relative velocity
v_t	tangential components of the relative velocity
W	width of the specimen

W_0	original width of the specimen
W_D	work of main fracture, i.e. the work of fracture which does not include the energy for stretching and fracture of the surface layers
W_e	essential work of fracture, i.e. the work performed within the FPZ
W_e^I	essential work of fracture in mode I
W_e^{II}	essential work of fracture in mode II
W_f	total work of fracture
W_f^I	total work of fracture in mode I
W_f^{II}	total work of fracture in mode II
W_g	work for fracture growth
W_i	work for fracture initiation
W_N	work for stretching and fracture of the surface layers
W_n	work for necking and tearing
W_{ni}	work for neck inception stage
W_p	work the for the plastic deformation
W_{np}	work for neck propagation stage
W_p^I	work the for the plastic deformation in mode I
W_p^{II}	work the for the plastic deformation in mode II
W_y	work for yielding
w_D	specific work of main fracture, i.e. $W_D / L_0 t_0$
$w_{e,1}$	specific EWF for the neck inception within the FPZ
$w_{e,2}$	specific EWF for the neck propagation in FPZ to the final fracture
$w_{e,i}$	specific EWF for the neck inception stage
$w_{e,p}$	specific EWF for neck propagation stage
$w_{e,n}$	specific EWF for necking

$w_{e,y}$	specific EWF for yielding
w_e^I	specific EWF in mode I
w_e^{II}	specific EWF in mode II
w_f	specific work of fracture, i.e. $W_f / L_0 t_0$
w_f^I	specific work of fracture in mode I
w_f^{II}	specific work of fracture in mode II
$w_{f,i}$	specific work for neck inception stage
$w_{f,p}$	specific work for neck propagation stage
w_i	specific work for fracture initiation, i.e. $W_i / L_0 t_0$
w_n^I	average work density for the neck forming in mode I
w_n^{II}	average work density for the neck forming in mode II
w_p	average plastic work density
$w_{p,i}$	specific plastic work for neck inception stage
$w_{p,p}$	specific plastic work for neck propagation stage
$w_{p,n}$	specific plastic work for necking
$w_{p,y}$	specific plastic work for yielding
w_p^I	average plastic work density in mode I
w_p^{II}	average plastic work density in mode II
w_y	specific work for yielding, i.e. $W_y / L_0 t_0$
w_e^{ε}	specific EWF for plane-strain fracture
w_e^{σ}	specific EWF for plane-stress fracture
Y	uni-axial yield strength of the material
$Y(\varepsilon)$	yield stress at the onset of plastic deformation
β	shape factor for the plastic deformation zone
β_1	shape factor for the neck

β_2	shape factor for the plastic deformation zone in mode I
β_3	shape factor for the plastic deformation zone in mode II
β_i	shape factor in the neck inception stage
β_p	shape factor in the neck propagation stage
Δ	displacement at the point of interest
Δ_1	crack tip opening displacement
Δ_f	displacement at fracture
Δ_n	displacement at which transition starts
$\Delta_n^{'}$	displacement at which transition ends
Δ_y	displacement at the maximum load
Γ_0^I	specific EWF in mode I
Γ_0^{II}	specific EWF in mode II
Γ_n	specific necking energy within the FPZ
ε	true strain
ε_0	transition strain
ε_E	engineering strain
ε^n	true stress at the onset of necking in the FPZ
ε_E^n	engineering strain at the onset of necking in the FPZ
$\bar{\varepsilon}$	equivalent strain
$\bar{\varepsilon}_{n,\max}$	maximum equivalent strain for the neck inception in the FPZ
$\bar{\varepsilon}_f$	equivalent strain at the final fracture
$\dot{\varepsilon}$	strain rate
θ_0	angle of crack propagation with respect to the original crack orientation
γ	angle between relative velocity and velocity discontinuity
λ	shape factor for the active plastic zone
σ	true stress

σ_1	maximum principal stress
σ_2	minimum principal stress
σ_C	tensile strength
σ_E	engineering stress
$\sigma_{\max}$	maximum tensile stress
σ_y	tensile yield stress
$\overline{\sigma}$	equivalent stress
τ_C	shear strength
$\tau_{\max}$	maximum shear stress

Chapter 1

Introduction

1.1 Background

Although polymers are, nowadays, widely used in many structural products because of their low costs and ease of processing, the end use in engineering applications is often restricted by their macroscopic mechanical properties. Among the various mechanical properties of polymers, the deformation behaviour in elastic or small plastic realm has been relatively well investigated. Accordingly, the fracture behaviour which occurs after some deformation has been studied extensively. However, for the fracture preceded by extremely small or large deformations, the theoretical or experimental scheme has been established depending on the deformation characteristic of the polymers. For example, if a polymer fails in a brittle manner, the fracture behaviour of this polymer after little deformation has been studied abundantly in the past. On the other hand, for ductile polymers, brittle fracture is hard to be generated, resulting in the scarcity of study in this area.

Since extent of plastic deformation involved in the fracture process depends on the stress state, such as deformation being highly suppressed in the plane-strain condition but not in the plane-stress condition, fracture after little plastic deformation is often called "plane-strain fracture", while that preceded by noticeable amount of plastic deformation "plane-stress fracture". Note that plane-stress fracture needs to be classified in a more detailed manner for polymers. Fracture can also be classified by the mode of stress that causes the fracture. For example, when tensile stress is applied to generate crack growth in the direction perpendicular to the stress, it can be classified as tensile (mode I) fracture. Likewise, in-plane shear (mode II) and out-of-plane shear (mode III) fracture can be classified in a similar manner. It has been known that most polymers have high tendency to be fractured in the tensile mode [1]. Therefore, methodologies and theories for the fracture behaviour of polymers in tensile mode have been well developed while those on shear mode rarely.

1.2 Objective

Table 1-1 shows how previous studies on the fracture behaviour has been biased towards the fracture involving limited deformation because that fracture behaviour is easy to be generated in laboratory testing. However, as the application of polymeric materials increases to load-bearing applications, unexpected fracture that has been rarely studied in the past can sometimes occur. For example, high-density polyethylene (HDPE) is a highly ductile polymer of which the fracture was always believed to involve extensive necking. Because of its ductility, HDPE has been widely used for critical applications such as natural gas pipe-line in the municipal area. However, it has been reported that pressurized polyethylene pipe may fail in a very brittle manner without any sign of the ductile deformation, commonly known as rapid crack propagation (RCP) [2]. RCP can cause catastrophic failure, thus it is highly necessary to study plane-strain fracture behaviour. On the other hand, fracture behaviour of poly(acrylonitrile-butadiene-styrene) (ABS) is known to be dominated by tensile mode even under pure shear loading. Since many products with complex shape have the tendency of shear fracture in the service loading environment, it is essential to obtain the correct information on the deciding factors for this fracture mode.

This current study has been focused on areas that have not been explored well in the past. Main objective of this study is to develop new methodologies to encourage plane-strain fracture in polymers that are known to be highly ductile, and shear fracture in ductile and highly ductile polymers, and evaluate the corresponding fracture toughness. Fracture behaviour of highly ductile polymers that involves stable necking was also investigated, which in the past has been treated in the same manner as that in unstable necking. The study investigated yielding behaviour and yield criterion under stable necking that are essential for the correct numerical simulation. The areas that have been dealt with in this study are summarized in Table 1-1.

1.3 Essential Work of Fracture

The fracture behaviour can be best represented by “fracture toughness”. Toughness is a measure of material’s resistance to failure. Used with “fracture”, it refers to the energy per unit area needed to generate a new crack surface. The measures of fracture toughness derived prior to 1960 have been based on linear elastic fracture mechanics (LEFM); therefore, they can be applied only to brittle materials that obey Hooke’s Law. Although modifications were later made to accommodate small-scale plasticity [3], these analyses are still restricted to structures of which global behavior is linear elastic. For example, energy release rate and stress intensity factor are two measures of the fracture toughness in the global deformation behavior that can be well described using LEFM. Since LEFM is valid only if nonlinear material deformation is confined to a small region surrounding the crack tip, fracture behaviors of many materials are virtually impossible to characterize using LEFM due to their elastic-plastic deformation, and nonlinearity between stress and strain. For these types of materials, J-integral has been used to characterize the crack growth resistance. However, when plastic deformation is not confined at the crack tip region, but occurs globally, J-integral presents coupled contribution from plastic deformation and crack formation [4]. As a result, a different approach that was firstly proposed by Broberg [5], known as essential work of fracture (EWF), was developed to extract the specific energy needed for the crack formation, by separating it from the non-essential work for the plastic deformation. Many researchers have since studied this concept [6-13], and obtained strong evidence to support validity of the EWF concept for the toughness characterization.

The essential work of fracture (EWF) concept is the scheme to determine the essential work which is the energy consumed within the region around the crack tip where necking and final fracture occurs, called fracture process zone (FPZ). If a double-edge-notched (DEN) sheet specimen (Fig. 1-1) yields completely before fracture, the height of the plastic deformation zone formed between the notches, h, is proportional to the ligament length (L_0). However, size of the plastic deformation zone does not increase after the initial yielding. Therefore, the work consumed for the whole fracture process,

W_f, can be separated into two components:

(i) The essential work consumed within the FPZ (W_e)

(ii) The non-essential work consumed in the plastic deformation zone (W_p).

The essential work, W_e, is proportional to the ligament cross-sectional area, $L_0 t_0$, that is to be fractured during the test where t_0 is the original specimen thickness, provided that the specific essential work remains constant. The non-essential work for the plastic deformation, W_p, is proportional to plastic deformation volume, $\beta L_0^2 t_0$, where β is the shape factor of plastic deformation zone. If w_p represents the plastic energy density, then the total work of fracture can be written as

$$W_f = W_e + W_p = L_0 t_0 w_e + \beta w_p L_0^2 t_0 \qquad (1.1)$$

where w_e is the specific essential work of fracture. By measuring the total work of fracture for specimens of different ligament lengths, and dividing W_f by the ligament cross sectional area ($L_o t_o$), the specific work of fracture, w_f, can be expressed as:

$$w_f = w_e + \beta w_p L_0 \qquad (1.2)$$

Thus, if the specific work of fracture, w_f, is plotted against the ligament length L_0, there should be a straight line with a positive intercept that is the specific essential work, w_e, representing the fracture toughness [11]. The basic assumption of this scheme is the energy consumed within the FPZ, w_e, is constant and can be regarded as material property which has been investigated in this study and will be discussed in Chapter 4.

When the shape of the plastic deformation zone is circular, W_p in Eq. (1.1) can be written as:

$$W_p = \int_0^{\bar{\varepsilon}_y} \bar{\sigma} d\bar{\varepsilon} \, (\pi/4) L_0^2 t_0 \qquad (1.3)$$

where $\bar{\sigma}$ is the effective stress, $\bar{\varepsilon}$ effective strain, and $\bar{\varepsilon}_y$ the effective strain at yielding. By substituting $\int_0^{\bar{\varepsilon}_y} \bar{\sigma} d\bar{\varepsilon}$ with w_p, Eq. (1.2) can be re-written as:

$$w_f = w_e + \frac{\pi}{4} w_p L_0 \qquad (1.4)$$

thus, β in Eq. (1.2) is equal to $\pi/4$ for circular plastic zone. When the plastic deformation zone is elliptical shape with the height being h, it can be derived that $\beta = \frac{\pi}{4}(\frac{h}{L_0})$. β value for other shapes of plastic zone can be determined from the plastic zone area if it can be measured with sufficient accuracy. However, the report from ESIS committee stated that the attempts to determine β were abandoned because the shape of the plastic deformation zone could not be measured with sufficient precision [13].

For metals with reasonably high strain hardening exponents, the plastic deformation zone is almost circular [11], while for small strain hardening exponent it is narrower and elliptically shaped. For polymers plastic deformation zone can be wedge shaped and very narrow [6]. However, in all cases the area of the plastic deformation zone and the work for the plastic deformation, W_p, are still proportional to L_0^2 [6]; therefore, it is not necessary to separate β and w_p in evaluating w_e. Since the EWF concept has been used in this study to evaluate w_e as the representative of fracture toughness, the attempt to separate β and w_p has not been made in this thesis.

Pardoen et al. [7] proposed that w_e can be further divided into the local fracture energy that accounts for material damage and separation to form new surfaces and the necking energy that comes from the development of a localized neck in front of the crack, both of which are within the FPZ. Therefore, w_e in Eq. (1.2), can be expressed as:

$$w_e = w_e^{\varepsilon} + \Gamma_n \tag{1.5}$$

where w_e^{ε} is the specific energy for generating the new surface, excluding the energy for necking, and is suggested to be the EWF for plane-strain fracture, and Γ_n is the specific necking energy within the FPZ. Ideally, Γ_n is negligible in the plane-strain fracture, while it is significant in plane-stress fracture.

1.4 Materials

Poly(acrylonitrile-butadiene-styrene) (ABS) and high density polyethylene (HDPE) are two polymers used for tests in this thesis. ABS is a rubber-toughened glassy polymer consisting of a matrix of random styrene-acrylonitrile (SAN) colopymer and a population of approximately spherical rubber particles. HDPE is a semi-crystalline polymer which is composed of both crystalline and amorphous regions as shown in Fig. 1-2. Crystalline region consists of entities known as shperulites in which multiple lamellae are stacked together. Lamella is the layered structure of folded entangled polymer chains. Difference of their micro structures resulted in very contrasting deformation behaviour. Excellent ductility and significant work-hardening of HDPE has enabled the development of stable necking during the plastic deformation [15,16]. On the other hand, ABS that does not show any work hardening behaviour, with its neck formation quickly leading to the final fracture. Also, HDPE shows shear-like fracture under pure shear loading while the fracture in ABS is always dominated by the tensile mode under any loading conditions. Therefore, they are the examples showing extremely different fracture behaviors.

The mechanical properties of ABS and HDPE used in this study are summarized in Table 1-2.

1.5 Thesis Overview

Structure of the thesis is like the following. Plane-strain fracture of highly ductile polymers will be discussed in Chapter 2 and 3. Because of its excellent ductility, the fracture of HDPE is known to involve extensive necking. Brittle fracture without necking is very difficult to be generated. As a result, the essential work usually contains a significant portion of necking energy, which makes it difficult to evaluate fracture toughness of HDPE under plane-strain condition. The method to evaluate plane-strain fracture toughness based on the EWF concept is proposed in Chapter 2. The results for the HDPE of two different thicknesses are presented, that are compared with the results of the new method for toughness evaluation based on the work partitioning principle presented in Chapter 3.

Compared to the fracture toughness in plane-strain condition, that in plane-stress has been explored well by using the EWF concept [9,10,17-19]. The original idea of EWF concept [6,9,10,11] assumes the state within the FPZ to be constant during the crack growth. However, for stable necking materials, the degree of necking within the

FPZ varies and its size increases with the neck propagation into the neighbouring region. Therefore, validity of the EWF concept when the stable necking occurs needs to be examined, which is discussed in Chapter 4.

The study of shear fracture toughness has been rarely conducted for polymers because their fracture in most mechanical tests mainly occurs in mode I. As a result, even though the crack is initiated in a shear-like mode, the fracture mode is often changed to mode I soon after the initiation [20,21]. To our knowledge, no experimental data are available to evaluate the shear fracture toughness for ductile polymers. A method has been developed for evaluating the shear fracture toughness and applied to ABS, a non-work-hardening material, in Chapter 5, and HDPE a work-hardening material with stable necking, in Chapter 6.

Chapter 7 presents two case studies that use finite element method (FEM) to simulate deformation behaviour when subjected to tensile loading. The first one is to deform HDPE in uni-axial tensile (UT) test beyond the initial yielding, i.e. to generate stable necking in the gauge section. Validity of conventional experimental yield stress is investigated using FEM simulation, and a simple correction process was developed to determine the effective yield stress for the FEM input from the experimental results. Variation of yield function with the necking development is also examined through the case study of double-edge-notched tensile (DENT) specimen. Appropriateness of the conventional von Mises yield function with the assumption of isotropic work hardening was examined, and an anisotropic yield function employing an empirical parameter is proposed.

The main conclusions are summarized in Chapter 8, together with the recommendations for future work, to substantiate the conclusions and explain some unresolved questions.

This thesis adopts the paper format based on six papers, submitted or published in technical journals. Reference of the papers and corresponding chapters are listed below.

Chap. 2: H. J. Kwon and P.-Y. Jar. "Toughness of High-Density Polyethylene in Plane-Strain Fracture," Polymer Engineering & Science. Vol. 66 (10), pp. 1428-1432 (Oct. 2006).

Chap. 3: H. J. Kwon and P.-Y. Jar. "New Work Partitioning Approach to the Measurement of Plane-Strain Fracture Toughness of High-Density Polyethylene based on the Concept of Essential Work of Fracture," Engineering Fracture Mechanics. In Press.

Chap. 4: H. J. Kwon and P.-Y. Jar. "On the Application of Essential Work of Fracture Concept to Toughness Characterization of High-Density Polyethylene," Polymer Engineering & Science. Accepted.

Chap. 5: H. J. Kwon and P.-Y. Jar. "Fracture toughness of polymers in shear mode," Polymer, Vol. 46 (26), pp. 12480-12492 (Dec. 2005).

Chap. 6: H. J. Kwon and P.-Y. Jar. "Fracture Toughness of High-Density Polyethylene in Shear Mode," International Journal of Fracture. Accepted.

Chap. 7: H. J. Kwon and P.-Y. Jar. "On the Application of Numerical Simulation to the Deformation of High-Density Polyethylene," International Journal of Solids and Structures. Submitted.

Figures

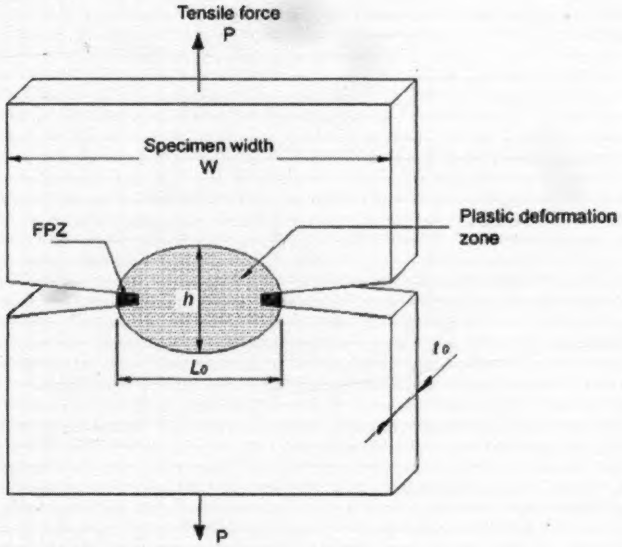
Tensile force
P
Specimen width
W
FPZ
Plastic deformation
zone
h
L_0
t_0
P

Fig. 1-1 Double-edge-notched (DEN) specimen.

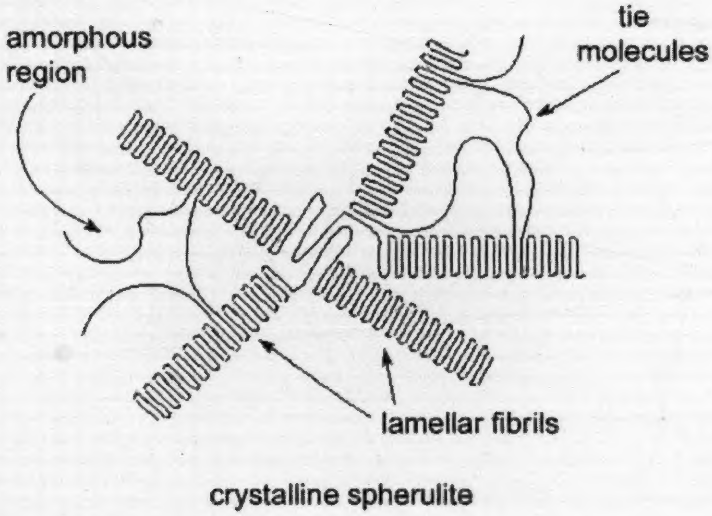
amorphous
region
tie
molecules
lamellar fibrils
crystalline spherulite

Fig. 1-2 Schematic illustration of HDPE.

Tables

Table 1-1. The map showing the degree of exploration on the deformation behaviour of the materials having different ductility: ■, explored extensively; ▨, explored moderately; □, explored rarely; ●, explored in this study.

Materials	Mode I		Mode II (polymer)	Yielding
	Plane-strain	Plane-stress		
Brittle	■	-	▨	■
Ductile	▨	■	□ ●	▨
Highly ductile	□ ●	▨ ●	□ ●	□ ●

Table 1-2. Material properties of ABS and HDPE (*: provided by the supplier.)

	ABS	HDPE
Supplier	Denki Kagaku Kogyo, Japan	McMaster, Canada
Material Type	Extruded Plate	Extruded Plate
Young's modulus	2.5 GPa	1 GPa
Tensile Strength	48 MPa	25 MPa
Elongation at Failure	20 %	> 500 %
Density	1.04 *	0.96
Glass Transition Temp.	100 °C *	-30 °C *
Water Absorption	0.3 % *	0.076 % *
Degree of crystallinity	-	80% *

References

1. J.G. Williams, Fracture Mechanics of Polymers, Ellis Horwood Limited, Chichester, England, 74 (1984).
2. S.J.K. Ritchie, P. Davis, and P.S. Leevers, "Brittle-tough transition of rapid crack propagation in polyethylene", Polymer, 39(25), 6657 (1998).
3. J.R. Rice, ASME Meeting APM-31, American Society of Mechanical Engineers (ASME), 8 (1968).
4. A.G. Atkins and Y.-W. Mai, Elastic and Plastic Fracture, Ellis Horwood Limited, Chichester, UK, 269 (1985).
5. K.B. Broberg, "Critical Review of some Theories in Fracture Mechanics", International Journal of Fracture Mechanics, 4, 11 (1968).
6. B. Cotterell, T. Pardoen, and A.G. Atkins, "Measuring Toughness and the Cohesive Stress-Displacement Relationship by the Essential Work of Fracture Concept", Engineering Fracture Mechanics, 72(6 SPEC ISS), 827 (2005).
7. T. Pardoen, Y. Marchal, and F. Delannay, "Essential Work of Fracture Compared to Fracture Mechanics-Towards a Thickness Independent Plane Stress Toughness", Engineering Fracture Mechanics, 69(5), 617 (2002).

8. P. Luna, C. Bernal, A. Cisilino, P. Frontini, B. Cotterell, and Y.-W. Mai, "The Application of the Essential Work of Fracture Methodology to the Plane Strain Fracture of ABS 3-Point Bend Specimens", Polymer, 44(4), 1145 (2003).

9. Y.-W. Mai, B. Cotterell, R. Horlyck, and G. Vigna, "ESSENTIAL WORK OF PLANE STRESS DUCTILE FRACTURE OF LINEAR POLYETHYLENES", Polymer Engineering and Science, 27(11), 804 (1987).

10. Y.-W. Mai and B. Cotterell, "ON THE ESSENTIAL WORK OF DUCTILE FRACTURE IN POLYMERS", International Journal of Fracture, 32(2), 105 (1986).

11. B. Cotterell and J.K. Reddel, "The Essential Work of Plane Stress Ductile Fracture", International Journal of Fracture, 13(3), 267 (1977).

12. S. Hashemi, "Work of Fracture of High Impact Polystyrene (HIPS) Film Under Plane Stress Conditions", Journal of Materials Science, 38(14), 3055 (2003).

13. S. Hashemi, "Work of Fracture of PBT/PC Blend: Effect of Specimen Size, Geometry, and Rate of Testing", Polymer Engineering and Science, 37(5), 912 (1997).

14. E.Q. Clutton, "ESIS TC4 EXPERIENCE WITH THE ESSENTIAL WORK OF FRACTURE METHOD", *Fracture mechanics testing methods for polymers, adhesives and composites,* Elsevier, Kidlington, UK, 177 (2001).

15. C. G'sell and J.J. Jonas, "DETERMINATION OF THE PLASTIC BEHAVIOUR OF SOLID POLYMERS AT CONSTANT TRUE STRAIN RATE", Journal of Materials Science, 14(3), 583 (1979).

16. J.W. Hutchinson and K.W. Neale, "NECK PROPAGATION", Journal of the Mechanics and Physics of Solids, 31(5), 405 (1983).

17. A.S. Saleemi and J.A. Nairn, "Plane-Strain Essential Work of Fracture as a Measure of the Fracture Toughness of Ductile Polymers", Polymer Engineering and Science, 30(4), 211 (1990).

18. Y.-W. Mai and P. Powell, "Essential Work of Fracture and J-Integral Measurements for Ductile Polymers", Journal of Polymer Science, Part B (Polymer Physics), 29(7), 785 (1991).

19. X.-H. Chen, Y.-W. Mai, and L.-C. Zhang, "Numerical simulation of the essential fracture work method", Fracture of Polymers, Composites and Adhesives, Elsevier, Amsterdam, 175-186 (1999).

20. K. Husaini, K. Kishimoto, M. Notomi, and T. Shibuya, "Fracture Behaviour of PC/ABS Resin Under Mixed-Mode Loading", Fatigue and Fracture of Engineering Materials and Structures, 24(12), 895 (2001).

21. J. Li, X. Zhang, and N. Recho, "J-Mp Based Criteria for Bifurcation Assessment of a Crack in Elastic-Plastic Materials Under Mixed Mode I-II Loading", Engineering Fracture Mechanics, 71(3), 329 (2004).

Chapter 2

Toughness of High-Density Polyethylene in Plane-Strain Fracture

2.1 Introduction

When studying the fracture resistance of very ductile materials, where a large plastic zone develops and the energy dissipation is no longer confined to a small region around the crack tip, the J-integral has been the traditional method to quantify the toughness. However, its value for ductile materials presents coupled contribution from plastic deformation and crack formation [1, 2]. As a result, a different approach that was firstly proposed by Broberg [3], known as essential work of fracture (EWF), was developed to extract the specific energy needed for the crack formation, by separating it from the non-essential work for the plastic deformation. Many researchers have since studied this concept [4-11], and obtained strong evidence to support validity of the EWF concept for the toughness characterization. The EWF concept is now increasingly popular for determining fracture toughness of ductile materials.

** A version of this chapter has been published. Polymer Engineering & Science. Vol. 66 (10), pp. 1428-1432 (Oct. 2006).

Using double-edge-notched tensile (DENT) specimens, the basic requirement for applying the EWF concept to the toughness measurement is twofold. Firstly, the ligament between two edge cracks, L_o in Fig. 2-1, should yield completely before the fracture commences, and secondly, the plastic deformation should occur only in the region around the ligament. When these requirements are met, the energy absorbed during the test, after normalized by the original ligament area, is known to be a linear function of the ligament length. The energy for the crack formation, known as specific EWF, can be determined by extrapolating the normalized energy absorption to zero ligament length, because the specimen with zero ligament length should no longer require any additional energy for plastic deformation. The specific EWF consists of two parts, that is, the energy for necking inside the fracture process zone (FPZ in Fig. 2-1) and the energy for generating new fracture surface [12]. In order to determine the latter, the necking energy within the FPZ should be excluded from the specific EWF.

The need for extracting the energy that is only for the formation of new fracture surface is justified here, using polyethylene as an example. Polyethylene is one of the most ductile materials, of which the fracture at room temperature usually occurs with a strain greater than 100%. Fracture of polyethylene specimens is known to involve extensive necking; however, as a pressurized pipe polyethylene can fail in a very brittle manner without any sign of neck formation, commonly known as rapid crack propagation (RCP). Several factors, such as high crack growth speed (sometimes exceeding the sound speed), low ambient temperature, deformation constraint, etc. [13-16], are known to prohibit the neck formation, resulting in the brittle fracture behaviour. This type of fracture is often referred to as the plane-strain fracture, in contrast to the plane-stress fracture that involves extensive necking. Toughness of polyethylene in the two fracture modes is expected to be significantly different, with the toughness in the plane-strain mode being much lower than that in the plane-stress mode.

In the plane-stress fracture, toughness of polyethylene was reported to be above 30 kJ/m^2. Some types of high-density polyethylene were reported to show the toughness around 35 kJ/m^2 [17]. But for ultra-high-molecular-weight polyethylene and high-molecular-weight polyethylene, the toughness can be as high as 78 and 138 kJ/m^2, respectively [7, 8]. Using arc-shaped specimens, the toughness for polyethylene pipe was reported to be around 80 kJ/m^2 [18]. It should be noted that all of the above values were measured in the plane-stress condition, with the involvement of necking in the fracture process. These values are much higher than the steady-state dynamic fracture toughness (G_d) of polyethylene pipe, estimated to be around 6 kJ/m^2 [16], which is known to occur without necking.

Several studies have used the EWF concept to determine the toughness of polyethylene in the plane-strain fracture. For example, Mai and co-workers observed a transition from plane-stress to plane-strain fracture by decreasing the ligament length at a given thickness [7, 8], evident by a distinct deviation of the trend line from linearity in the plot of specific work of fracture versus ligament length. Fig. 2-2 illustrates the general phenomenon observed in these studies. Attempts have been made to use the non-linear trend line to determine the specific EWF value for the plane-strain fracture, such as using power-law fitting of the data in the transition region of Fig. 2-2 to zero ligament length [20, 22-24]. However, the specific EWF values for polyethylene from these approaches

(w_e^e in Fig. 2-2) show a wide range of values, from as low as 7 kJ/m^2 to above 20 kJ/m^2 [7, 23].

We recently observed that in the EWF test of HDPE specimens with very short ligament length, i.e. less than the specimen thickness, the fracture occurred in a very brittle manner without necking. When the ligament length is short enough, the trend line of specific work of fracture vs. the ligament length was found to resume the linear relationship, of which the slope is similar to that in the plane-stress region. This observation is consistent with the speculation proposed by Luna et al. [6] that when the specimen thickness is larger than the ligament length, plane-strain fracture is expected to occur. It is believed that the true plane-strain specific EWF can be determined by extrapolating values of specific work of fracture in this region to zero ligament length.

This paper presents the experimental observation of the fracture behaviour in the plane-stress and plane-strain conditions and the corresponding specific EWF values. The specific EWF values in both extrusion and transverse directions of the HDPE plate are reported here.

2.2 EWF Concept

The EWF concept is to extract the energy for the formation of crack surface from the total energy absorbed in the fracture process. The basic requirement of the EWF concept is that the ligament between two edge cracks, L_o in Fig. 2-1, should yield completely before the crack growth commences, but the plastic deformation should be confined to regions around the ligament [9]. Therefore, the energy absorbed for the formation of crack surface can be determined by extrapolating the value of energy absorption per unit fracture area (known as specific work of fracture) to the case with zero ligament length, as the corresponding energy for plastic deformation is zero.

Using the above concept, work provided to fracture the specimen can be classified into two parts. The first part is the work for plastically deforming the region around the ligament, which is expected to be proportional to the volume of plastic deformation zone. Provided that the plastic deformation has been fully developed before the crack growth commences, the height of the plastic deformation zone, h in Fig. 2-1, is then proportional to the initial ligament length, L_0, and the total work for plastic deformation, W_p, is proportional to $L_0^2 \times t_o$. The second part is the essential work required for the formation of fracture surface, W_e, which is proportional to the cross sectional area of the ligament $(L_o \times t_o)$.

The total work of fracture, W_f, is the sum of the two parts of energy consumption. That is,

$$W_f = W_e + W_p = w_e L_0 t_0 + \beta w_p L_0^2 t_o \qquad (2.6)$$

where t_0 is the initial specimen thickness, w_e the specific essential work of fracture, w_p the average plastic work density, and β the shape factor for the plastic deformation zone. By measuring the total work of fracture for specimens of different ligament lengths, and dividing W_f by the ligament cross sectional area ($L_o \times t_o$), the specific work of fracture, w_f, can be expressed as:

$$w_f = w_e + \beta w_p L_0 \qquad (2.7)$$

The specific essential work of fracture, w_e, can then be determined by extrapolating w_f to zero ligament length [9].

Pardoen et al. [5] proposed that in thin plates, w_e can be further divided into the fracture energy that accounts for damage and material separation to form new surfaces and the necking energy that comes from the development of a localized neck in front of the crack, both of which are within the FPZ. In the plane-stress fracture, the corresponding specific EWF, w_e in Eq. (2.2), can be expressed as:

$$w_e = w_e^c + \Gamma_n \tag{2.3}$$

where w_e^c is the specific energy for generating the new surface, excluding the energy for necking, and is suggested to be the EWF for plane-strain fracture, and Γ_n is the specific necking energy within the FPZ. Value of w_e for metals was suggested to be proportional to the specimen thickness because the value of Γ_n was found to be thickness-dependent. However, for many polymers, w_e turned out to be independent of thickness [26-28]. Therefore, Γ_n for these polymers must be independent of the thickness.

Since the basic requirement of the EWF concept is the complete yielding of the ligament region prior to the commencement of crack growth, the w_e value obtained from the above approach should represent the toughness for the plane-stress fracture. According to the ESIS protocol for the EWF test [19], the plane-stress fracture is expected to occur when the ligament length L_o satisfies the following condition:

$$(3-5)t_0 \le L_0 \le \min(\frac{W}{3} \; or \; 2r_p) \tag{2.4}$$

where t_o is specimen thickness, W specimen width, and $2r_p$ size of the plastic zone which can be estimated using the following equation:

$$r_p = \frac{1}{2\pi}\frac{Ew_e^{\sigma}}{\sigma_y^2} \qquad (2.5)$$

with E and σ_y being the elastic modulus and tensile yield stress of the material, respectively, and w_e^{σ} the plane-stress specific EWF.

Even though the EWF concept was developed for the fracture in the plane-stress condition, there have been several studies that apply this concept to evaluate plane-strain fracture. As described earlier, this is done by extrapolating w_f values to zero ligament length in the plot that has the ligament length in a range less than that specified in Eq. (2.4). Sometimes power-law curve-fitting was used in the extrapolation because the trend line between w_f and L_o was not linear in this range; however, this approach does not have any support from theoretical analysis, as indicated by Saleemi and Nairn [23].

Recently, Luna et al. [6] speculated that the plane-strain fracture occurs when the following conditions for specimen thickness t_0 and ligament length L_0 are met [6, 20-21]:

$$t_o \geq 25\frac{w_e^{\varepsilon}}{\sigma_y} \quad \textit{and} \quad L_0 \leq t_0 \qquad (2.6)$$

where w_e^{ε} is the specific EWF in the plane-strain fracture, based on ASTM standard for J_{IC} testing [29]. Using the above condition for specimen design, in this study we searched for the feasibility of applying the EWF concept to determine fracture toughness in the plane-strain condition. This paper summarizes the test results and provides plausible explanation for their validity.

2.3 Experiments

A commercial-grade, extruded high-density polyethylene of 6.25 mm thick was used for the study, which was much thicker than the polyethylene specimens used in the past [7, 23]. With a reasonable ligament length, plane-strain fracture is expected to occur in the specimens of such thickness.

As shown in Fig. 2-1, DENT specimens with the dimensions of 90 mm wide (W), 260 mm long (H) and ligament length L_o ranging from $5.3t_o$ (33 mm) to $0.32t_o$ (2 mm) were prepared for the testing. Due to the extrusion process, polymer molecules may have been slightly oriented in the extrusion direction, causing anisotropy of the fracture toughness. To examine the possible toughness anisotropy, two batches of specimens were prepared, one with specimen length along the rolling direction (i.e. the notches perpendicular to the rolling direction) and the other with specimen length along the transverse direction (i.e. the notches parallel to the rolling direction). Tests were conducted by applying tensile load in the specimen length direction using an Instron universal testing machine at a crosshead speed of 5 mm/min. Test details are described in Appendix A.

2.4 Results and Discussion

The specific work of fracture w_f was calculated using the area under the load-displacement curve, which is presented in Fig. 2-3 as a function of ligament length L_o.

Fig. 2-3 clearly shows a linear relationship between w_f and L_o at $L_0 \geq 15\,mm$ (about $2.5t_0$). This is consistent with the prediction by Eq. (2.4) that specimens with L_o larger than 3 to 5 times of t_o should have fracture dominated by the plane-stress condition. Post-fractured DENT specimens, as presented in Fig. 2-4(a), show that fracture occurred after extensive elongation. The corresponding specific EWF value (w_e^σ , with the superscript σ representing the plane-stress condition) is 49.7 kJ/m^2 for specimens in the transverse direction ("Δ" in Fig. 2-3) and 75.5 kJ/m^2 for specimens in the rolling directions ("o" in Fig. 2-3). The correlation coefficients (*R*) for the curve fitting are 0.9996 and 0.9997, respectively.

For specimens with ligament length shorter than 15 mm (2.5 t_o), the trend of w_f with L_o in Fig. 2-3 clearly shows deviation from the above linearity. The corresponding post-fracture behaviour is presented in Fig. 2-4(b) which shows the evident suppression of neck formation, suggesting that the fracture is no longer dominated by the plane-stress condition. As discussed earlier, this is probably the result of mixed plane-stress and plane-strain fracture [6, 23-25]. Orientation introduced by the extrusion process still shows a visible effect on the w_f value, but difference of the w_f values due to specimen orientation is reduced with the decrease of L_o. For specimens in the rolling direction, extrapolating the w_f values in the transition region of Fig. 2-3 to zero ligament length yields 8.03 kJ/m^2 which is very close to that reported by Mai et al. [7] using linear extrapolation, also obtained from a similar region.

Further decrease of the ligament length below the transition region, i.e. with L_o below 5 mm for specimens in the rolling direction and 8 mm for specimens in the transverse direction, the w_f values seem to resume a linear relationship with L_o. Although the polymer orientation still affects the w_f values, its effect is much less than that shown in the other two regions. As shown in Fig. 2-3, by extrapolating the w_f values in this region to zero ligament length 5.0 and 6.0 kJ/m^2 were obtained for specimens in the transverse and rolling directions, respectively. The corresponding correlation coefficients (*R*) are 0.991 and 0.999. These specific EWF values are much smaller than those for the plane-stress fracture (w_e^σ). Typical post-fracture behaviour of these specimens is presented in Fig. 2-4(c) which shows that most of the necking is suppressed. Therefore, Γ_n in Eq. (2.3) that represents the energy for necking within the FPZ should be negligibly small, and the specific EWF, w_e, should be close to the pure plane-strain specific EWF (w_e^ε , with the superscript ε representing the plane-strain condition). In other words, w_f in the plane-strain condition can be expressed in a way similar to Eq. (2.2), except $\Gamma_n = 0$, thus w_e is equivalent to w_e^ε .

Results in Fig. 2-3 and the above discussion suggest that the plots of w_f vs. L_o for the plane-strain and the plane-stress fracture should show similar slopes, but the trend line for the plane-strain fracture is shifted downward in the plot due to negligible Γ_n value. It is interesting to note that the w_e^ε values in Fig. 2-3 are very close to the dynamic fracture toughness of polyethylene pipe, reported to be 6 kJ/m^2 by Zhuang et al. [16], though no material information was provided in their paper for comparison.

It should also be noted that the range of ligament length for the transition region in Fig. 2-3 (for the mixed plane-stress and plane-strain fracture) depends on the crack growth directions. For specimens in the rolling direction ("o" in Fig. 2-3) lower bound value of L_o for the transition region extends to below 5 mm, but that for specimens in the transverse direction ("Δ" in Fig. 2-3) is about 8 mm (marked by a dash line below the data points). Fig. 2-3 also shows that data in the transition region are much more scattered from linearity than those in the plane-stress or in the plane-strain regions, possibly due to the variation in the involvement of necking before the final fracture.

Karger-Kocsis and co-workers [26-27], using energy partitioning methods, expressed the total work of fracture in terms of the deformation processes involved. Since each process consumes essential and non-essential energies for fracture, they proposed that each of the terms, w_e and $\beta w_p L_0$ in Eq. (2.2), should include both types of energy. That is, the value of w_e which is conventionally regarded as constant, irrespective of the crack length or deformation behaviour, should have contributions from each of the deformation processes, such as yielding, necking and tearing. Therefore, values of w_e may vary during the crack growth, depending on the deformation processes involved. In the brittle, plane-strain fracture where necking is negligible, the deformation process may not vary much during the crack growth. However, for the plane-stress fracture of very ductile materials, the deformation process may vary significantly during the fracture evolvement. In this case, w_e may need further classification to reflect the essential work of fracture for each of the deformation processes involved. This type of study will be conducted in the near future using ductile polymers such as HDPE.

2.5 Conclusions

The concept of essential work of fracture has been applied to high-density polyethylene plate of 6.25 mm thick to determine its fracture toughness. By varying ligament length of the DENT specimens, three distinct regions were found in the plot of specific work of fracture (w_f) versus ligament length (L_o). These three regions correspond to plane-stress, mixed plane-stress and plane-strain, and plane-strain fractures, respectively. The plot bears similar features as those predicted by Luna et al., and proves that a plane-strain-dominant region exists when L_o is smaller than the specimen thickness. Excellent linear relationship was found between w_f and L_o in the plane-strain region, which allows the adoption of linear regression for the curve fitting. By extrapolating L_o to zero in this region, the specific EWF for the plane-strain fracture was determined, which is about 10 times smaller than the plane-stress counterpart.

Further study is being conducted for the plane-stress fracture, in view of the possible variation of deformation processes during the crack growth. This follow-up study is expected to establish expressions of specific work of fracture accompanied with necking or plastic deformation in the surrounding ligament region. The study is also expected to elucidate the fracture mechanisms involved in the DENT specimen, and the cause for the huge difference between the fracture toughness in the plane-strain and plane-stress conditions.

Figures

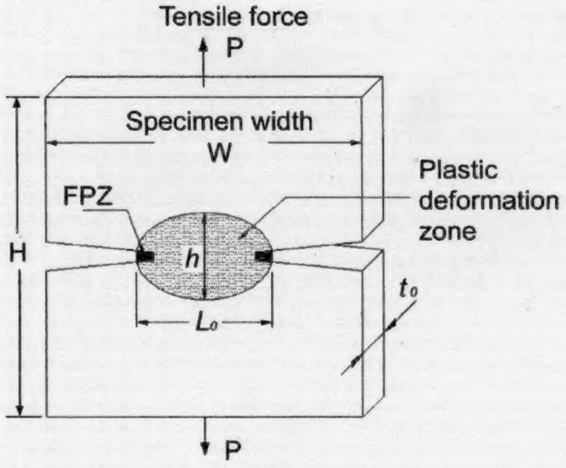
Tensile force
P
Specimen width
W
Plastic deformation zone
FPZ
H
h
L_o
t_o
P

Fig. 2-1 Double-edge-notched tensile (DENT) specimen.

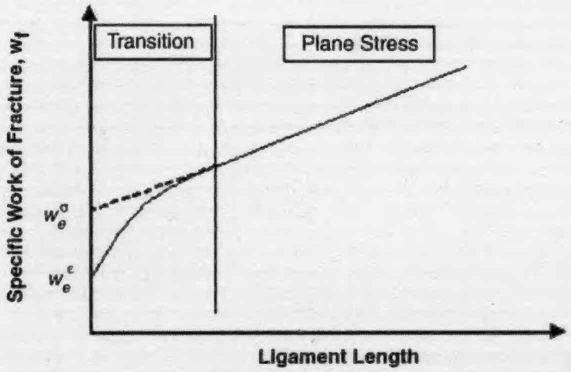

Fig. 2-2 Schematic plot of the specific work of fracture (w_f) versus ligament length (L_o), adopted from ref. [6, 7]. The plot suggests the existence of transition from plane-stress to mixed plane-stress and plane-strain conditions, which has been used in the past to determine EWF value in the plane-strain condition.

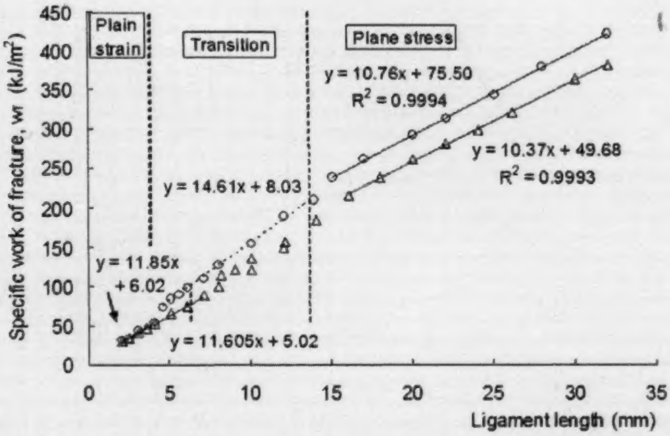

Fig. 2-3 Specific work of fracture of HDPE as a function of ligament length: "O" for specimens in the rolling direction and "△" for specimens in the transverse direction.

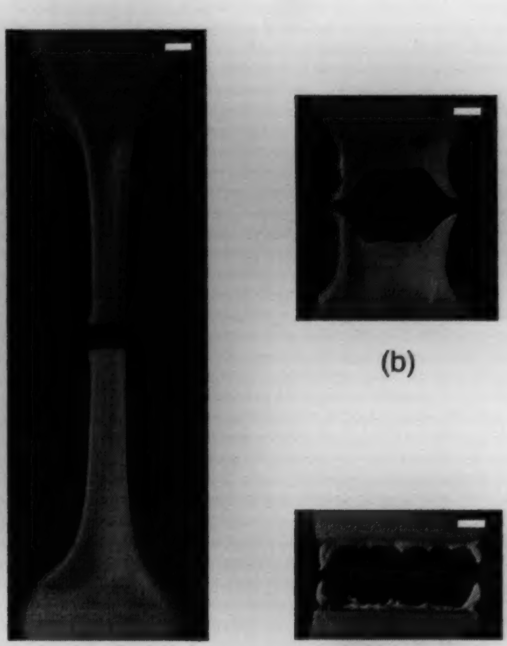

(b)

(a)

(c)

Fig. 2-4 Photographs of fracture behaviours in: (a) plane-stress region, (b) transition region, and (c) plane-strain region of Fig. 2-3. Photos were taken from the side of the specimens to show the variation of specimen thickness. Length of the white bar in each photograph corresponds to 1mm.

References

1. A.G. Atkins and Y.-W Mai, *Elastic and Plastic Fracture,* Ellis Horwood Limited, Chichester, England, 269 (1985).
2. X.-H. Chen, Y.-W. Mai, and L.-C. Zhang, *Fracture of Polymers, Composites and Adhesives, ESIS Publication 27*, Elsevier, Amsterdam, 175-186 (1999).
3. K.B. Broberg, *Int. J. Fract. Mech.*, **4**, 11 (1968).
4. B. Cotterell, T. Pardoen, and A.G. Atkins, *Eng. Fract. Mech.,* **72**, 827 (2005).
5. T. Pardoen, Y. Marchal, and F. Delannay, *Eng. Fract. Mech.,* **69**, 617 (2002).
6. P. Luna, C. Bernal, A. Cisilino, P. Frontini, B. Cotterell, and Y.-W. Mai, *Polymer,* **44**, 1145 (2003).
7. Y.-W. Mai, B. Cotterell, R. Horlyck, and G. Vigna, *Polym. Eng. Sci.,* **27**, 804 (1987).
8. Y.-W. Mai and B. Cotterell, *Int. J. Fract.,* **32**, 105 (1986).
9. B. Cotterell and J.K. Reddel, *Int J Fract,* **13**, 267 (1977).
10. S. Hashemi, *J. Mater. Sci.,* **38**, 3055 (2003).
11. S. Hashemi, *Polym. Eng. Sci.,* **37**, 912 (1997).
12. T. Pardoen, F. Hachez, B. Marchioni, P.H. Blyth, and A.G. Atkins, *J. Mech. Phys. Solids,* **52**, 423 (2004).

13. A. Ivankovic and G.P. Venizelos, *Eng. Fract. Mech.*, **59**, 607 (1998).

14. P.S. Leevers, G.P. Venizelos, and R.E. Morgan, *Proceedings of the Symposium on Buried Plastic Pipe Technology: 2nd Volume,* ASTM, Philadelphia, PA, USA, 133 (1994).

15. L. Moreno and P.S. Leevers, *Plastics, Rubber and Composites,* **33**, 149 (2004).

16. Z. Zhuang and P.E. O'Donoghue, *Int. J. Fract.*, **101**, 251 (2000).

17. Y.-W. Mai and P. Powell, *J. Polym. Sci., Part B,* **29**, 785 (1991).

18. L. Han, Y. Deng, and C. Liu, *Int. J. Pressure Vessels Piping,* **76**, 647 (1999).

19. E. Clutton, *Fracture mechanics testing methods for polymers, adhesives and composites,* Elsevier, Kidlington, UK, 177 (2001).

20. C.A. Paton and S. Hashemi, *J. Mater. Sci.*, **27**, 2279 (1992).

21. Y.-W. Mai, S.-C. Wong, and X.-H. Chen, *Application of Fracture Mechanics for Characterization of Toughness of Polymer Blends,* Wiley (John) and Sons, New York, 17 (2000).

22. J. Wu and Y.-W. Mai, *Polym. Eng. Sci.*, **36**, 2275 (1996).

23. A.S. Saleemi and J.A. Nairn, *Polym. Eng. Sci.*, **30**, 211 (1990).

24. G. Levita, L. Parisi, A. Marchetti, and L. Bartolommei, *Polym. Eng. Sci.*, **36**(20), 2534 (1996).

25. Y.-W. Mai, *Int. J. Mech. Sci.*, **35**(12), 995 (1993).

26. J. Karger-Kocsis, T. Czigany and E.J. Moskala, *Polymer*, **38**(18), 4587 (1997).

27. M.LI. Maspoch, J. Gamez-Perez and J. Karger-Kocsis, *Polym. Bul.*, 50, 279 (2003).

28. H.J. Kwon and P.-Y.B. Jar, *Polymer*, **46**(26), 12480 (2005).

29. E 1820-01, "Standard Test Method for Measurement of Fracture Toughness", American Society for Testing and Materials, Philadelphia (2001).

Chapter 3

New Work Partitioning Approach to the Measurement of Plane-Strain Fracture Toughness of High-Density Polyethylene based on the Concept of Essential Work of Fracture

3.1 Introduction

When a ductile material deforms in tension, the initial flow stress increases with the increase of plastic deformation, until one cross section reaches the condition that further increase in the flow stress does not compensate for the decrease of the cross-sectional area. From this stage onward, plastic deformation evolves around that particular section, which is known as the necking process. High-density polyethylene (HDPE) that fractures in plane-stress condition usually involves extensive necking; however, it is known that pressurized polyethylene pipe can fail in a very brittle manner without any sign of the neck formation, commonly known as rapid crack propagation (RCP) [1]. Factors such as high crack growth speed (sometimes exceeding the sound speed), low ambient temperature, deformation constraint, etc. [2-5], are known to suppress the necking in

** A version of this chapter has been accepted. Engineering Fracture Mechanics (Dec. 2006).

polyethylene, resulting in a brittle, plane-strain fracture. This is in contrast with the ductile, plane-stress fracture that involves extensive necking. The different fracture behaviour is expected to result in significantly different toughness, with that for the plane-strain fracture being much lower than that for the plane-stress fracture.

Zhuang and Ivankovic [2,5], through finite element simulation of dynamic fracture in a small-scale steady-state (S4) test, estimated that toughness of high-density polyethylene pipe in the plane-strain fracture should be around 5 to 6 kJ/m^2. In plane-stress fracture, on the other hand, the toughness has been reported to be several times higher, ranging from 35 to 138 kJ/m^2 [6-8]. Since fracture behaviour of polyethylene strongly depends on the type of applications, it is important to ensure that toughness used in design is consistent with the expected fracture behaviour for the specific applications in concern.

The basic concept of essential work of fracture (EWF), since proposed by Broberg [9], has been studied by many researchers [7,10-14], and is now widely accepted for measuring toughness of ductile materials in plane-stress fracture. In plane-strain fracture, on the other hand, J-integral is the standard method for the toughness evaluation, but the results in the literature for HDPE show a wide range of variation, from as low as 2 kJ/m^2 to above 100 kJ/m^2 [15-19]. Such variation is very unlikely to represent the true range of plane-strain toughness for HDPE, even after taking into account the difference of materials used in these studies. It is believed that some of the methods used in these studies may have introduced the fracture in a mixed mode of plane-stress and plane-strain conditions. A method that can reliably measure toughness for HDPE in the pure plane-strain fracture is thus highly desired, but yet to be available.

Several attempts have been made to use the EWF concept to evaluate the plane-strain fracture toughness. In applying the EWF concept to the plane-stress fracture, specimens should have ligament length more than 3 times of the specimen thickness. Otherwise, the fracture is generated in a mixed mode of plane-stress and plane-strain conditions, which is also known as a transition or mixed condition [7,20]. For estimating the plane-strain fracture toughness, some EWF studies have used linear extrapolation in the transition region to zero ligament length [7,21]. However, the data have shown a non-linear trend that made it difficult to justify the use of a linear regression method [22]. Attempts have also been made to use non-linear curve-fitting techniques, such as power-law functions, [22-23], but no theoretical basis can support these approaches [22]. For HDPE, values determined in those approaches show significant variation, from as low as 7 kJ/m^2 to above 20 kJ/m^2 [8,22].

Karger-Kocsis et al. [24-25] proposed an approach that was based on the principle of energy partitioning to divide the total work of fracture into the work for yielding and the work for necking and fracture. They suggested that the corresponding work is equivalent to the areas under the load-displacement curve before and after the point at the maximum load, respectively. They observed that the value obtained by extrapolating the specific work for yielding to zero ligament length in the plane-stress region agrees well with the specific EWF value determined using the total work of fracture in the transition region. Based on this observation, they suggested that the plane-strain EWF value can be obtained by applying the EWF concept to work for yielding [24-25].

In the previous work on HDPE toughness using double-edge-notched tensile (DENT) test, we discovered that when the ligament length was shorter than the specimen thickness, fracture occurred in the plane-strain condition, i.e. brittle fracture with little necking [27]. The corresponding trend line for the total specific work of fracture versus the ligament length was found to be linear, with the slope similar to that in the plane-stress condition. By applying linear extrapolation to data in the plane-strain region, the specific EWF values at zero ligament length were estimated to be 5.02 and 6.02 *kJ/m*^{2} for 6.25-*mm*-thick HDPE specimens, with the specimen length along the rolling and the transverse directions, respectively.

This paper presents results from a follow-up study, using HDPE specimens of 12.5 mm thick, as it is expected that the plane-strain fracture toughness should be independent of the specimens thickness used for the testing [22]. Following the notation used in the previous paper [27], the specimens with length along the rolling direction is also referred to as "rolling direction" here, and likewise the specimens with length in the transverse direction as "transverse direction".

It is worth mentioning that in the current study, the plane-strain EWF values are determined in two ways, one based on total work of fracture and the other on the concept of energy partitioning but in a different way from that proposed by Karger-Kocsis et al. [24-25]. The new energy partitioning approach is also applied to the analysis of data reported previously [27], and the results are included in the discussion.

3.2 Brief Review of EWF Method

EWF method is a methodology to measure toughness of ductile materials, and becomes increasingly popular for toughness measurement in the plane-stress fracture [20]. The traditional EWF method uses DENT specimens and is based on the concept that plastic deformation should be fully developed around the ligament region prior to the crack growth. Work required for the fracture of the DENT specimen consists of two parts: (i) the essential work for the formation of new fracture surface, and (ii) the work for plastically deforming the ligament region. Since the height of the plastic deformation zone, h in Fig. 3-1, is proportional to the ligament length, L_0, the work for plastic deformation is proportional to L_0^2. The total work of fracture, W_f, is expressed below as the sum of the part that is essential for fracture, W_e, and the part that is not essential, i.e. the work for the plastic deformation, W_p. That is,

$$W_f = W_e + W_p = w_e L_0 t_0 + \beta w_p L_0^2 t_0 \tag{3.1}$$

where t_0 is the initial thickness, w_e the specific essential work of fracture, w_p the average plastic work density, and β the shape factor for the plastic deformation zone. By measuring the total work of fracture from specimens of different ligament lengths, and dividing the total work of fracture by the ligament cross sectional area ($L_o t_o$), the specific work of fracture, w_f, can be expressed as [10]:

$$w_f = w_e + \beta_p w_p L_0 \tag{3.2}$$

According to Eq. (3.2), w_e can be obtained by linear extrapolation of w_f values to zero ligament length, i.e. $L_o = 0$, as long as the deformation mechanisms involved are the same. Traditionally, the EWF method is applied to the plane-stress condition, and w_e so determined is known as the plane-stress EWF (w_e^σ). To ensure the occurrence of the plane-stress fracture, specimen dimensions should satisfy the following condition [7,20]:

$$(3-5)t_0 \leq L_0 \leq \min(\frac{W}{3} \; or \; 2r_p) \tag{3.3}$$

where W is the specimen width and $2r_p$ the size of the plastic zone which can be estimated using the following equation:

$$r_p = \frac{1}{2\pi}\frac{Ew_e^{\sigma}}{\sigma_y^2} \tag{3.4}$$

with E being the elastic modulus and σ_y tensile yield stress. For HDPE, value of w_e^{σ} consists of the energy for necking inside the FPZ and the fracture energy for forming the new surface.

Pardoen et al. [28] proposed that the specific essential work of fracture, w_e, can be divided into the energy for deformation and necking and the energy for the formation of new surfaces, both of which are for deformation within the FPZ. In this approach, w_e can be expressed as:

$$w_e = w_e^s + \Gamma_n \tag{3.5}$$

where w_e^s is the specific energy for the formation of new surfaces and Γ_n the specific energy for necking within the FPZ. The former is suggested to be the EWF for the plane-strain fracture, and the latter to be proportional to the specimen thickness, resulting in w_e being thickness-dependent. However, w_e values for many polymers were found to be thickness-independent [13,29].

Alternatively, under the concept that the plane-strain EWF is the energy for the formation of fracture surface, several attempts were made to distinguish the deformation mechanisms involved in the fracture process of DENT specimen. Mai et al. [7-8]

proposed the partitioning of the total work of fracture W_f into the work for fracture initiation (W_i) and the work for fracture growth (W_g), as shown in Fig. 3-2(a). The corresponding specific work for fracture initiation, $w_i = W_i / L_0 t_0$, was suggested to be independent of the ligament length L_0, and is believed to be less than w_e^σ but greater than the plane-strain specific EWF, w_e^ε.

In a similar approach, Karger-Kocsis et al. [11,25,30] divided the total work of fracture into work for yielding (W_y) and that for subsequent necking and tearing (W_n), as shown in Fig. 3-2(b), each of which was suggested to be a function of ligament length. Therefore, the specific work of fracture is split into the following two terms:

$$w_f = w_y + w_n = \left(w_{e,y} + \beta_y \, w_{p,y} \, L_o\right) + \left(w_{e,n} + \beta_n \, w_{p,n} \, L_o\right) \qquad (3.6)$$

where, respectively, $w_{e,y}$ and $w_{e,n}$ are specific EWF for yielding and necking, and $w_{p,y}$ and $w_{p,n}$ are specific work of plastic deformation for yielding and necking. They proposed that $w_{e,y}$ is the critical plane-strain EWF value that represents the generic toughness of the material [24,29]. This was based on the experimental observation that values of $w_{e,y}$ are consistent with those determined by extrapolating w_f values to zero ligament length, from specimens with ligament length shorter than the lower threshold value for the plane-stress fracture, i.e. (3-5)t_o. However, this approach has little support from the theoretical analysis.

Based on energy partitioning, this paper proposes a new approach to determine plane-strain EWF value for extremely ductile polymers like HDPE.

3.3 Experiments

Commercially extruded HDPE plates of 12.5 mm thick were used in the experimental study. DENT specimens, as shown in Fig. 3-1, with dimensions of 90 *mm* wide (W), 260 mm long (L), and ligament length L_0 in the range from 2 to 32 *mm* (equivalent to $0.16t_0$ and $2.56t_0$, respectively) were prepared for the testing. Difference of fracture toughness due to preferential molecular orientation, possibly introduced by the extrusion process, was examined by preparing two batches of specimens, with specimen length along the rolling and the transverse directions, respectively. Tensile load was applied in the specimen length direction using an Instron universal testing machine, at a crosshead speed of 5 *mm/min*. Test details are described in Appendix A.

3.4 Results and Discussion

Fig. 3-3(a) shows representative load-displacement curves, from 12.5-*mm*-thick specimens in the transverse direction, and Fig. 3-3(b) the $w_f - L_0$ plots for all specimens in both directions, based on the total work of fracture. A vertical dash line in Fig. 3-3(b) marks the ligament length that is equivalent to the specimen thickness, corresponding to the upper bound of ligament length for the plane-strain fracture. In contrast to 6.25-*mm*-thick specimens that show significantly different trend lines between the transition and the plane-strain regions [27], Fig. 3-3(b) shows little change of the trend lines between the two regions, especially for specimens in the rolling direction.

By extrapolating the w_f values in the transition region (right half of Fig. 3-3(b)) to zero ligament length, values of 8.3 and 12.9 kJ/m^2 were obtained for specimens in the rolling and the transverse directions, respectively. The corresponding values in the plane-strain region (left half of Fig. 3-3(b)) are 7.2 and 7.9 *kJ/m*^{2}. These values are higher than those reported previously using 6.25-mm-thick specimens, 6.0 and 5.0 *kJ/m*^{2}, respectively. In addition, Fig. 3-3(b) suggests that slope of the trend line in the transition region is slightly lower than that in the plane-strain region, which is opposite to the phenomenon for the 6.25-*mm*-thick specimens. Therefore, appropriateness is questioned about the use of the total work of fracture to determine the EWF value for the plane-strain fracture.

It should be noted that due to the thickness of 12.5 *mm*, the plane-stress fracture cannot be produced in these specimens, as the ligament length could not meet the requirement of at least 3 to 5 times of the thickness.

Front and side views of selected post-fracture 12.5-mm-thick specimens are presented in Fig. 3-4, including fracture in the transition region, Fig. 3-4(a), and in the plane-strain region, Figs. 3-4(b) and 3-4(c). It should be noted that none of these photographs shows extensive necking, except in the surface layers that are clearly visible in the side-view photographs, as marked by the two horizontal white lines in the figures. These photographs suggest that all of the 12.5-mm-thick specimens have similar fracture behaviour, with fracture in the mid-thickness region involving little plastic deformation.

A typical load-displacement curve in the plane-strain condition is presented in Fig. 3-5 (a), which was generated from a specimen with ligament length of 6 *mm*. The image insert in Fig. 3-5(a) is a side view of the specimen at displacement Δ_n at which a significant, sudden drop of the load occurred. The load drop was caused by the formation of fracture surface in the mid-thickness region. However, two halves of the specimen were still connected by the surface layers, as pointed by two white arrows in the image insert. Further increase of the displacement from Δ_n caused elongation, necking and gradual fracture of the surface layers. Therefore, the corresponding area under the load-displacement curve should be irrelevant to the fracture that occurred earlier. By selecting the area W_D, i.e. the area covered by the oblique lines in Fig. 3-5(a), the energy for stretching and fracture of the surface layers is excluded from the calculation of the specific work of fracture, and the data become a highly linear function of ligament length, as shown in Fig. 3-5(b). The extrapolation to zero ligament length yields values of 5.9 and 5.7 kJ/m^2 for the rolling and the transverse directions, respectively, with the corresponding correlation coefficients (R) of 0.999 and 0.998.

The above work-partitioning approach was also applied to data obtained from 6.25-*mm*-thick specimens of which the typical load-displacement curve in the plane-strain condition is presented in Fig. 3-6(a). The load drop in the figure is not as steep as that in Fig. 3-5(a), but the point on the curve where the main fracture commences could still be identified and the work up to that point was used to calculate w_D. By extrapolating the w_D values to zero ligament length, as shown in Fig. 3-6(b), values of 6.0 and 5.7 kJ/m^2 were determined for specimens in the rolling and the transverse directions, respectively. The plots are also highly linear, with the corresponding R values of 0.9992 and 0.9991, respectively. These values are consistent with those obtained from 12.5-*mm*-thick specimens. As a result, we believe that the above work partitioning approach has successfully produced specific EWF value that is independent of the specimen thickness, and can represent EWF values of HDPE in the plane-strain fracture (w_e^ε).

Although the use of total work of fracture for 6.25-mm-thick specimens yielded values very close to those based on the new energy partitioning approach, the two approaches do not generate consistent values for 12.5-mm-thick specimens. This suggests that the use of the total work of fracture is not always reliable for determining the plane-strain EWF value.

As mentioned before, Karger-Kocsis et al. [24-25] proposed that the plane-strain EWF value can be obtained by extrapolating the work for yielding (W_y in Fig. 3-2(b)) to zero ligament length in the plane-stress region. To further examine this idea, the work for yielding (W_y in Fig. 3-2(b)) was calculated from our results, by excluding the work after the maximum load. The resulting $w_y - L_0$ plots for 6.25-*mm*-thick and 12.5-*mm*-thick specimens are presented in Figs. 3-7(a) and 3-7(b), respectively. For 6.25-*mm*-thick specimens, Fig. 3-7(a), the extrapolated w_y values in the plane-stress region are 14.6 kJ/m^2 along the rolling direction, and 11.5 kJ/m^2 along the transverse direction, that are significantly different from the plane-strain EWF values obtained in Fig. 3-5, i.e. 5.9 and 5.7 kJ/m^2.

To examine the thickness dependency, the extrapolated works for yielding (w_y) to the zero ligament length in the transition region were compared between specimens of different thickness. For 6.25-*mm*-thick specimens, Fig. 3-7(a), the extrapolated w_y values in the transition region are 7.8 kJ/m^2 along the rolling direction, and 6.4 kJ/m^2 along the transverse direction. For 12.5-*mm*-thick specimens, Fig. 3-7(b), the data show large scattering and the linearly extrapolated values in the transition region are about 31.3 and 26.9 kJ/m^2, along the rolling and transverse directions, respectively. Therefore, it is concluded that the approach proposed by Karger-Kocsis et al. is not appropriate for estimating the plane-strain fracture toughness of HDPE.

3.5 Conclusions

The concept of essential work of fracture is applied to HDPE plate of 12.5 *mm* thick to determine its plane-strain fracture toughness. The use of total fracture energy showed variation in the EWF values, different from those reported previously using 6.25-mm-thick specimens. An alternative approach is proposed, which uses energy partitioning to exclude the work for plastic deformation and for fracture of the surface layers from the calculation of specific work of fracture. By extrapolating the extracted specific work of fracture to zero ligament length in the plane-strain region, the specific EWF for the plane-strain fracture was determined, of which the values show little dependence on the specimen thickness. The study also concludes that the work-partitioning approach proposed by Karger-Kocsis et al. is not suitable for extremely ductile materials like HDPE.

Figures

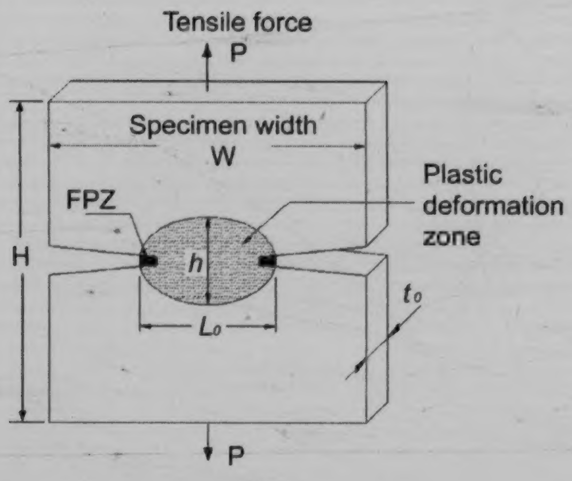
Tensile force
P
Specimen width
W
FPZ
Plastic
deformation
zone
H
h
L_o
t_o
P

Fig. 3-1 Double-edge-notched tensile (DENT) specimen.

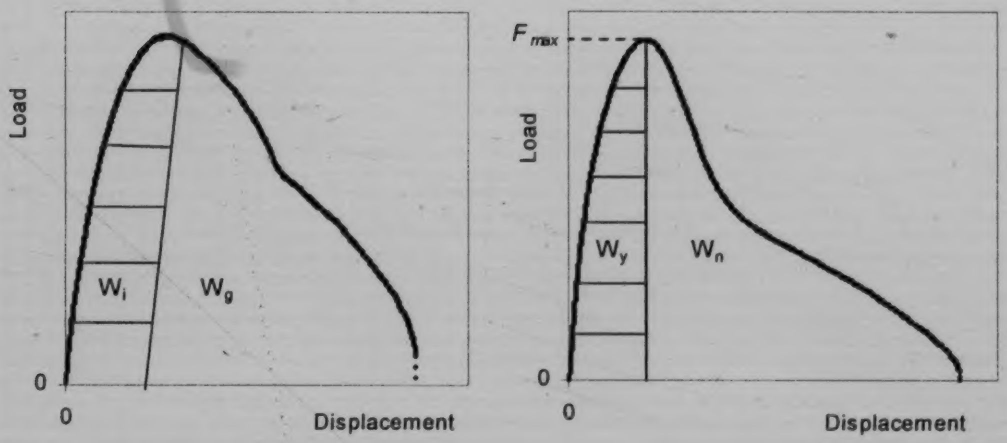

(a) (b)

Fig. 3-2 Partitioning of the total work of fracture into work for (a) fracture initiation (W_i) and fracture growth (W_g) [7, 8], and (b) yielding (W_y) and necking and tearing (W_n) [11, 26, 30].

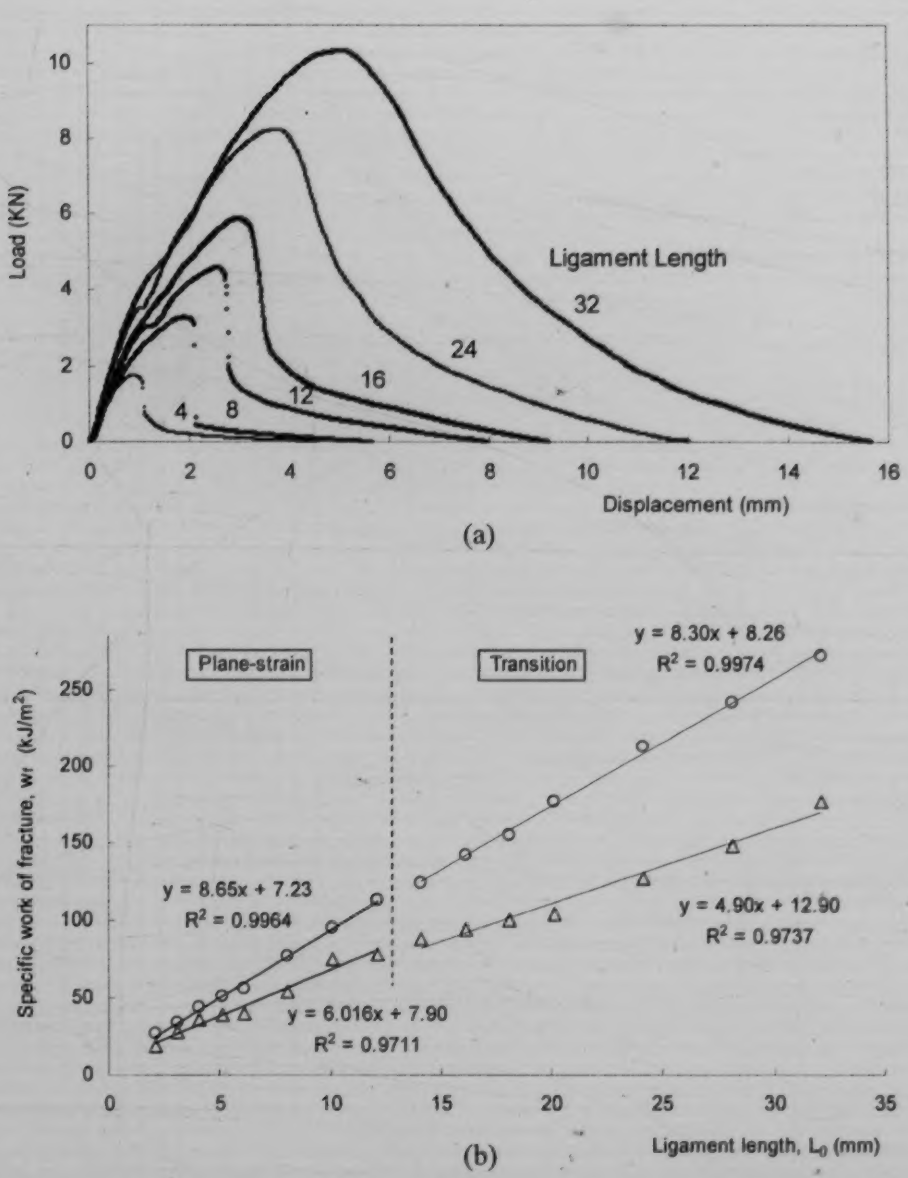

Fig. 3-3 DENT test results from 12.5mm-thick specimens: (a) Representative load-displacement curves with different ligament lengths, taken from specimens in the transverse direction, and (b) specific work of fracture based on the total work of fracture, plotted as a function of ligament length in the rolling (O) and the transverse (△) directions.

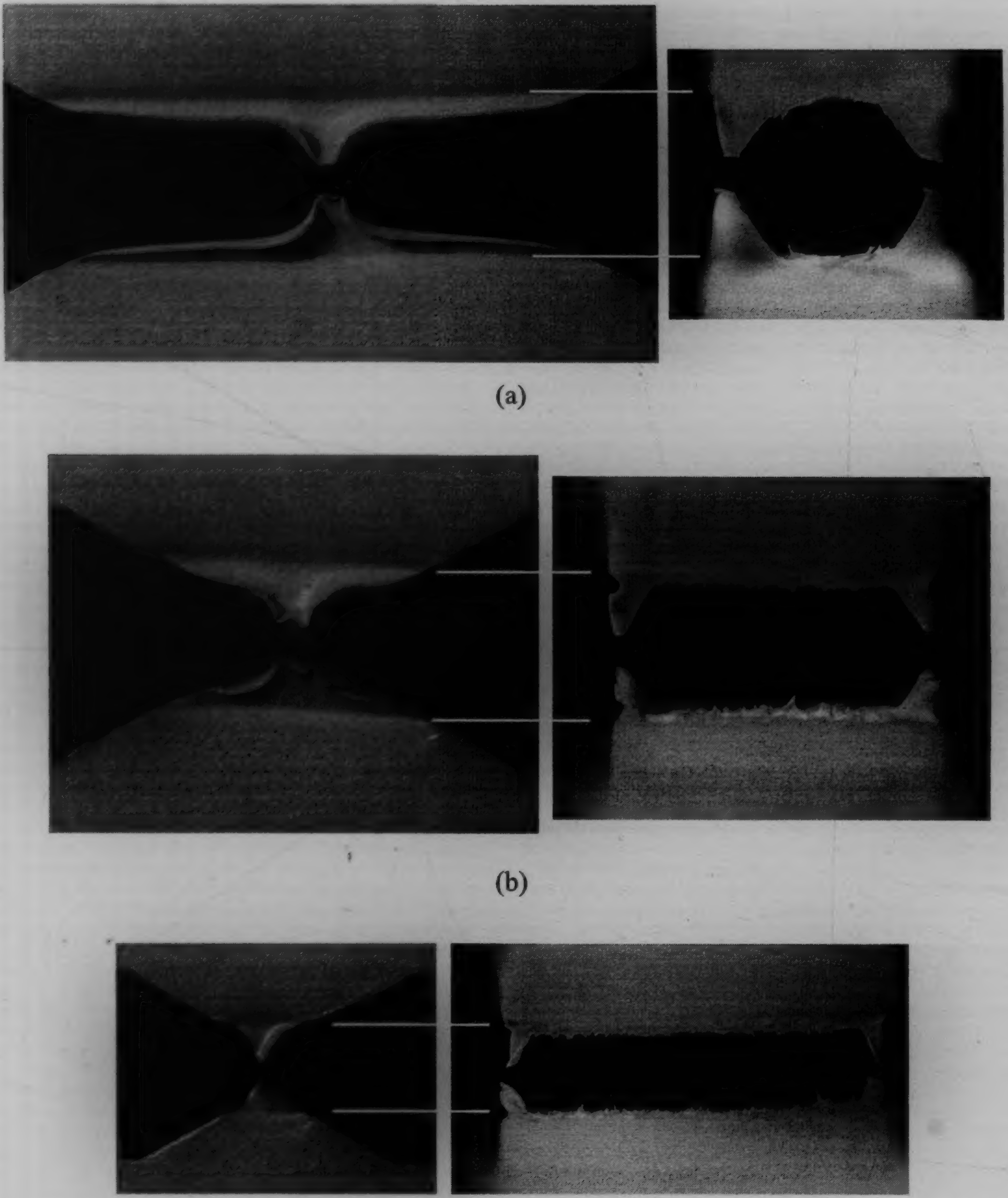

(a)

(b)

(c)

Fig. 3-4 Front and side views of 12.5mm-thick specimens after fracture, with (a) L_0 = 32 mm, (b) L_0 = 10 mm, and (c) L_0 = 3 mm.

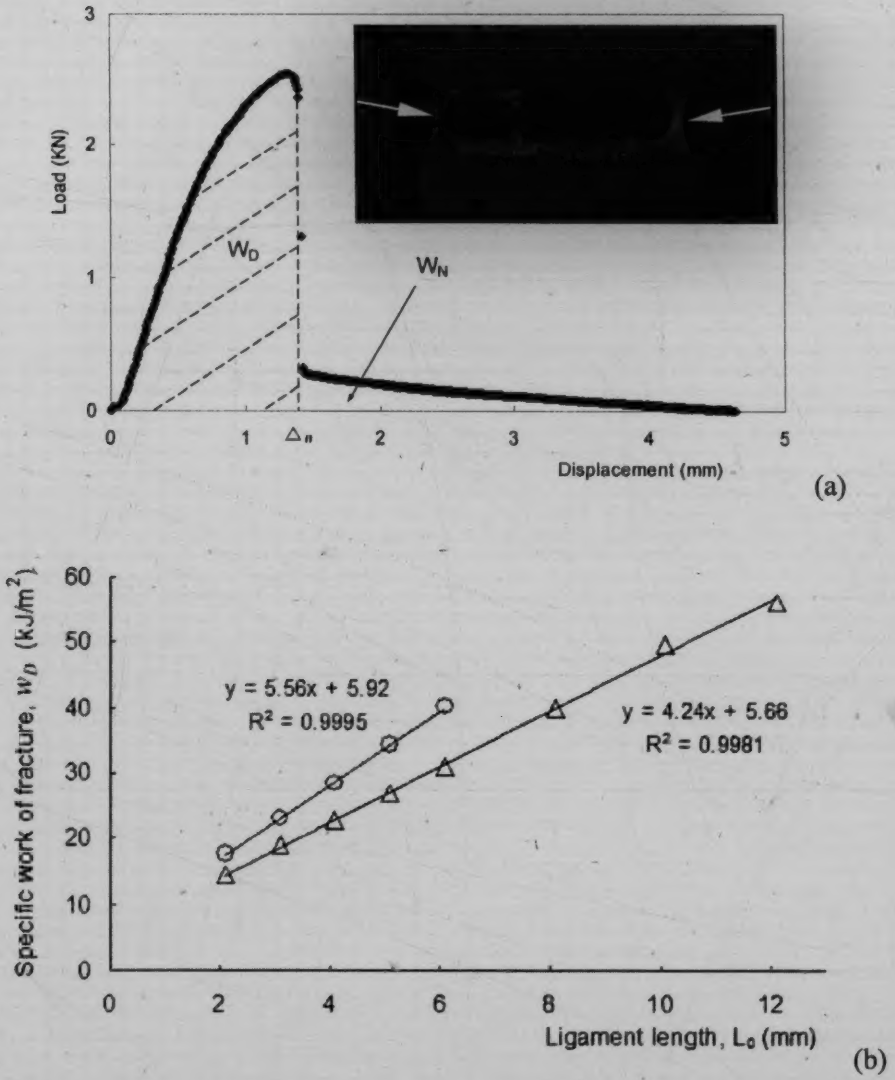

Fig. 3-5 Energy partitioning of the DENT test results for 12.5mm-thick specimens: (a) Typical load-displacement curve in the plane-strain region, from a specimen in the transverse direction with L_0 = 6mm, and (b) specific work of fracture, w_D , based on W_D in (a), plotted as a function of ligament length, L_0.

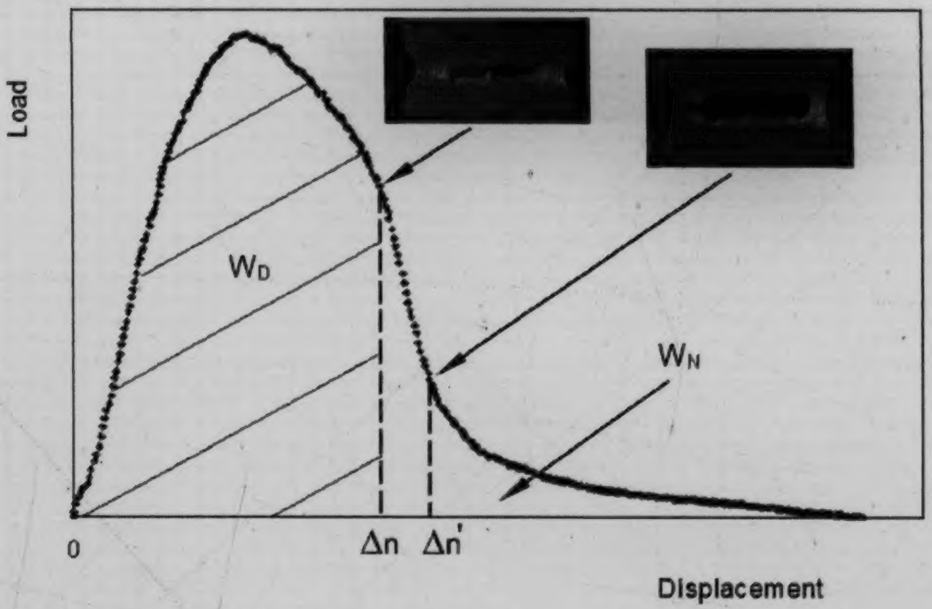
Load
W_D
W_N
0
Δn
Δn'
Displacement

(a)

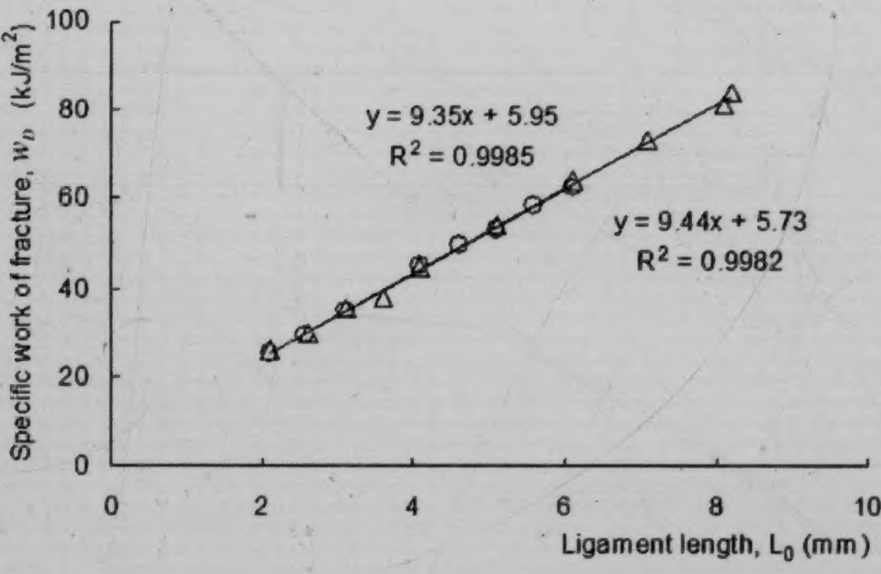
Specific work of fracture, w_D (kJ/m^2)
100
80
60
40
20
0
0
2
4
6
8
10
Ligament length, L_0 (mm)
y = 9.35x + 5.95
R^2 = 0.9985
y = 9.44x + 5.73
R^2 = 0.9982

(b)

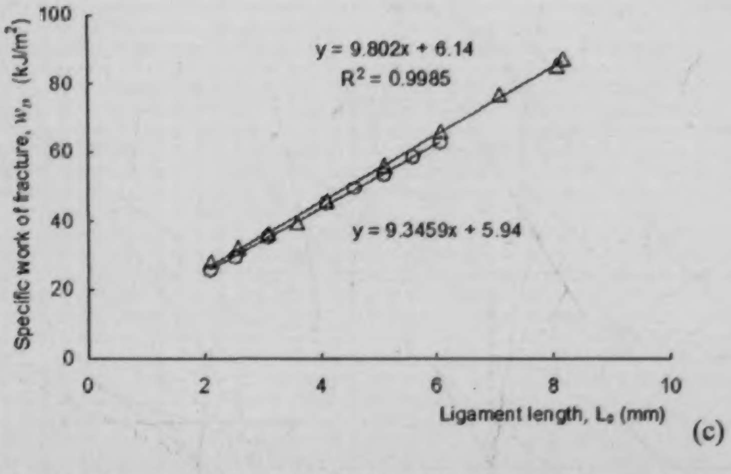

Fig. 3-6 DENT test results for 6.25mm-thick specimens: (a) Typical load-displacement curve in the plane-strain region, from a specimen in the transverse direction with $L_0 = 3.5$ mm, (b) specific work of fracture (w_D), as a function of ligament length (L_0) based on W_D calculated up to Δ_n in (a), and (c) w_D as a function of L_0 based on W_D calculated up to Δ'_n in (a).

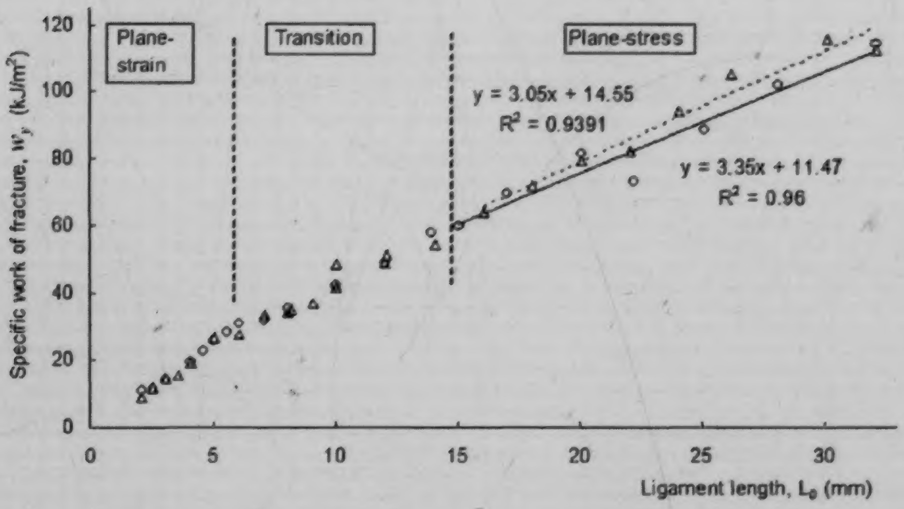

Fig. 3-7 Plots of specific work of fracture, w_y, based on W_y in Fig. 2(b), as a function of ligament length L_0 for specimens of 6.25 *mm* thick, in the rolling (—) and the transverse (- - -) directions.

References

1. Ritchie SJK, Davis P, Leevers PS. Brittle-tough transition of rapid crack propagation in polyethylene. Polymer. 1998;39(25):6657-6663.

2. Ivankovic A, Venizelos GP. Rapid crack propagation in plastic pipe: Predicting full-scale critical pressure from S4 test results. Engng Fract Mech. 1998;59(5):607-622.

3. Leevers PS, Venizelos GP, Morgan RE. Proceedings of the Proceedings of the Symposium on Buried Plastic Pipe Technology: 2nd Volume, Feb 28-Mar 2 1994, New Orleans, LA, USA: Publ by ASTM, Philadelphia, PA, USA, 1994. p. 133-148.

4. Moreno L, Leevers PS. Effect of axial surface scores on rapid crack propagation in polyethylene pipe. Plastics, Rubber and Composites. 2004;33(4):149-154.

5. Zhuang Z, O'Donoghue PE. Determination of material fracture toughness by a computational/experimental approach for rapid crack propagation in PE pipe. Int J Fract. 2000;101(3):251-268.

6. Mai YW, Powell P. Essential work of fracture and J-integral measurements for ductile polymers. J Polym Sci , Part B. 1991;29(7):785-93.

7. Mai YW, Cotterell B. On the essential work of ductile fracture in polymers. Int J Fract. 1986;32(2):105-125.

8. Mai YW, Cotterell B, Horlyck R, Vigna G. Essential work of plane stress ductile fracture of linear polyethylenes. Polym Engng Sci. 1987;27(11):804-809.

9. Broberg KB. Critical Review of Some Theories in Fracture Mechanics. Int J Fract Mech. 1968;4:11-17.

10. Cotterell B, Reddel JK. The essential work of plane stress ductile fracture. Int J Fract. 1977;13(3):267-277.

11. Karger-Kocsis J, Czigany T, Moskala EJ. Thickness dependence of work of fracture parameters of an amorphous copolyester. Polymer. 1997;38(18):4587-4593.

12. Pardoen T, Marchal Y, Delannay F. Essential work of fracture compared to fracture mechanics-towards a thickness independent plane stress toughness. Engng Fract Mech. 2002;69(5):617-631.

13. Kwon HJ, Jar P-B. Fracture toughness of polymers in shear mode. Polymer. 2005;46(26):12480-12492.

14. Cotterell B, Pardoen T, Atkins AG. Measuring toughness and the cohesive stress-displacement relationship by the essential work of fracture concept. Engng Fract Mech. 2005;72:827-848.

15. Frassine R, Rink M, Pavan A. Size effects in the fracture of a pipe-grade high density polyethylene. Fat Fract Engng Mater & Struct. 1997;20(8):1217-1223.

16. Han L, Deng Y, Liu C. Determination of J_{IC} for polyethylene pipe using non-standard arc-shaped specimen. Int J Pressure Vessels Piping. 1999;76(9):647-651.

17. Manoharan M. Mixed-mode fracture toughness of polyethylene. Scripta Metallurgica et Materialia. 1994;30(11):1383-1386.

18. Chan MKV, Williams JG. Plane strain fracture toughness testing of high density polyethylene. Polym Engng Sci. 1981;21(15):1019-1026.

19. Swei H, Crist B, Carr SH. J integral fracture toughness and damage zone morphology in polyethylenes. Polymer. 1991;32(8):1440-1446.

20. Clutton E (ed). Essential Work of Fracture. In: Moore DR, Pavan A, Williams JG, editors. Fracture mechanics testing methods for polymers, adhesives and composites. Kidlington, UK: Elsevier, 2001. p. 177-95.

21. Wu J, Mai YW. Essential fracture work concept for toughness measurement of ductile polymers. Polym Engng Sci. 1996;36(18):2275-2288.

22. Saleemi AS, Nairn JA. Plane-strain essential work of fracture as a measure of the fracture toughness of ductile polymers. Polym Engng Sci. 1990;30(4):211-218.

23. Levita G, Parisi L, Marchetti A, Bartolommei L. Effects of thickness on the specific essential work of fracture of rigid PVC. Polym Engng Sci. 1996;36(20):2534-2541.

24. Karger-Kocsis J, Ferrer-Balas DE-. On the plane-strain essential work of fracture of polymer sheets. Polymer Bulletin. 2001;46(6):507-512.

25. Mouzakis DE, Karger-Kocsis J, Moskala EJ. Interrelation between energy partitioned work of fracture parameters and the crack tip opening displacement in amorphous polyester films. J Mater Sci Lett. 2000;19(18):1615-1619.

26. Paton CA, Hashemi S. Plane-stress essential work of ductile fracture for polycarbonate. J Mater Sci. 1992;27(9):2279-90.

27. Kwon HJ, Jar P-YB. Toughness of High-Density Polyethylene in Plane-Strain Fracture. Polym Engng Sci. accepted.

28. Pardoen T, Hachez F, Marchioni B, Blyth PH, Atkins AG. Mode I fracture of sheet metal. J Mech Phys Solids. 2004;52(2):423-52.

29. Maspoch ML, Gamez-Perez J, Karger-Kocsis J. Effects of thickness, deformation rate and energy partitioning on the work of fracture parameters of uPVC films. Polymer Bulletin. 2003;50(4):279-286.

30. Karger-Kocsis J, Czigany T, Moskala EJ. Deformation rate dependence of the essential and non-essential work of fracture parameters in an amorphous copolyester. Polymer. 1998;39(17):3939-3944.

Chapter 4

On the Application of Essential Work of Fracture Concept to Toughness Characterization of High-Density Polyethylene Introduction

4.1 Introduction

The essential work of fracture (EWF) [1-5] is a concept for material toughness evaluation. Its value represents the energy consumed within the fracture process zone (FPZ) where new surface is generated. For crack growth subjected to tensile loading, the EWF value is often determined using double-edge-notched tensile (DENT) test [6] for which the specimen is shown in Fig. 4-1. Under the plane-stress condition, total work consumed in a DENT test consists of two parts: (i) the essential energy for the formation of new fracture surface, and (ii) the energy for plastic deformation around the ligament section. The EWF concept is a scheme to extract the energy for part (i) from the total fracture energy in the DENT test, and is increasingly popular for evaluation of the toughness for ductile fracture [6].

For materials in ductile fracture, FPZ is known to undergo a necking process that

** A version of this chapter has been accepted. Polymer Engineering and Science (Mar. 2007).

eventually breaks down to form fracture surface. It has been suggested that in order for necking to be fully developed in the FPZ, specimen dimensions have to meet the following constraints [3,7]. The EWF value so determined is known as the plane-stress specific EWF (w_e).

$$(3-5)t_0 \leq L_0 \leq \min\left(\frac{W}{3} or\, 2r_p\right) \tag{4.1}$$

where t_0, L_0 and W are specimen thickness, ligament length and specimen width, respectively, and $2r_p$ is the size of the plastic zone that can be estimated using the following equation:

$$2r_p = \frac{1}{\pi}\frac{Ew_e}{\sigma_y^2} \tag{4.2}$$

where E is the elastic modulus and σ_y the tensile yield stress. Value of w_e represents energy consumed for the formation of neck and new fracture surface inside the FPZ. Some work [3,8-10] has attempted to express the EWF value in terms of the energy consumed before and after the neck formation in FPZ, in order to take into account the energy for the necking explicitly.

There are two types of necking behaviour, based on the stability of the necking process [11]. For many ductile materials, the neck development is an unstable process that leads to final fracture soon after the neck is initiated. This is because increase of strength by the work-hardening from the neck formation cannot keep up with the stress increase caused by the cross section reduction. However, for some very ductile materials like HDPE, the work-hardening rate in the neck is fast enough to compensate for the decrease of the cross-sectional area, so that the neck development process is stabilized, and its size grows at a constant rate [12].

In a plane-stress DENT test of HDPE, neck is initially initiated along the ligament section. As to be shown in this paper, after the neck is formed through the whole ligament, it propagates into the neighbouring region that has been plastically deformed at the early stage of the test. In the past, studies that evaluated w_e of HDPE [3,8,13] have largely ignored the neck development process for the energy consumption analysis.

Objective of this study is to examine the deformation behaviour of DENT specimens of HDPE in the plane-stress condition, in order to identify the deformation mechanisms involved and to quantify the associated energy consumption. Uni-axial tensile (UT) tests were also conducted to extract the stress-strain relationship of HDPE during the necking process. The information is used to facilitate the understanding of the neck development process.

This paper will firstly present results from the UT tests, for analysis of the stress-strain relationship during the necking process. With the assumption that the stress-strain relationship from the UT test is applicable to the DENT test, deformation process involved in the latter is examined, the associated energy consumption at each stage of the crack growth quantified, and their specific EWF values determined. The specific EWF values are then compared with those determined from the conventional method that uses total energy consumption for the analysis.

4.2 Experimental Details

Specimens used in the study were machined from a commercial-grade, extruded HDPE plate of 6.25 *mm* thick and density of 0.96 g/cm^3, provided by McMaster-Carr, USA. The

In the DENT tests, the transition from the plane-stress fracture to the mixed plane-stress/plane-strain fracture could easily be detected by the deviation of the linear trend line, in the plot of specific work of fracture versus ligament length. It has been suggested that the lower bound of the initial ligament length for the plane-stress fracture should be three times of the initial ligament thickness ($L_0 = 3t_0$) [3,8,13]; however, our previous study [14] has shown that for HDPE, the plane-stress fracture could occur with L_0 down to $2.4t_0$. Therefore, the DENT specimens used in this study, Fig. 4-1, were designed to have width (W) 90 mm and the initial ligament length (L_0) ranging from 15 to 32 mm (corresponding to 2.4 and 5.12 times of t_0). Overall length of the specimens was 260 mm. Because the plane-stress specific EWF value (w_e) of the HDPE depends on the specimen orientation [14], DENT tests were conducted on both types of specimens that have length along either the rolling or the transverse direction. The tests were conducted using an Instron testing frame that has a load capacity of 250 kN, at a crosshead speed of 5 mm/min.

The strain in the ligament section of the DENT specimens was also determined using the change of the cross sectional dimensions. Following the assumption that the strain of the DENT specimens in the ligament length direction is negligible [16], the true strain in the loading direction in the ligament section was determined using the following equation:

$$\varepsilon = \ln\left(\frac{t_0}{t}\right) \tag{4.5}$$

where t_0 is the original specimen thickness and t the thickness during the test.

4.3 Stress-Strain Relationship from the UT Test

A typical time function of the loading curve from the UT tests is presented in Fig. 4-2(a). The corresponding $\sigma-\varepsilon$ curve is shown in Fig. 4-2(b), and $\sigma_E-\varepsilon_E$ curve in Fig. 4-2(c). Necking started at the maximum load where ε was around 0.12 (the equivalent ε_E was about 0.127). As expected, increase of the strain after the onset of necking was mainly caused by the reduction of the cross section. The term "neck inception stage" will be used here to refer to the deformation process in which reduction of the cross sectional area was localized for the neck formation. After the load passed through the minimum point, the neck started growing into the neighbouring region, and the total length of the neck increased significantly. This part of the necking process will be referred to as the "neck propagation stage" in which the load never decreased again until the specimen fractured. Although the load increased, decreased, and then increased again in the UT tests, the true stress-strain curve, Fig. 4-2(b), shows monotonic increase of the true stress without any drop, at both the neck inception and the neck propagation stages.

Fig. 4-2(b) also contains a curve that was generated numerically to fit the experimental data in the plastic deformation regime. The curve in the low-strain section, i.e. below ε_0 in Fig. 4-2(b), was generated based on a constitutive equation that was originally proposed by Hollomon [17]:

$$\sigma(\varepsilon)=K\varepsilon^N \tag{4.6}$$

where K is the strength coefficient and N the work-hardening coefficient. The section above ε_0 in the curve was generated using an expression proposed by G'Sell and Jonas [12]:

$$\sigma(\varepsilon,\dot{\varepsilon}) = k\exp(M\varepsilon^{n})\cdot\dot{\varepsilon}^{m} \qquad (4.7)$$

where k, M, n, and m are material constants and $\dot{\varepsilon}$ the strain rate. With the assumption that the true stress-strain curve is insensitive to the strain rate, the above expression can be rewritten as:

$$\sigma(\varepsilon) = k'\exp(M\varepsilon^{n}) \qquad (4.8)$$

where k' can also be regarded as a material constant.

Hill [16] proposed that the necking occurs when the following condition is satisfied:

$$\frac{1}{Y}\frac{dY}{d\varepsilon} \le \left(\frac{\partial f}{\partial\sigma_1}+\frac{\partial f}{\partial\sigma_2}\right)\Big/\frac{\partial f(Y,0)}{\partial Y} \qquad (4.9)$$

where Y is uni-axial yield strength of the material, f a yield function, and σ_1 and σ_2 the principal stresses. By choosing von Mises function as f for plane stress, that is,

$$f \equiv \sigma_1^2 - \sigma_1\sigma_2 + \sigma_2^2 = Y^2 \qquad (4.10)$$

it can be shown that based on Eq. (4.9), necking occurs under uni-axial loading when

$$\frac{1}{Y}\frac{dY}{d\varepsilon} \le 1 \qquad (4.11)$$

A strain range for the necking in the UT test can be determined by combining Eq. (4.11) with Eqs. (4.6) and (4.8), which is

$$N \le \varepsilon \le \left(\frac{1}{Mn}\right)^{\left(\frac{1}{n-1}\right)} \qquad (4.12)$$

However, the above strain range is not directly applicable to the necking process in the DENT test. Following the assumption by Hill [16] that the plastic strain along the ligament length direction remains constant during the DENT test, with the use of von Mises function as f in Eq. (4.9) the necking in the test is expected to occur when the following condition is met:

$$\frac{1}{Y}\frac{dY}{d\varepsilon} \le \frac{\sqrt{3}}{2} \tag{4.13}$$

The corresponding strain range for the necking in the DENT test is:

$$\frac{N}{\sqrt{3}/2} \le \varepsilon \le \left(\frac{\sqrt{3}/2}{Mn}\right)^{\left(\frac{1}{n-1}\right)} \tag{4.14}$$

In this study, data from the UT tests were used to determine the constants in Eqs. (4.6) and (4.8), with the value of N (equivalent to the strain for the onset of necking in the UT tests) being 0.12. Value of K in Eq. (4.6) was determined to be 37.5 MPa for the best curve fit in the plastic strain range, which is for strain in Fig. 4-2(b) to be up to ε_o (0.32).

Values of M and k' were determined by imposing continuity of the stress and the tangent modulus ($d\sigma / d\varepsilon$) between Eqs. (4.6) and (4.8) at the strain 0.32, which yielded the following expressions for M and k' in terms of β:

$$M = \frac{N}{n\,\varepsilon_0^n} \tag{4.15}$$

$$k' = \frac{K\,\varepsilon_0^N}{\exp(N/n)} \tag{4.16}$$

Through trial and error, the best curve that fits data in Fig. 4-2(b) in the strain range above ε_0 was generated by Eq. (4.8) based on n value of 1.6. The corresponding k' and M values are 30.4 and 0.47, respectively. Note that the n value is close to 2 that was suggested by G'Sell and Jonas [12] for HDPE.

Using the above N, M and n values, Eq. (4.12) estimates that the true strain range for HDPE to develop necking in the UT test is between 0.12 and 1.61, equivalent to the nominal strain range from 0.13 to 3.99, as illustrated by the shaded area in Fig. 4-2(c).

The corresponding loading range is presented in Fig. 4-2(a) in the section that is also high-lighted by the shaded area.

As predicted by Eq. (4.12), the maximum strain for necking in the UT test is equivalent to 55% reduction of the specimen width, defined as $\left(1-\frac{W}{W_0}\right)$. The width reduction in the fractured UT specimens was examined and found to vary from 58% at the centre of the neck to 50% at the end of the neck. Since these specimens are already fractured, the measured values should have excluded the width reduction due to the elastic deformation, of about 5%. Therefore, the upper limit predicted by Eq. (4.12), 55%, can serve as a conservative estimate of the maximum strain that can possibly be generated by the necking process in the UT tests. Note that the nominal strain in Fig. 4-2(c) was measured from the position where the neck was initiated. After the neck propagation commenced, cross section in the already necked region was reduced continuously but at a much slower rate, as shown by the dense data points at the very end of Fig. 4-2(c).

At the molecular level, the neck development is attributed to the uncoiling and alignment of polymer chain segments [18]. When tensile stress on the specimen increases to a critical level, the entangled molecular chains starts to uncoil at a particular section, which corresponds to the "neck inception stage". The uncoiling and alignment continues at the "neck propagation stage". It has been reported that at an elevated temperature HDPE can be drawn to a draw ratio Λ (defined as the ratio of the final length to the initial length) between 8 and 10 [19]. However, at room temperature the maximum Λ of HDPE is about 6 that is equivalent to an engineering strain (ε_E) of 500% [20]. When the elongation approaches this level, the specimen becomes noticeably more rigid. These phenomena are consistent with those shown in Figs. 4-2(b) and 4-2(c) in which a sharp rise of the stress occurs in the right-most region of ε_E , of around 550% which corresponds to Λ of about 6.5. When a sufficient strain is generated in the neck, fracture occurs.

4.4 Deformation Behaviour in the DENT Test

Fig. 4-3(a) demonstrates the typical shape of load-displacement curves from DENT tests in the plane-stress condition. The curves always contain a transition of the load drop rate which is indicated by point B on the top curve. Fig. 4-3(b) presents all values of specific work of fracture (w_f , defined as the total work divided by the area in the ligament section) in the plane-stress condition, plotted as a function of the ligament length L_0. Through linear regression to zero ligament length, Fig. 4-3(b) suggests that specific EWF values (w_e) in the plane-stress fracture for specimens in the transverse and the rolling directions are 49.7 and 75.5 KJ/m^2 , respectively. These values are comparable to values published in the literature, in the range from 35 kJ/m^2 [13] to 78 kJ/m^2 [3,8], though no specific specimen orientation was provided in the literature.

The above data deduction process has been widely adopted for the DENT test, which is based on the following assumptions for determining w_e: (i) the plastic zone is fully developed around the ligament section prior to the crack growth, (ii) the necking is confined within the FPZ, and (iii) the height of FPZ and fracture strain within the FPZ remain constant during the crack growth [3,5,21]. The latter two assumptions imply that work hardening in the material should not be significant enough to generate stable necking. However, the UT tests suggest that the work hardening in the HDPE is strong enough to stabilize the neck development process, to allow the neck propagation before the specimen fractures. This raises concerns on whether the above data deduction process is applicable to the HDPE.

It is worth mentioning that in Broberg's original paper that introduced the EWF concept [1], fracture is categorized in three main classes based on the characteristics of the end region (FPZ): (i) with an autonomous unstable end-region in brittle materials, (ii) with an unstable end-region in ductile materials, of which dimensions are proportional to the crack length, and (iii) with a stable end-region in very ductile materials. Since the EWF concept is based on the assumption of unstable necking in FPZ, it is applicable to materials in the 1st class. The concept may also be applicable to materials in the 2nd class, provided that fracture in FPZ is autonomous and fracture criteria for the 1st class are applicable to their crack growth process. However, the assumption of constant height of FPZ during the crack growth is not applicable to materials in the 3rd class such as HDPE that generates stable FPZ. As a result, validity of the above data analysis that is based on the EWF concept, but without the consideration of its limitation, needs to be examined.

The curves from the DENT tests, Fig. 4-3(a), clearly indicate that the HDPE specimens used in this study fractured in two stages, between which transition caused the change of the load drop rate. Deformation in the two stages is demonstrated in Fig. 4-4. The top photograph in the figure was taken above the fracture surface (top view); the bottom left from the specimen surface (front view); and the bottom right along the ligament length direction (side view). The front view clearly shows two stages of deformation during the crack growth. The first stage, marked $L_i/2$ for the left half in the front view, was initiated soon after the maximum load was reached, i.e. point A in Fig. 4-3(a). As to be explained later, neck development at this stage is equivalent to the "neck inception stage" in the UT test. The second stage, marked L_p in the front view of Fig. 4-4, was initiated after the change of the load drop rate, as indicated by point B in Fig. 4-3(a). Neck development at this stage is equivalent to the "neck propagation stage" in the UT test.

Thickness decrease in the ligament section of the DENT specimens was examined after the test. Typical thickness change is shown in Fig. 4-4 which was taken from a specimen with $L_0 = 27\,mm$. Top view of Fig. 4-4 suggests that at the neck inception stage the ligament thickness decreases continuously with the crack growth. The strain range that corresponds to the thickness decrease at this stage was found to be within that specified by Eq. (4.14). At the neck propagation stage, i.e. after the necking has been initiated through the entire ligament section, strain in the ligament section only increased slightly with the crack growth. The ligament thickness maintained almost constant of around 1.6 mm (from the initial thickness of 6.25 mm). With the assumption of zero strain in the ligament length direction, as suggested in ref. [16], the strain in the loading direction, based on the specimen thickness reduction, was found to be around 320%. This value is far below the strain in the very right region of the stress-strain curve from the UT test, as shown in Fig. 4-2(c) where the stress increases sharply.

The deformation and fracture process in the DENT test is schematically presented in Fig. 4-5. The top two drawings depict the development of the plastic zone, the FPZ and the onset of crack growth when the maximum load is reached, i.e. point A in Fig. 4-3(a).

Note that the drawings suggest that the plastic zone in these specimens has a rather flat elliptical shape, in contrast to the nearly circular shape for metallic specimens. Fig. 4-5 also suggests that the crack growth is accompanied with the increase of the FPZ size, with the size increase in the ligament length direction being faster than that in the specimen length direction. Since the length of FPZ increased faster than the crack growth, the two FPZs met at the centre of the specimen, as illustrated by the 3rd drawing in Fig. 4-5, with the crack tips still at a distance L_p away from each other. The corresponding point on the load-displacement curve is point B in Fig. 4-3(a), known as the transition point. Further specimen elongation caused stable neck propagation in the loading direction, while the two crack tips proceeded steadily towards the centre. The fracture process after the transition point resulted in a necked zone of a triangular shape, as shown by the bottom drawing in Fig. 4-5.

Fig. 4-6 shows an example of the DENT specimens at the transition point, at which the neck has developed across the whole ligament section. This necking process bears some similarity with that in the UT test. The main difference is that in the DENT tests, the crack growth was involved in both the neck inception and the neck propagation stages, while in the UT tests, the crack growth occurred only at the end of the neck propagation stage.

Interestingly, crack growth speed in the DENT tests remained nearly constant during both stages of the neck development. This is evident in Fig. 4-7 which presents the reduction of the ligament length as a function of time for two specimens of the same L_0, with time zero being the point when the maximum load is reached. The constant crack growth speed allowed us to use the load-displacement curve to determine the remaining ligament length at any point during the DENT test. That is, based on values of L_0 and displacement at the point of interest, Δ, we can determine the ligament length L between the two crack tips using the following expression:

$$L = \frac{\Delta - \Delta_y}{\Delta_f - \Delta_y} L_0 \qquad (4.17)$$

where Δ_y is the displacement at the maximum load, and Δ_f the displacement at fracture. Eq. (4.17) suggests that lengths of the ligament sections for the two stages of crack growth, L_i and L_p, can be determined using the following expressions:

$$L_i = \frac{\Delta_n - \Delta_y}{\Delta_f - \Delta_y} L_0; \quad L_p = \frac{\Delta_f - \Delta_n}{\Delta_f - \Delta_y} L_0 \qquad (4.18)$$

where Δ_n is the displacement at the transition point.

Experimental results suggest that values of Δ_y / Δ_f and Δ_n / Δ_f are nearly constant in the whole range of ligament lengths used in the study, as shown in Fig. 4-8. Mean value of Δ_y / Δ_f is 0.20 for both rolling and transverse directions, and that of Δ_n / Δ_f is 0.39 and 0.42, respectively. Since these values are independent of L_0, the ratios of L_i to L_0 and L_p to L_0 should also be independent of L_0. The latter ratio for the HDPE used in this study is 0.75 and 0.72, respectively, in the rolling and the transverse directions.

Neck Propagation in DENT Test

For polymers with limited ductility, the plastic deformation does not generate sufficient work hardening to stabilize the neck development process. Their DENT specimens are expected to fracture at the neck inception stage. For polymers with high ductility such as HDPE in the plane-stress condition, significant work hardening slows down the crack formation and allows the occurrence of neck propagation before the final fracture.

In addition to the above mechanism that is based on the different stability in the necking process, the plastic zone shape is also believed to contribute to the occurrence of neck propagation in the DENT test of highly ductile polymers. The explanation is as follows. Strain increment ($d\varepsilon$) in the active plastic zone can be expressed in terms of displacement increment (du), the remaining ligament length (L), and the active plastic zone shape (represented by the shape factor λ) [5]:

$$d\varepsilon = \frac{du}{\lambda L} \tag{4.19}$$

Since the cross-head speed ($\frac{du}{dt}$) is constant during the test, the strain rate ($\frac{d\varepsilon}{dt}$) in the FPZ of a given L depends only on the λ value. For metallic materials, shape of the plastic zone is nearly circular, thus λ being close to 1. But for polymeric materials like HDPE, due to the flat shape of the plastic zone, λ is much smaller than 1. Therefore, the strain rate in the ligament section of the polymeric specimens should be much higher than that in the metallic specimens when subjected to the same testing conditions, allowing the former to reach the strain for neck propagation before the crack tips reach the centre of the ligament. As a result, the central section of the ligament for polymeric specimens could go through the neck propagation stage before the specimen fractured completely.

Transition of the Load Drop Rate in the DENT Test

Another interesting phenomenon in the DENT test is the transition of the load drop rate, i.e. point B in Fig. 4-3(a). This phenomenon can be explained based on the variation of the average nominal stress (σ_E)between the neck inception stage and the neck propagation stage. Let F be the load carried by the remaining ligament section during the DENT test. F can be expressed as:

$$F = \sigma_E \, t_0 \, L \tag{4.20}$$

The load drop rate ($\frac{dF}{dt}$) during the crack growth is:

$$\frac{dF}{dt} = \frac{d\sigma_E}{dt} t_0 \, L + \sigma_E \, t_0 \frac{dL}{dt} \tag{4.21}$$

With a constant crack growth speed through the test, i.e. a fixed, negative value of $\frac{dL}{dt}$, difference of $\frac{dF}{dt}$ between the two stages of neck development is dominated by the difference of the 1st term on the right-hand side of Eq. (4.21). Results from the UT tests, Fig. 4-2(c), suggest that $\frac{d\sigma_E}{dt}$ should be negative in the neck inception stage, but zero or slightly positive in the neck propagation stage. Therefore, the load drop rate (the absolute value of $\frac{dF}{dt}$) in the neck inception stage should be higher than that in the neck propagation stage.

Fracture Criterion

The deformation behaviour observed in the DENT tests clearly suggests that critical elongation, though being a common fracture criterion for ductile materials, is not suitable for the FPZ fracture in HDPE. Chen et al. [22] proposed an alternative criterion for the crack growth in HDPE that is based on the crack-tip opening angle (CTOA). Since the load-displacement curves of their HDPE specimens did not show any existence of a neck propagation stage, suitability of CTOA as a criterion for the HDPE used in this study needs to be re-evaluated.

Here, the crack tip angle was measured in-situ in both the neck inception and the neck propagation stages, as presented in Figs. 4-9(a) and 4-9(b), respectively. CTOA for ten DENT specimens were monitored, and were found to maintain around 130° through the entire necking process, supporting that the CTOA is a valid criterion for the crack growth in the HDPE used in this study, even in the neck propagation stage.

Maintaining a constant crack tip angle in the DENT test can also be rationalized in the following way. As shown in Fig. 4-9(c), angle at the crack tip (α), specimen elongation (Δ) and ligament length (L) have the following relationship:

$$\frac{d\Delta}{dL} = -\tan(\frac{\alpha}{2}) \tag{4.22}$$

Since the DENT tests were conducted at a constant cross-head speed ($\frac{d\Delta}{dt}$) and the crack growth rate ($\frac{dL}{dt}$) maintained constant during the test, $\frac{d\Delta}{dL}$ should be constant, resulting in a constant α value.

4.5 Energy Consumption in the DENT Test and the EWF Values

In view of the significant difference in the deformation behaviour between the neck inception and the neck propagation stages in the DENT test, toughness of HDPE determined from the test may need more than single w_e to characterize. Instead of using the total energy consumption, a work-partitioning scheme is proposed here to isolate the energy consumption for each stage of the crack growth to determine the corresponding w_e values.

Several work partitioning schemes have been proposed in the past for various purposes. The first scheme proposed for polyethylene was by Mai et al. [3,8] who divided the total work of fracture into the work for fracture initiation (W_i) and the work for fracture (W_f), as shown in Fig. 4-10(a). The corresponding specific work for fracture initiation (w_i) is determined by linear regression of $\frac{W_i}{L_0\, t_0}$ to zero ligament length, which is suggested to represent some kind of material toughness that is less than w_e, but greater than the plane-strain specific EWF. Later, Karger-Kocsis et al. [4,23,24] proposed a work partitioning scheme to determine the work for yielding (W_y) and the work for the subsequent necking and tearing (W_n), as shown in Fig. 4-10(b). Through normalization by the area of the original ligament section ($L_0\, t_0$), based on the linear regression to zero ligament length, the specific work of fracture (w_f) is expressed as:

$$w_f = w_{f,y} + w_{f,n} = \left(w_{e,y} + \beta_y\, w_{p,y}\, L_o\right) + \left(w_{e,n} + \beta_p\, w_{p,n}\, L_0\right) \qquad (4.23)$$

where $w_{e,y}$, $w_{e,n}$, $w_{p,y}$, and $w_{p,n}$ are specific EWF for yielding, specific EWF for necking, specific work for plastic deformation in yielding, and specific work for plastic deformation in necking, respectively. They proposed that $w_{e,y}$ is the critical EWF for plane-strain fracture that represents generic toughness of the material [25,26]. However, little evidence was provided to support the claim.

Based on our experimental observation of the HDPE deformation in the plane-stress DENT test, the total work of fracture should be divided into two parts, to determine the EWF values for the two stages of the crack growth. The division is depicted in Fig. 4-10(c), by a vertical line at point B where the transition of the necking process occurs. With the assumption that the work for elastic deformation is negligible in comparison with the total work consumed for fracture, the work for each stage of crack growth is represented by the area under the corresponding load-displacement curve, that is, W_{ni} for the neck inception stage and W_{np} for the neck propagation stage. Crack growth length in each stage is L_i and L_p, which can be determined using Eq. (4.18).

The work of fracture is normalized by the original ligament area for the corresponding stage of crack growth. The expressions for the specific work of fracture for two stages of crack growth are:

$$w_{f,i} = W_{ni} / L_i t_0 \quad and \quad w_{f,p} = W_{np} / L_p t_0 \tag{4.24}$$

Similar to the approach proposed by Karger-Kocsis et al., each specific work of fracture is believed to contain an essential term that is independent of the ligament length and a non-essential term that is proportional to the ligament length. That is,

$$\begin{aligned} w_{f,i} &= w_{e,i} + \beta_i w_{p,i} L_i \\ w_{f,p} &= w_{e,p} + \beta_p w_{p,p} L_p \end{aligned} \tag{4.25}$$

The above equations can also be expressed in terms of η (defined as L_p / L_0) as:

$$\begin{aligned} w_{f,i} &= w_{e,i} + \beta_i w_{p,i} (1-\eta) L_0 \\ w_{f,p} &= w_{e,p} + \beta_p w_{p,p} \eta L_0 \end{aligned} \tag{4.26}$$

Using linear regression to zero ligament length, $w_{e,i}$ and $w_{e,p}$ for the HDPE in the rolling direction are 201.5 and 44.3KJ/m^2, respectively, as shown in Fig. 4-11(a). The corresponding values in the transverse direction are 144.0 and 21.7 KJ/m^2, Fig. 4-11(b). These values suggest that w_e for the HDPE is not constant during the crack growth in the DENT test, but varies with the deformation mechanisms involved in the crack growth. Value of w_e measured by the conventional method can be regarded as an average value for the fracture toughness that may actually vary during the crack growth.

It should be noted that Eq. (4.26) can be used to determine $w_{e,i}$ and $w_{e,p}$ only because the η values are insensitive to the change of the ligament length, as shown in Fig. 4-12. Otherwise, values of $w_{e,i}$ and $w_{e,p}$ have to be determined using Eq. (4.25).

The above $w_{e,i}$ and $w_{e,p}$ values did not take into account the thickness change during the crack growth, thus the values may have underestimated the fracture toughness of the HDPE. If the thickness change had been considered in the above calculation, values of $w_{e,i}$ and $w_{e,p}$ would have been bigger, with the latter being more than 3 times of the above values due to the thickness decrease from 6.25 mm to about 1.6 mm. That is, values of $w_{e,p}$ would have been 168 and 83 kJ/m^2 for specimens in the rolling and transverse directions, respectively. Nevertheless, the above analysis suggests that the specific EWF values for HDPE are not constant. Further study will be conducted to elucidate the variation of w_e during the DENT test, especially with the consideration of the change of the specimen thickness.

Discussion

The difference between $w_{e,i}$ and $w_{e,p}$ could have been caused by the difference of the deformation mechanisms involved in the crack growth. Before the transition of the load drop rate (prior to point B in Fig. 4-3(a)), the deformation mechanisms included the neck inception across the whole ligament section and the neck propagation within the distance of $L_i/2$ from the notch tips. After point B, the deformation was dominated by the neck propagation in the active plastic zone.

Mai et al. [3,8-10] suggested that the energy consumed within the FPZ can be expressed as the sum of two terms, one for the plastic deformation before the onset of necking and the other for the neck formation and fracture. Based on this concept, Mai et al. expressed w_e as [3,8-10]:

$$w_e = h\int_0^{\varepsilon^n} \sigma d\varepsilon + \int_{\varepsilon_E^n h}^{\Delta_F} \sigma_E(\Delta_1) d\Delta_1 \qquad (4.27)$$

where h is the height of the FPZ and is assumed to be constant during the test, σ and ε are the true stress and true strain in the FPZ, ε^n and ε_E^n are the true strain and engineering strain, respectively, at the onset of necking, σ_E is the engineering stress during the necking process which is a function of the crack tip opening displacement (Δ_1), and Δ_F is the displacement Δ_1 at fracture. However, Eq. (4.27) can be applied only if unstable necking occurs within the FPZ. In the case that the deformation transition occurs during the crack growth, contribution from the two terms in Eq. (4.27) to the w_e value may vary, due to the change of the deformation mechanisms.

To investigate the possible variation of the two terms in Eq. (4.27) for contributing to the w_e, value for the crack growth with stable necking is divided into two terms, $w_{e,1}$

that represents the specific EWF for the neck inception within the FPZ and $w_{e,2}$ for the specific EWF for the neck propagation in FPZ to the final fracture. With the assumption that strain within FPZ is constant, $w_{e,1}$ and $w_{e,2}$ can be expressed as:

$$w_{e,1} = h_1 \int_0^{\bar{\varepsilon}_{n,\max}} \bar{\sigma} d\bar{\varepsilon} \tag{4.28}$$

$$w_{e,2} = h_2 \int_{\bar{\varepsilon}_{n,\max}}^{\bar{\varepsilon}_f} \bar{\sigma} d\bar{\varepsilon} \tag{4.29}$$

where $\bar{\varepsilon}_{n,\max}$ is the maximum equivalent strain for the neck inception in the FPZ, $\bar{\varepsilon}_f$ the equivalent strain at the final fracture.

The total essential work of fracture consumed in the neck inception stage ($W_{e,i}$) of the DENT test should be the summation of the work for the neck inception through the entire ligament section and the work for the neck propagation within the distance $L_i/2$ from each notch tip. That is,

$$W_{e,i} = 2t_0 \left[\int_0^{L_0/2} w_{e,1} dL + \int_0^{L_i/2} w_{e,2}\, dL \right] \tag{4.30}$$

On the other hand, the total essential work of fracture consumed at the neck propagation stage ($W_{e,p}$) of the DENT test is only due to neck propagation within the central ligament section of L_p in length ($L_p = L_0 - L_i$). That is,

$$W_{e,p} = 2t_0 \int_{L_i/2}^{L_0/2} w_{e,2}\, dL \tag{4.31}$$

The specific essential work of fracture for each stage of crack growth can be determined by dividing Eqs. (4.30) and (4.31) by the corresponding ligament area for the crack growth:

$$w_{e,i} = W_{e,i} / (L_i t_0) = (1 + \frac{1}{\eta}) w_{e,1} + w_{e,2}$$

$$w_{e,p} = W_{e,p} / (L_p t_0) = w_{e,2} \qquad (4.32)$$

The above expressions indicate that $w_{e,i}$ may be much larger than $w_{e,p}$ due to the inclusion of the 1st term, $\left(1+\frac{1}{\eta}\right) w_{e,1}$, provided that difference between h_1 and h_2 is not significant.

For HDPE that shows stable necking in the DENT test, further modification is needed for the above expressions to take into account the increase of h_1 and h_2 with the crack growth. Once $\bar{\sigma}$ can be expressed explicitly as a function of $\bar{\varepsilon}$, and h_1 and h_2 as a function of L, analytical expressions for $w_{e,i}$ and $w_{e,p}$ can then be established to show their dependence on the fundamental material behaviour such as the stress variation as a function of strain. We believe that the analysis will also lead to the development of the resistance curve for the crack growth in the DENT test. This will be studied in the near future.

4.6 Conclusions

Plastic deformation and necking of HDPE under tensile loading were investigated using UT and DENT tests. Results from the UT tests suggest that the neck development in the HDPE can be divided into two stages, for neck inception and neck propagation, respectively, with fracture occurring only at the end of the neck propagation stage. The neck development in the DENT tests was similar, except that the crack growth was involved in both stages of the neck development. By quantifying the energy consumed for each stage of the neck development in the DENT tests, the specific EWF values for each stage of the crack growth were determined using linear regression to zero ligament length. The results suggest that EWF values for the two stages are different, and the EWF values may actually vary continuously as a function of the crack growth length in the DENT test.

The study also observed two interesting phenomena in the DENT tests. One is a constant crack growth speed throughout the whole fracture process, despite two distinctively different stages of the neck development. The other is a fixed fraction of the total ligament length for each stage of the neck development, which is independent of the original ligament length used in the study.

Figures

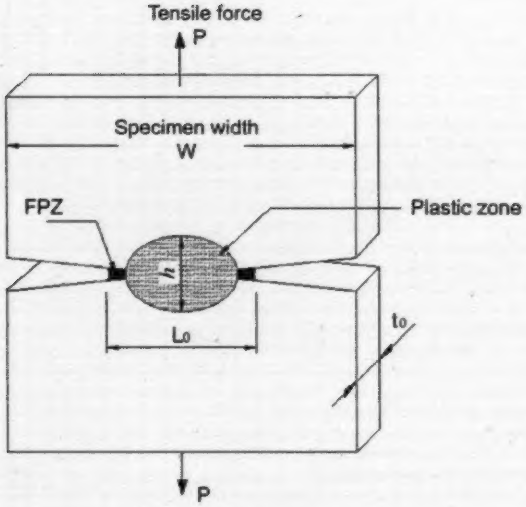
Tensile force
P
Specimen width
W
FPZ
Plastic zone
h
L_0
t_0
P

Fig. 4-1 Double-edge-notched tensile (DENT) specimen.

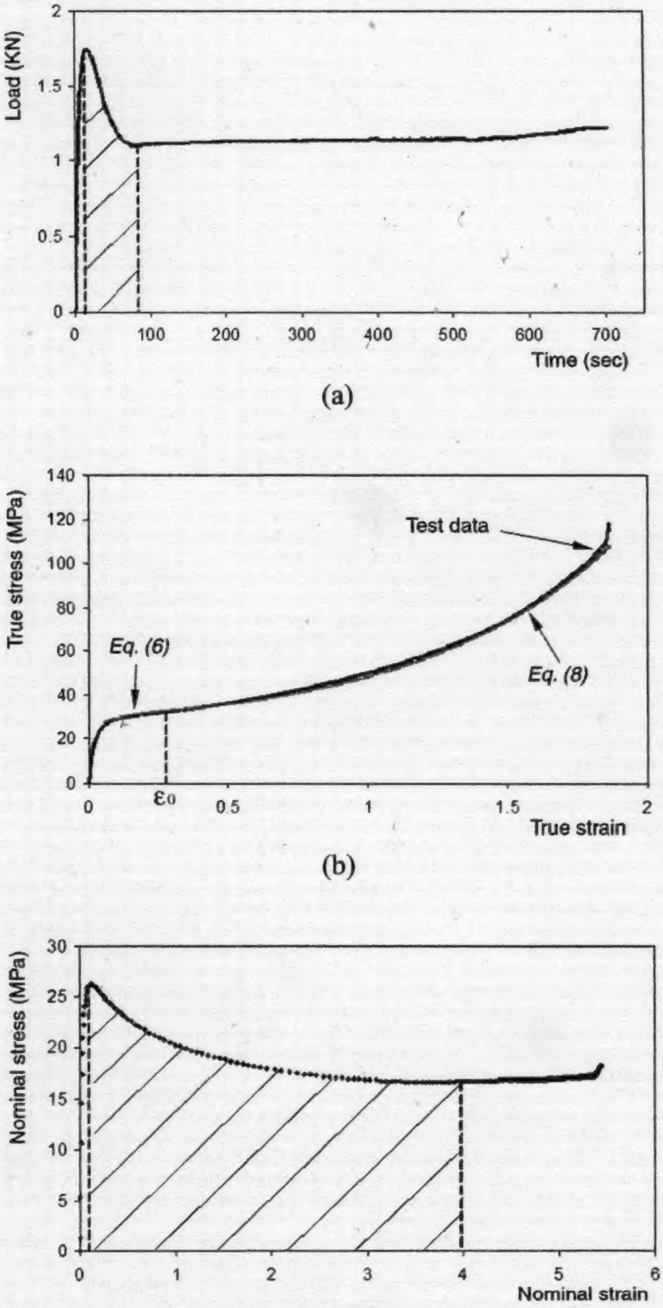

(a)

(b)

(c)

Fig. 4-2 Typical UT test results for HDPE: (a) load versus time, (b) true stress-strain curve, and (c) nominal stress-strain curve.

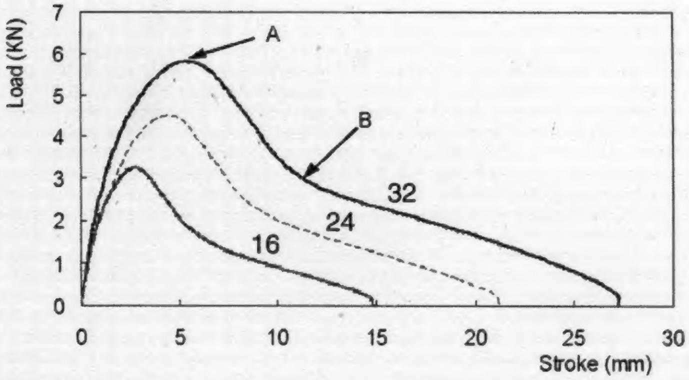

(a)

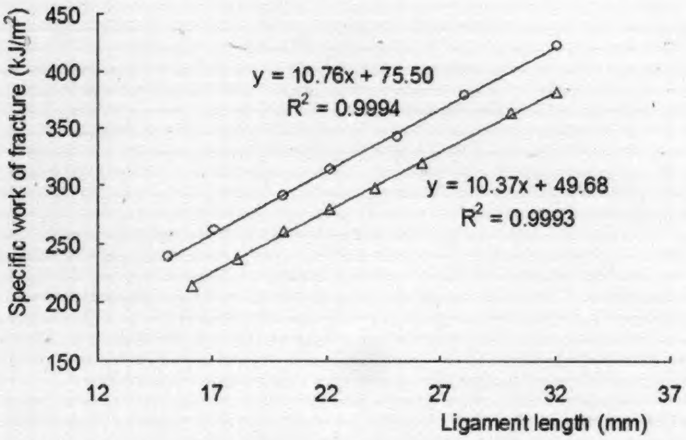

(b)

Fig. 4-3 DENT test results: (a) Typical load-displacement curves for specimens in the transverse direction (ligament length is indicated on each curve), and (b) specific work of fracture as a function of the ligament length (O for specimens in the rolling direction and △ for specimens in the transverse direction).

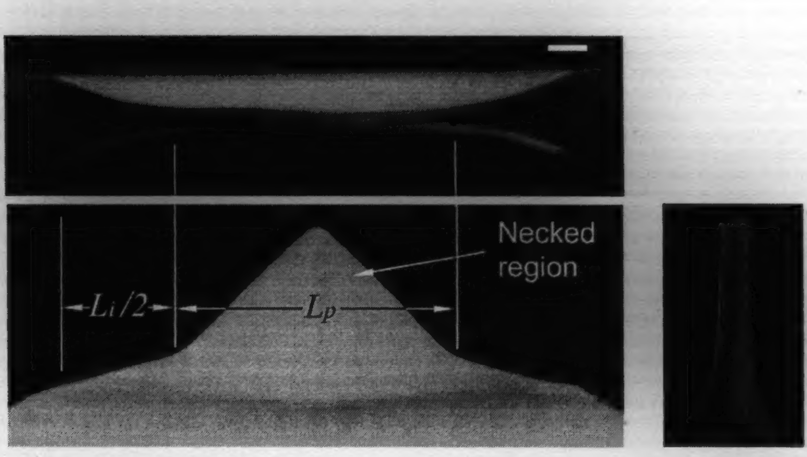
Necked region
Li/2
Lp

Fig. 4-4 Top, front and side views of a fractured DENT specimen, $L_0 = 27$ mm. Length of the white bar corresponds to 1mm.

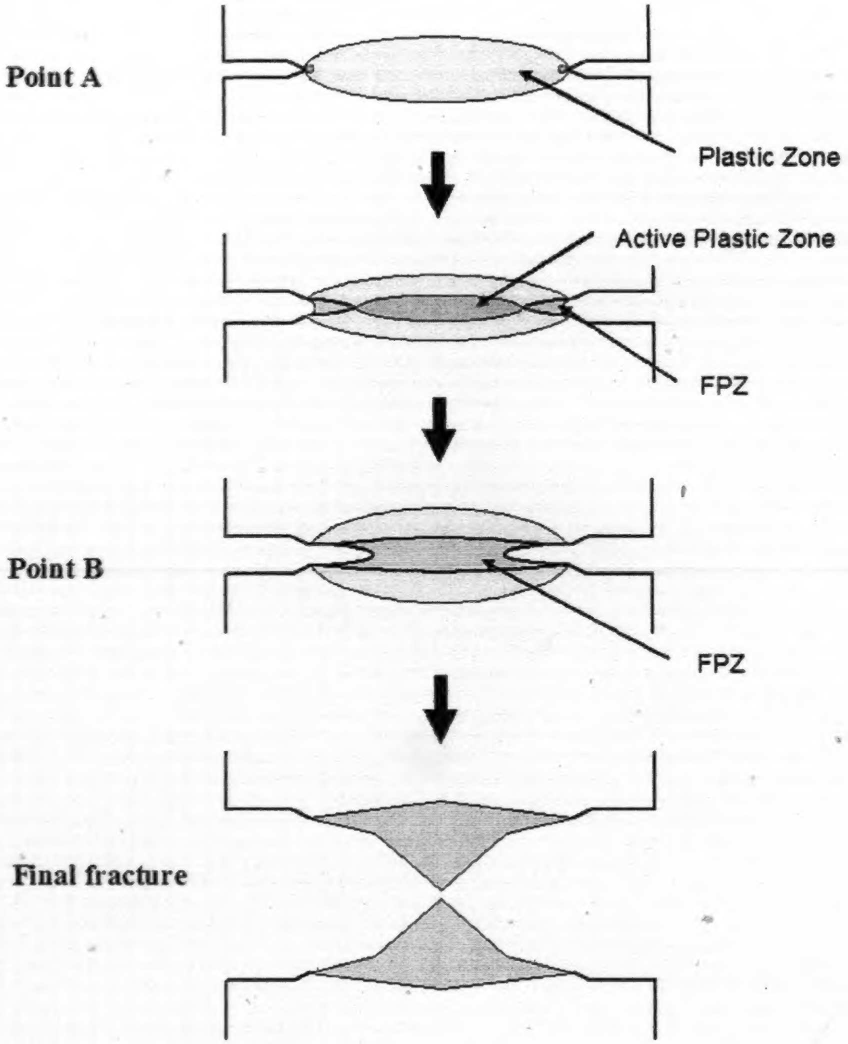
Point A
Plastic Zone
Active Plastic Zone
FPZ
Point B
FPZ
Final fracture

Fig. 4-5 Development of FPZ in the DENT test from point A of Fig. 3(a) to the final fracture.

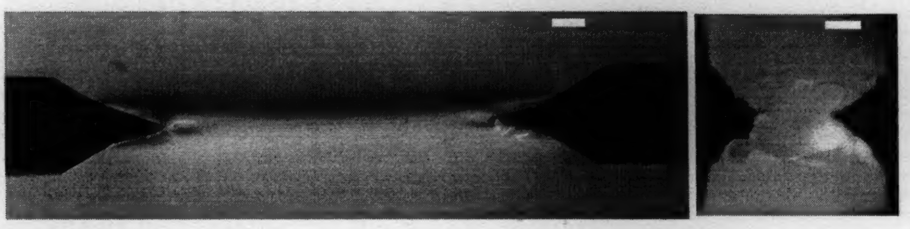

(a) (b)

Fig. 4-6 Deformation of a DENT specimen at point B of Fig. 3(a): (a) front view and (b) side view. Length of the white bar in each photograph corresponds to 1mm.

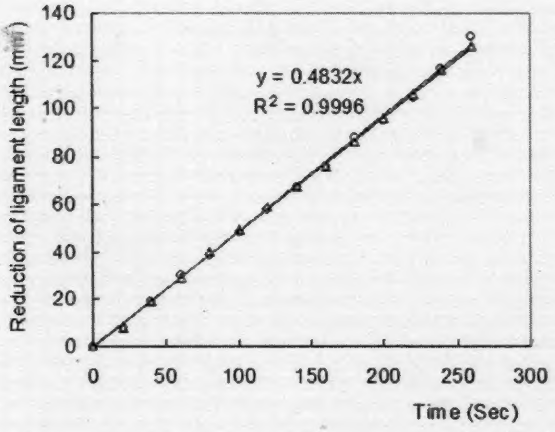

Fig. 4-7 Plots of ligament length reduction versus time from two DENT tests with L_0 = 30 mm.

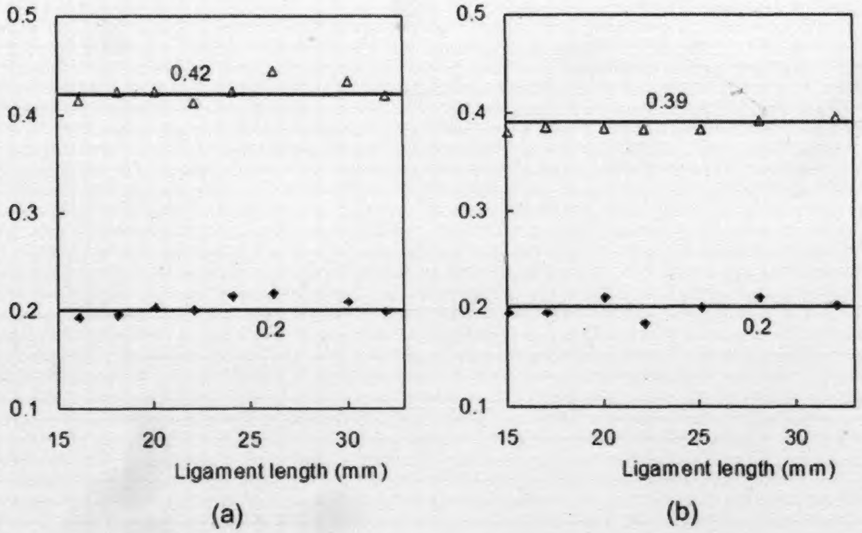

Fig. 4-8 Variation of Δ_n / Δ_f (△) and Δ_y / Δ_f (◆) of DENT specimens in (a) the rolling direction and (b) the transverse direction.

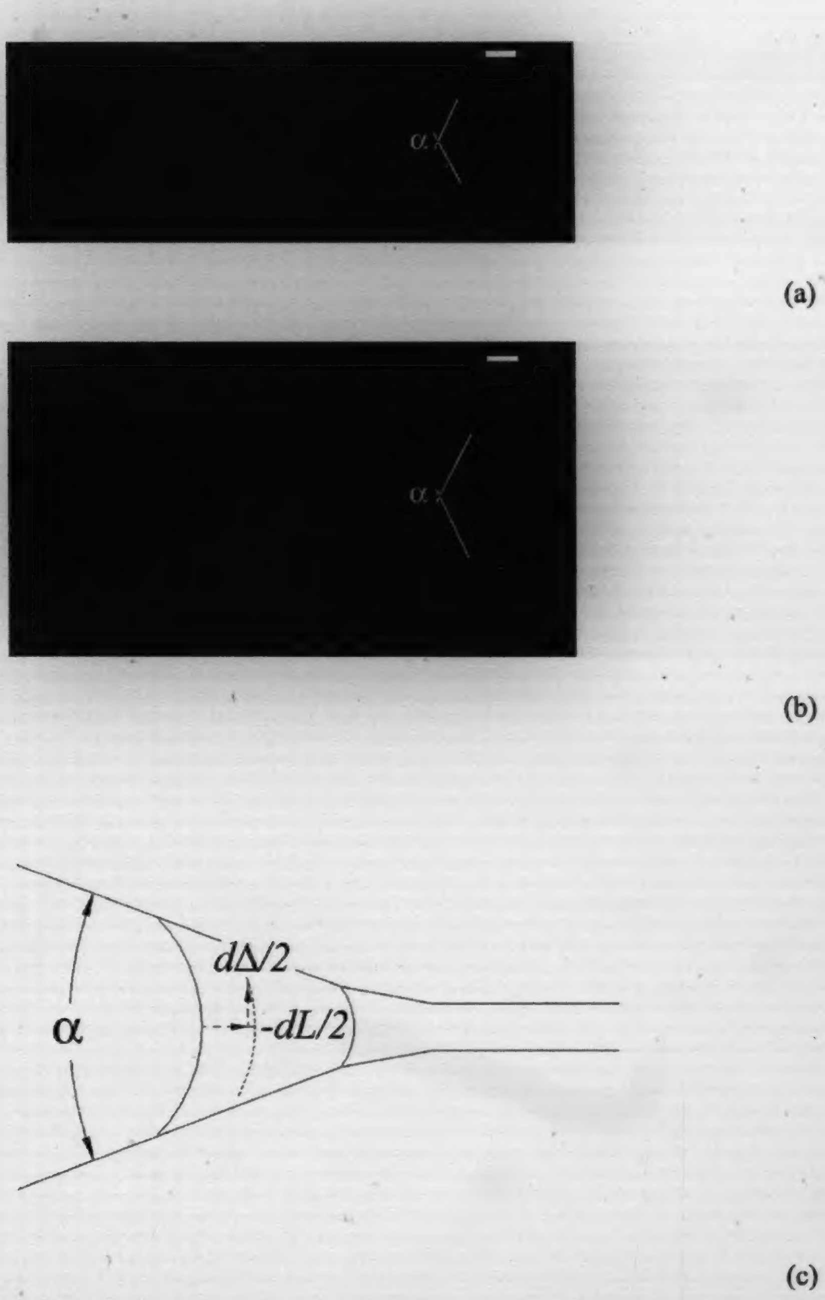

Fig. 4-9 Angle at the tip (α) of a growing crack in the DENT test: (a) α in the neck inception stage, and (b) α in the neck propagation stage, and (c) a schematic illustration of the relationship of α with displacement Δ and ligament length *L*. Length of the white bar in each photograph corresponds to 1 mm.

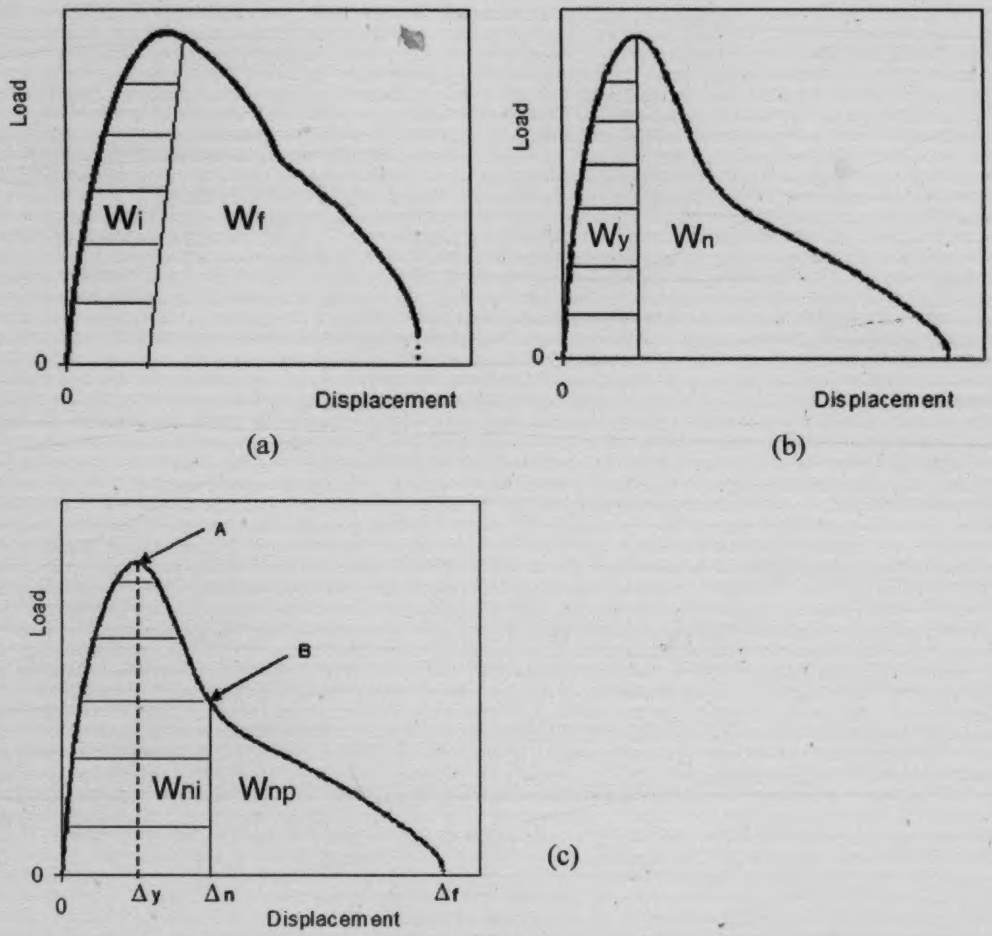

(a)

(b)

(c)

Fig. 4-10 Partitioning of the total work of fracture: (a) for fracture initiation (W_i) and fracture (W_f) [3,8], (b) for yielding (W_y) and necking and tearing (W_n) [4,23,24], and (c) for the neck inception stage (W_{ni}) and the neck propagation stage (W_{np}).

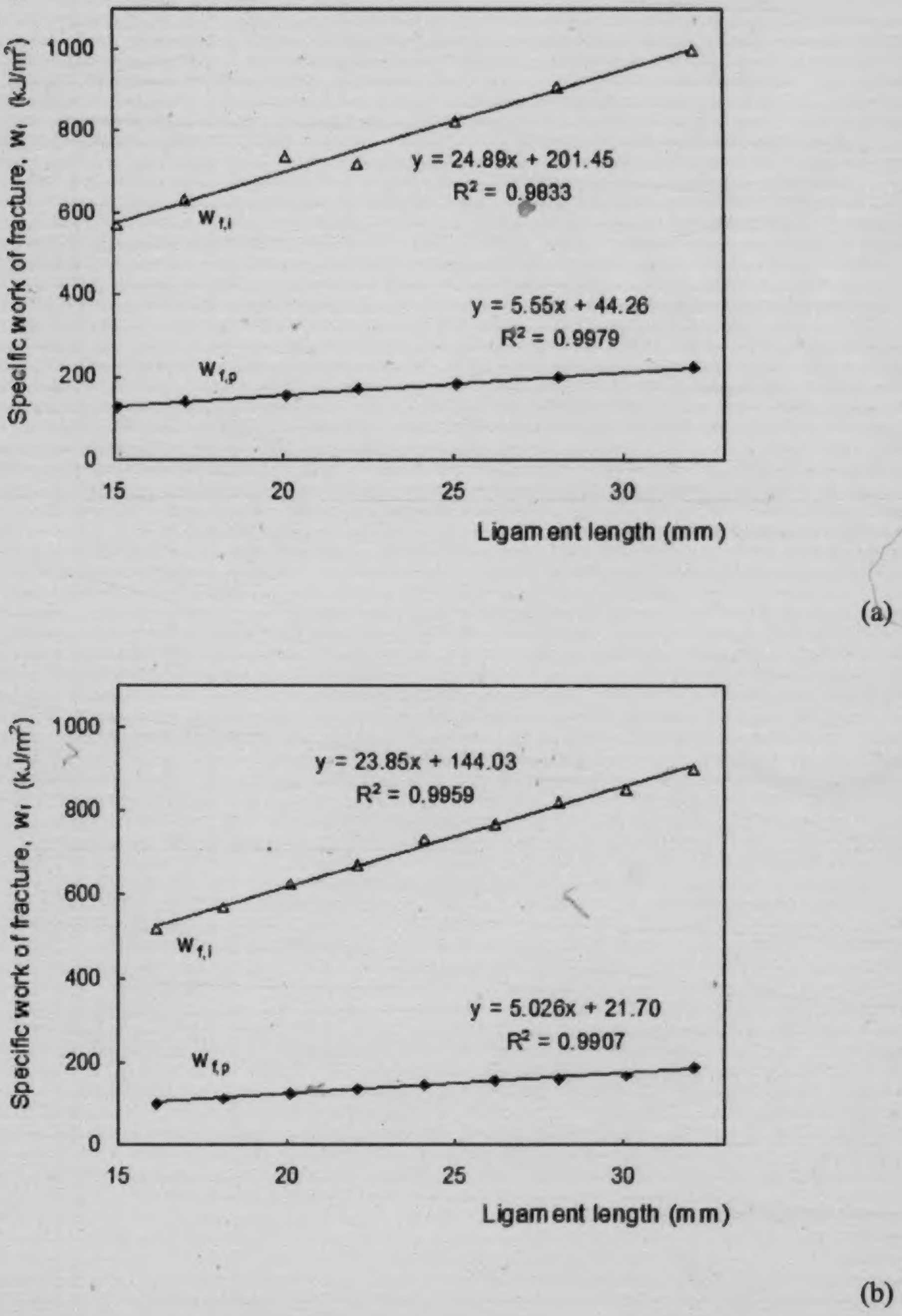

Fig. 4-11 Partitioned specific work of fracture as a function of the ligament length: (a) for specimens in the rolling direction, and (b) for specimens in the transverse direction.

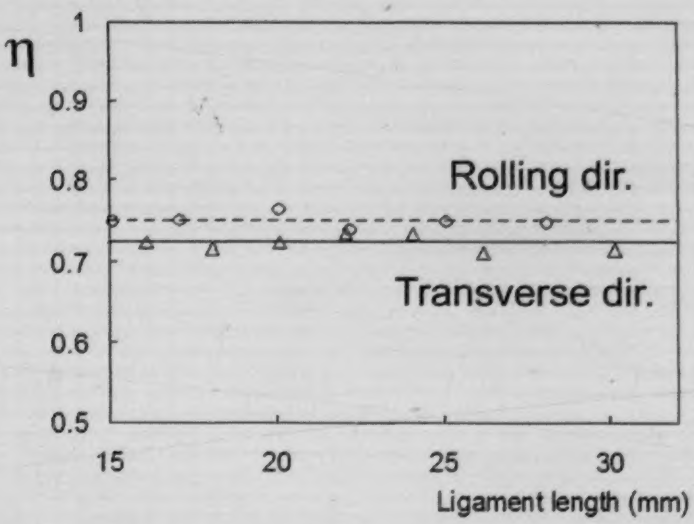

Fig. 4-12 The variation of η (defined as L_p / L_0) in the rolling (○) and the transverse (△) directions.

References

1. K.B. Broberg, *Int. J. Fract. Mech.*, **4**, 11 (1968).

2. B. Cotterell and J.K. Reddel, *Int. J. Fract.*, **13**(3), 267 (1977).

3. Y.-W. Mai and B. Cotterell, *Int. J. Fract.*, **32**(2), 105 (1986).

4. J. Karger-Kocsis, T. Czigany, and E.J. Moskala, *Polymer,* **38**(18), 4587 (1997).

5. B. Cotterell, T. Pardoen, and A.G. Atkins, *Eng. Fract. Mech.*, **72**(6 SPEC ISS), 827 (2005).

6. E. Clutton, *Fracture mechanics testing methods for polymers, adhesives and composites,* Elsevier, Kidlington, UK, 177-95 (2001).

7. A.S. Saleemi and J.A. Nairn, *Polym. Eng. Sci.*, **30**(4), 211 (1990).

8. Y.-W. Mai, B. Cotterell, R. Horlyck, and G. Vigna, *Polym. Eng. Sci.*, **27**(11), 804 (1987).

9. Y.-W. Mai, *Int. J. Mech. Sci.*, **35**(12), 995 (1993).

10. J. Wu and Y.-W. Mai, *Polym. Eng. Sci.*, **36**(18), 2275 (1996).

11. J.W. Hutchinson and K.W. Neale, *J. Mech. Phys. Solids,* **31**(5), 405 (1983).

12. C. G'sell and J.J. Jonas, *J. Mater. Sci.*, **14**(3), 583 (1979).

13. Y.-W. Mai and P. Powell, *J. Polym. Sci.* , *Part B,* **29**(7), 785 (1991).

14. H.J. Kwon and P.-Y.B. Jar, *Polym. Eng. Sci.*, **46**(10), 1428 (2006).

15. *Standard Test Method for Tensile Properties of Plastics, D 638-01, Annual Book of ASTM Standards,* ASTM.

16. R. Hill, *J. Mech. Phy. Solids,* **1**, 19 (1952).

17. J.H. Hollomon, *American Institute of Mining and Metallurgical Engineers -- Technical Publications*, 22 (1945).

18. R.J. Young and P.A. Loevll, *Introduction to Polymers*, 2nd Ed. Chapman & Hall, London (1991)

19. A. Peterlin, *J. App. Phy.*, **48**(10), 4099 (1977).

20. A. Peterlin, *Collid & Polym. Sci.*, **265**, 357 (1987).

21. B. Cotterell and Y.-W. Mai, *Advances in Fracture Research, (Fracture 81) : Proceedings of the 5th International Conference on Fracture (ICF5),* Pergamon, Oxford ; New York, 1683-1695 (1982).

22. X.-H. Chen, Y.-W. Mai, and L.-C. Zhang, *Fracture of Polymers, Composites and Adhesives,* Elsevier, Amsterdam, 175-186 (1999).

23. D.E. Mouzakis, J. Karger-Kocsis, and E.J. Moskala, *J. Mater. Sci. Lett.,* **19**(18), 1615 (2000).

24. J. Karger-Kocsis, T. Czigany, and E.J. Moskala, *Polymer,* **39**(17), 3939 (1998).

25. J. Karger-Kocsis and D.E.-. Ferrer-Balas, *Polymer Bulletin,* **46**(6), 507 (2001).

26. M.L. Maspoch, J. Gamez-Perez, and J. Karger-Kocsis, *Polymer Bulletin,* **50**(4), 279 (2003).

Chapter 5

Shear Fracture Toughness of Polymers in Shear Mode

5.1 Introduction

Toughness, a measure of resistance to fracture, has long been evaluated for polymeric materials using concepts such as critical stress intensity factor (Kc), energy release rate (Gc), J-integral (Jc), etc. Test methods developed using the first two concepts are based on linear elastic fracture mechanics (LEFM), originally developed for brittle materials, that is, they are normally used when linear elasticity dominates the deformation behaviour. J-integral only allows small plastic deformation limited to the vicinity around the crack tip. Validity of this principle, however, has been questioned when considered for toughness measurement of ductile materials in which the fracture is accompanied with significant plastic deformation. Furthermore, current methods have difficulties in measuring toughness of polymers in shear mode (mode II). The reason, as Williams [1] stated, is that most polymers have much lower toughness in tension mode (mode I) than

** A version of this chapter has been published. Polymer, Vol. 46 (26), pp. 12480-12492 (Dec. 2005).

that in shear mode (mode II). Therefore, global failure behaviour of polymers in most load-bearing structures is believed to be in mode I even though in the initiation stage the behaviour can be in a shear-like mode [2,3]. Since current testing methods are not suitable for the measurement of mode II fracture toughness, especially for ductile polymers, no quantitive experimental data are available to support the above statement. The lack of testing method to measure mode II fracture toughness also hinders the capability of failure analysis in loading scenarios that involve mainly shear forces.

A relatively new test method based on the concept of essential work of fracture (EWF) [4] was proposed to characterize fracture toughness of ductile materials. The EWF concept was firstly proposed by Broberg [5,6], and has been accepted widely as a means to quantify fracture toughness of ductile materials in the sheet form where the deformation occurs in the plane-stress conditions. Up to now, most studies using the EWF concept have been limited to mode I fracture [7,8] and some special cases of mode III fracture [9]. The EWF concept has not yet been shown the applicability to the measurement of mode II fracture toughness.

The purpose of this study is to establish a testing method, based on the EWF concept, to evaluate mode II fracture toughness of polymeric materials. The testing method uses Iosipescu loading to apply a shear force [10,11] in the middle section of the specimen where edge notches are machined on both sides of the specimen. In addition to the notches, grooves were introduced along the specimen surfaces between the notch tips to encourage fracture in a direction parallel to the shear force, thus the mode II fracture. This paper firstly provides the background knowledge for the development of the new test method for mode II fracture, and then presents some experimental evidence on the mode II fracture toughness for a rubber-modified polymer and the associated deformation behaviour.

5.2 Theoretical Analysis

5.2.1 Review of fracture analysis using classical LEFM

Most criteria for material fracture are based on LEFM, under the assumption that crack extension is governed by a specific fracture parameter, such as stress, strain, or energy. Three common criteria used in the past are maximum circumferential stress [12], maximum strain energy release rate [13], and minimum strain energy density [14]. For 2-dimensional cases, stress intensity factors (*K_1* and *K_2*) are used to estimate the stress amplification at certain point away from the crack tip, which are defined as $K_1(\theta) = \lim_{r\to 0}(\sigma_\theta\sqrt{2\pi r})$ for mode I, and $K_2(\theta) = \lim_{r\to 0}(\tau_{r\theta}\sqrt{2\pi r})$ for mode II, where σ_θ and $\tau_{r\theta}$ are circumferential normal and shear stresses, respectively, in polar coordinates in the singularity dominated zone [15]. For example, under pure tensile loading, using the criterion of maximum circumferential stress, it has been shown that $K_{1(\max)} = \sigma\sqrt{\pi a}$ along $\theta_0 = 0^\circ$ and $K_{2(\max)} = 0.38\sigma\sqrt{\pi a}$ along $\theta_0 = 70.5^\circ$ where θ_0 is the angle of crack propagation with respect to the original crack orientation, and σ the remote tensile stress. Similarly, under pure shear loading $K_{2(\max)} = 0.866\tau\sqrt{\pi a}$ along $\theta_0 = 0^\circ$ while $K_{1(\max)} = \tau\sqrt{\pi a}$ along $\theta_0 = -70.5^\circ$ where τ is the remote shear stress. Fig. 5-1 depicts the variations of the normalized $K_1(\theta)$ and $K_2(\theta)$, by dividing K_1 and K_2 by $\sigma\sqrt{\pi a}$ and $\tau\sqrt{\pi a}$, respectively, where σ and τ are the applied normal and shear stresses. The curves in Fig. 5-1 show that $K_{1(max)}$ is always greater than $K_{2(max)}$. Other conditions such as mixed tension-shear or compression-shear loadings give similar results, i.e. $K_{2(max)} < K_{1(max)}$. Therefore, in terms of stress intensity factor generated by the applied load, mode I is the preferred mode of fracture. Similar conclusions can be drawn from other fracture criteria, such as strain energy release rate, and have been verified using finite element (FE) modeling [16]. For polymers, the critical stress intensity factor in mode II (K_C^{II}) is expected to be much larger than that in mode I (K_C^{I}) [1]. Therefore, in terms of material properties (critical stress intensity factor) mode I also dominates fracture in most polymers.

It should be noted that local yielding mode can be very different from global fracture mode. Since shear strength for some polymers are lower than their tensile strength [3,17], shear type cracking can occur at the yielding and crack initiation stage [2] in cases that the ratio of the applied shear stress to tensile stress is high. However, the subsequent fracture mode may switch to mode I as the crack and the accompanied plastic deformation zone evolve. This is because most polymers have higher fracture toughness in mode II than in mode I. As a result, it is believed that the global crack development process is dominated by mode I fracture; while the crack initiation can occur in shear mode.

The LEFM approach is known to have limited validity when extensive plastic deformation is accompanied with fracture or when fracture toughness needs to be evaluated beyond the crack initiation stage. One way to overcome the problem is to use the concept of essential work of fracture (EWF) to quantify the toughness, as to be discussed in the following section.

5.2.2 Review of essential work of fracture (EWF)

The EWF concept is to extract the energy for the formation of crack surface from the total energy absorbed in the fracture process. The basic requirement of the EWF concept is that the ligament between two edge cracks, L_o in Fig. 5-2, should yield completely before fracture occurs, but the plastic deformation should be confined to regions around the ligament. Therefore, the energy absorbed for the formation of crack surface is determined by extrapolating the value of energy absorption per unit crack area to the case with zero ligament length, as the corresponding energy for plastic deformation is zero.

Using the EWF concept, work provided to fracture the specimen can be divided into two parts: (i) the work for plastically deforming the region around the ligament, which is expected to be proportional to the volume of plastic deformation zone provided that full plastic deformation is developed before crack growth commences, and (ii) the essential work required for the formation of fracture surface, which is proportional to the cross sectional area of the ligament. Value of EWF has been found to increase with the increase of specimen thickness due to localized necking [18]. The height of the plastic deformation zone, h in Fig. 5-2, on the other hand, is known to be proportional to initial ligament length, L_0. Therefore, the total work of plastic deformation, W_p^I, is proportional to L_0^2. As a result, the total work of fracture, W_f^I, can be expressed as the sum of the essential work of fracture (W_e^I), the work for the necking (W_n^I), and the work for plastic deformation (W_p^I):

$$W_f^I = W_e^I + W_n^I + W_p^I = \Gamma_0^I L_0 t_0 + \beta_1 w_n^I L_0 t_0^2 + \beta_2 w_p^I t_0 L_0^2 \qquad (5.1)$$

where t_0 is the initial thickness, Γ_0^I the specific essential work of fracture in mode I, w_n^I

the average work density for the neck forming, w_p^I the average plastic work density, and β_1 and β_2 the shape factors for the neck and the plastic deformation zone, respectively. By measuring the total work of fracture for specimens of different thickness and ligament lengths, and dividing the total work of fracture by the ligament cross sectional area ($L_o \times t_o$) using specimens with geometry depicted in Fig. 5-2, the specific work of fracture, w_f^I, can be expressed in terms of Γ_0^I, w_n^I and w_p^I as:

$$w_f^I = \Gamma_0^I + \beta_1 w_n^I t_0 + \beta_2 w_p^I L_0 = w_e^I + \beta_2 w_p^I L_0 \qquad (5.2)$$

The first term in the very right expression, w_e^I, is a combinations of Γ_0^I and $\beta_1 w_n^I t_0$, i.e. $w_e^I = \Gamma_o^I + \beta_1 w_n^I t_o$, which is known as the specific essential work of fracture for a given thickness.

The EWF concept has made a great success in measuring toughness of metal plates. As a result, interests have increased tremendously in last few years in applying the EWF concept to evaluate toughness of polymer plates . However, as mentioned earlier, its current applications are limited to mode I fracture and special cases of out-of-plane tearing (mode III fracture). Very few studies have been reported on the use of the EWF concept to characterize the toughness in mode II fracture, except one study on metallic plates [19] for which mode II is known to be the preferred mode of fracture.

5.2.3 Velocity discontinuity in plastic deformation zone

During the plastic deformation, velocity field in a plate specimen may show an abrupt change in a very narrow region, known as velocity discontinuity [20] that leads to thickening or thinning of the region. Hill [21] considered the velocity discontinuity for the neck forming process in a plate that is subjected to plane-stress deformation, and correlated the velocity discontinuity with the strain rate in the necking process. For an idealized neck that is subjected to a uniform strain rate, as shown in Fig. 5-3, with the region on the right-hand side of the neck moving at a velocity v relative to the left-hand side, the strain-rate components that are tangential and normal to the neck, i.e. $\dot{\varepsilon}_{tt}$, $\dot{\varepsilon}_{nt}$ and $\dot{\varepsilon}_{nn}$, can be expressed as:

$$\dot{\varepsilon}_{nn} = \frac{v_n}{b} = \frac{v}{b}\sin\gamma,\ \dot{\varepsilon}_{tt} = 0,\ \textbf{and}\ \dot{\varepsilon}_{nt} = \frac{v_t}{b} = \frac{v}{b}\cos\gamma \qquad (5.3)$$

where b is the width of the neck, γ the angle between velocity v and the neck, and v_n and v_t normal and tangential components of v, respectively. When pure mode II fracture occurs, the neck should have negligible width ($b \approx 0$) and the two halves in Fig. 5-3 are expected to move relative to each other in a sliding mode, i.e. $\gamma = 0$.

5.2.4 The proposed EWF analysis for mode II fracture

In addition to the limited deformation, the classical fracture mechanics does not clearly distinguish the loading mode from the deformation or fracture mode. For the three fundamental modes of fracture, i.e. tension, in-plane shear and out-of-plane tearing (i.e. mode I, II and III, respectively), the underlying assumption in the classical fracture mechanics is that the crack growth direction (at the macroscopic level) is associated with the loading mode. This, however, is well known to fail in many polymers when subjected to mode II loading, as mode I fracture usually occurs at the crack tip due to their low mode I fracture toughness value. To resolve the inconsistency between the loading mode and the fracture mode, it is proposed here that the mode of fracture should be considered independently from the mode of loading. In other words, the loading mode should not be used as a criterion to identify the fracture mode, and it is possible that a fracture mode may occur in any loading mode. Therefore, the mode II fracture toughness should be measured when mode II fracture occurs, not when mode II loading is applied.

Without the loading mode to serve as a criterion, other criteria are needed to identify the mode II fracture. At the microscopic level, the crack growth in mode II fracture is expected to be in a direction parallel to the fracture surface and perpendicular to the crack front, which is known to seldom occur in amorphous polymers. An example is given by O'Brien [22] who observed the formation of "hackles" in a resin-rich layer of fibre-reinforced polymers (FRP) that had been subjected to mode II loading. He suggested that the hackles were a result of formation and coalescence of micro-cracks that were not parallel to the global fracture surface, and concluded that the maximum shear stress does not generate the mode II fracture locally at the crack tip. Numerous other studies also showed that polymers do not deform and fracture in mode II at the microscopic level. Therefore, new criteria are proposed below for the mode II fracture, based on the fundamental concept of the expected deformation behaviour.

i) Crack orientation: In the aforementioned classical fracture mechanics [12-14], the macroscopic crack orientation in mode II fracture, when subjected to pure shear loading, should be parallel to the maximum shear stress.

ii) Development of fracture process zone (FPZ): The conventional definition of mode II fracture in a double-edge-notched specimen is that the fracture process should occur across the entire section between the two notches, i.e. the fracture process zone (FPZ) should be formed in the entire section prior to the crack evolvement, as shown in Fig. 5-4.

This is different from the crack development in mode I fracture, as shown in Fig. 5-2 in which the FPZs are limited at the notch tips [7,23] and progress towards each other as the crack grows.

iii) Work of fracture: Since the FPZ is formed across the entire ligament section uniformly, size of the plastic deformation zone should also be uniform in the ligament section, as shown in Fig. 5-4, and the total work for the plastic deformation, W_p^{II}, should be proportional to the cross sectional area of the ligament, $L_0 t_0$, instead of $L_0^2 t_0$ for the mode I fracture (Fig. 5-1). Under this condition, the total work of fracture, W_f^{II}, for the mode II fracture can be expressed as:

$$W_f^{II} = W_e^{II} + W_p^{II} = w_e^{II} L_0 t_0 + \beta_3 w_p^{II} L_0 t_0 \qquad (5.4)$$

where W_e^{II} is the essential work of fracture, w_e^{II} the specific essential work of fracture for a given thickness, β_3 a shape factor, w_p^{II} the average plastic work density, and superscript "*II*" represents mode II fracture. The corresponding specific work of fracture, w_f^{II}, is:

$$w_f^{II} = w_e^{II} + \beta_3 w_p^{II} \qquad (5.5)$$

It should be noted that there is a possibility for w_f^{II} to be dependent on the specimen dimensions, similar to that shown by Fig. 5-2. Experiments have been conducted to elucidate such dependence, and the results will be shown later in this paper.

Eqs. (5.2) and (5.5) indicate that a significant difference exists between the expressions of the specific work of fracture w_f in mode I and mode II, especially as a function of the ligament length L_0. For the mode I fracture, the specific work of fracture

w_f^I is proportional to the ligament length L_0; but for the mode II fracture, w_f^{II} should be independent of L_0. Experimental study, as to be shown later in this paper, has been carried out to verify this difference.

5.3 Experimental Study

5.3.1 Material

Poly(acrylonitrile-butadiene-styrene) (ABS) that is known to have higher fracture toughness in mode II than in mode I was selected for the study. The ABS used was an extrusion grade in the plate form with nominal thickness of 6 mm produced by Chi-Mei in Taiwan as the commercial name ABS PA-747F which is synthesized through emulsion polymerization. The content of Styrene-acrylonitrile(SAN) is 83% and the rubber particles have sizes in a range from 0.05 to 5 μm with the content of 17%. Preliminary tensile tests showed that the plates are isotropic in mechanical properties, with tensile strength close to 48 MPa and Young's Modulus 2.5 GPa.

5.3.2 Mode I fracture toughness

The EWF test method used in references [4,24,25] was adopted to measure the w_f^I value. Dimensions of double-edge-notched (DEN) specimens were 90 mm (width, W) x 270 *mm* (total length, L) with varying thickness and ligament length. Tests were conducted using an Instron universal testing machine at a crosshead speed of 2.5 *mm/min*. Test details are described in Appendix A.

5.3.3 Mode II fracture toughness

Several test devices were considered to apply the shear force to ABS, including off-axis tensile test [26], Arcan test [27] and Iosipescu shear test [28]. Among them, the Iosipescu test has relatively good precision in applying uniform pure shear force across the central cross section between the notches [29], thus being chosen for this study. Both sides of the specimens were bonded with aluminium tabs to minimize flexural deformation during the test.

The commonly used notch angles for Iosipescu specimens are either 90° or 110° [30,31] both of which were found to be improper for our test because these specimens could not avoid the generation of a secondary crack on the notch faces (details to be shown in Section 5.4). Instead, a reduced notch angle of 60° was selected for our study, and introduced to DEN specimens of 17 *mm* (W) x 90 *mm* (L) with varying ligament length and specimen thickness. One study that used Iosipescu loading to measure mode II fracture toughness [32] chose single-edge-notched (SEN) specimen and J-integral method. However, due to asymmetric fracture behaviour in the SEN specimen the EWF concept cannot be applied to determine the fracture toughness.

In our study, V-shaped grooves were introduced to some of the specimens along the ligament section between the notch tips to enhance the alignment of the relative velocity with the direction of the ligament length. The Iosipescu device and the DEN specimen without the grooves are shown in Fig. 5-5(a) and the specimen with grooves in Fig. 5-5(b). Again, Instron universal testing machine at a cross-head speed of 2.5 *mm/min* was used for the test. Fracture behaviour was recorded using a digital video camera with a micro-zoom lens.

5.3.4 Fractography

A scanning electron microscope (SEM, JEOL JSM-6301F), a digital video camera, and a profile projector (Mitutoyo PH-3500) were used to record the fracture behaviour. Each specimen of interest for SEM was mounted on a sample holder and coated with a thin layer of gold just before the examination.

5.4 Results and Discussion

5.4.1 Mode I fracture toughness

Preliminary results from mode I EWF test are summarized in Fig. 5-6, using specimens with ligament length in the range from 3 to 30 *mm* and thickness 6 *mm*. The data show a transition from pure plane-stress condition to mixed plane-stress and plane-strain condition at the ligament length around 8 mm, as suggested in ref. [33]. For ligament length in the range from 8 to 25 mm, the data show a linear variation between the specific work of fracture (w_f^I) and ligament length. Above 25 mm, the change of w_f^I and ligament length no longer followed a linear relationship. Therefore, the ligament lengths in the range from 8 to 25 mm were selected to measure the specific essential work of fracture (w_e^I) in the plane-stress condition. Fig. 5-6 suggests that the w_e^I for ABS is 12.7 kJ/m^2.

It has been recommended [4] that the range of ligament length L_0 for metals when subjected to the plane-stress condition should be:

$$(3-5)t \le L_0 \le \min(\frac{W}{3}, 2r_p) \qquad (5.6)$$

where t is specimen thickness, W specimen width, and $2r_p$ the plastic zone size that can be determined by:

$$2r_p = \frac{Ew_e^I}{\pi\sigma_y^2} \tag{5.7}$$

where E is the Young's modulus and σ_y the uni-axial tensile yield strength. By substituting values of E, σ_y and w_e^I for ABS into Eq. (5.7), $2r_p$ was found to be around 4.0 mm that is much shorter than $\frac{W}{3}$ (around 30 mm for our specimens). Therefore, the condition of $\min\left(\frac{W}{3}, 2r_p\right)$ to ensure the plane-stress condition seems to be too restrictive for ABS. Our speculation is consistent with that reported for polyethylene terephthalate glycol (PETG) [34].

The data in Fig. 5-6 also suggest that to ensure the plane-stress condition, the upper limit of ligament length for ABS specimens should be around 25 *mm* that is slightly less than the other option of the upper limit, $W/3$ (30 *mm* for our specimens). Based on results shown in Fig. 5-6, we decided to use ligament lengths in the range from 8 to 24 *mm* for the follow-up EWF tests to determine toughness in mode I fracture. For the follow-up tests, at least 5 specimens were used for each ligament length at an increment of 2 *mm*, to ensure repeatability of the test results.

Fig. 5-7 presents results of the follow-up tests, in which specific work of fracture for mode I (w_f^I) is plotted as a function of the ligament length, from ABS specimens of various thickness. The w_f^I values show very good linear relationship with the change of ligament length, with little dependence on the thickness change from 2 to 6 *mm*. As shown in Fig. 5-7, the estimated w_e^l value is 13.1 *kJ/m*^{2}. The results suggest that in the thickness range from 2 to 6 *mm*, specimen thickness has little effect on the w_f^l values. Therefore, w_n^l in Eq. (5.2) must be very small, implying that the necking effect in mode I fracture of these specimens is negligible.

5.4.2 Iosipescu test on specimens without grooves

When loaded in the Iosipescu device, specimens without the grooves developed the first pair of cracks from the notch tips, which grew in a direction that was about 25° from the centre line connecting the notch tips, as shown in the circle of Fig. 5-8(a). The cracks opened up and grew only for a very short distance. Then, a second pair of cracks were generated nearby the tip of the first pair cracks, as shown in Fig. 5-8(b), in a direction of about 70° from the centre line. Further loading resulted in the growth of the second pair of cracks. It should be noted that the crack development in Fig. 5-8 occurred around both notch tips but in the opposite direction. The asymmetric growth of the two cracks resulted in a rolling movement that eventually formed a cylinder with diameter proportional to the original ligament length, as shown in Fig. 5-8(c). Fig. 5-8(d) is the SEM micrograph of the fractured surface formed by the growth of the second crack as pointed by the arrow in Fig. 5-8(c).

The above crack development process is also reflected in the load-displacement curve from the Iosipescu test. Fig. 5-9 shows a typical load-displacement curve from ABS specimens without the grooves, in which point A indicates the position where the first pair of cracks occurred (Fig. 5-8(a)) and point B the position for the second pair of cracks (Fig. 5-8(b)). Generation of the cracks has caused the load drop, with the rate of load drop induced by the first pair of cracks being much faster than that by the second pair of cracks.

The generation of the first pair of cracks caused a sharp drop of the load, from point A to point B in Fig. 5-9. The first pair of cracks are "shear–like cracks" that were also observed by Husaini et al. [2]. Formation of the first pair of cracks can be explained by the competition of maximum principal stress and maximum shear stress [17]. The corresponding critical stresses are derived from the yielding theories (von-Mises or Tresca for ductile materials), with the concept that material yields and crack initiation occurs when either stress components reaches the critical value. It should be noted that after the crack is initiated, we believe that the mode of the following fracture process is independent of that for the crack initiation. This is based on the concept that in the crack initiation stage the fracture toughness is yet to be involved in the fracture process, and that the crack initiation is governed by the critical yielding stresses. In the following crack propagation stage, after the full development of FPZ, the fracture toughness plays a major role in the mode for the crack development. At this stage, difference of fracture toughness in the two modes of fracture is a critical factor to determine the mode of crack development [35]. It should be pointed out that crack development in the initiation stage could be very different from that in the following crack growth stage. Since the crack development can be divided into two stages, the energy consumed in the crack initiation stage should not be included in the energy consumption for the crack growth that is used to determine the fracture toughness. At present, however, mode transition in the crack development has not been thoroughly investigated, with very few parameters, such as stress triaxiality, being considered to be the cause of the mode transition [35].

Since the second pair of cracks are clearly visible in the fracture process presented in Fig. 5-8, their bifurcation angle can be used to determine the fracture mode. In our Iosipescu tests using specimens without grooves, the growth direction for the second pair of cracks is at 70° with respect to the centre line, which suggests that the second pair of cracks were generated in mode I fracture, surrounded by plastic deformation and possibly necking. The fractured surface by the second crack in Fig. 5-8(d) also shows slanted torn structures that are typical in mode I fracture of ABS. Therefore, specific essential work of fracture for mode I, w_e^I, can be determined from the Iosipescu test using the EWF concept, provided that the fracture energy for the second pair of cracks can be plotted as a function of the length of the second pair of cracks. However, in our attempt to determine w_e^I value from the Iosipescu test shown in Fig. 5-8, existence of the first pair of cracks was ignored. This was deemed acceptable as the length of the first pair of cracks is very short and the corresponding fracture energy (the triangular area *OAB* in Fig. 5-9) is only a very small portion of the total fracture energy (the total area under the curve). As a result, the existence of the first pair of cracks should have little influence on the determination of the w_e^I value.

Based on the above concept, the specific work of fracture in mode I (w_f^I) for these Iosipescu tests was plotted against the arc length of the second pair of cracks, and the results are presented in Fig. 5-10. It should be noted that the crack length used in Fig. 5-10 is the true crack length for the second pair of cracks, which is about 2.5 times of the ligament length. The corresponding w_e^I value is 13.4 kJ/m^2 that is very close to the w_e^I value measured from DEN specimens under tension, 13.1 kJ/m^2. Slope of the curve

(βw_p) in Fig. 5-10 is 8.6 kJ/m^3 that is much larger than that in Fig. 5-7, 1.3 kJ/m^3, which suggests that the plastic work density generated in the DEN specimen in Iosipescu test is much higher than that generated in the tensile test. The steep slope in Fig. 5-10, however, yields high sensitivity of the w_e^I value to possible experimental errors. Therefore, the Iosipescu test is not recommended for the measurement of w_e^I.

5.4.3 Iosipescu test on specimens with grooves

V-shaped grooves, as shown in Fig. 5-5(b), were introduced to the specimen to generate velocity discontinuity along the ligament length direction so that the crack development is forced to be along the direction of the maximum shear stress. As stated in Section 2.4, deformation in the mode II fracture is expected to occur in the whole ligament section before crack growth commences. However, the initial cracking in the grooved specimens is similar to that shown in Fig. 5-8(a), i.e. at an angle about 25° with respect to the direction of the ligament length, but resulting in much shorter crack length. This was probably due to the increase of growth resistance caused by the increase of specimen thickness in the crack growth direction. As discussed earlier, the initial cracking cannot be categorized as pure mode II fracture, and the consumed energy at this stage should not be included in the calculation of mode II fracture toughness. However, the second pair of cracks that were observed in the specimens without grooves, as shown in Fig. 5-8(b), did not occur in the grooved specimens. Instead, an array of multiple, short cracks were generated along the whole ligament section, as shown in Fig. 5-11(a). With further deformation, as shown in Fig. 5-11(b), the short cracks were connected to form the fracture surfaces along the ligament length. It should be noted that at the stage shown in

Fig. 5-11(b), the two halves of the specimen were still connected through some fibrils that were eventually broken after extensive elongation.

A typical load-displacement curve from the grooved DEN specimens is presented in Fig. 5-12 in which point A indicates the loading level for the initiation of the first pair of cracks. Advancement of the first pair of cracks stopped at point B. In the plateau region from points B to C, an array of short cracks started. Coalescence of these short cracks was reflected by a steady drop of the load in the section from C to D in Fig. 5-12. The section after point D was generated during the extensive elongation of the remaining fibrils, which was a deformation process after the main crack was formed, and involved mainly fibril fracture in mode I. Therefore, the deformation in the section after point D of Fig. 5-12 should be classified as local mode I fracture.

Based on the experimental observation, as presented in Fig. 5-11, the fracture development from points B to D in Fig. 5-12 was in the direction of the maximum shear stress with the crack evolving simultaneously in the whole ligament section, which satisfies the first and second criteria for mode II fracture (crack orientation and development of FPZ, respectively). The remaining criterion that needs to be satisfied is the work of fracture, as expressed by Eq. (5.4), that is, the specific work of fracture should not be a function of ligament length. This, however, requires the extraction of energy consumption from crack growth in this part of curve.

As a first attempt to extract energy consumption for mode II fracture from the Iosipescu test using the grooved DEN specimens, the energy consumption before point B in Fig. 5-12 was included in the calculation for the specific work of fracture, w_f. This was deemed acceptable because the curve in Fig. 5-12 suggests that the energy consumed before point B (0-A-B-0' of which point O' is slightly to the right of point O to take into account the plastic deformation) is a very small fraction of the energy consumed in the test. On the other hand, the energy consumed after point D in Fig. 5-12, which is for fibril fracture in mode I, is significant and should be excluded from the calculation for w_f. Fig. 5-13 compares w_f values calculated using the grooved specimens. Specimens with three different groove depths, labelled in terms of the remaining specimen thickness (to be named groove thickness in the rest of the paper) were used for the comparison. Fig. 5-13(a), based on the total area under the curve, shows much more scattering than Fig. 5-13(b) that has excluded the area after point D in Fig. 5-12. The average w_f values for the groove thickness of 3 *mm*, 3.5 *mm* and 4 *mm* are in Fig. 5-13(a) are 57.0, 60.1 and 67.9 *kJ/m*^{2}, with the standard deviation of 2.93, 4.10 and 1.55 *kJ/m*^{2}, while those in Fig. 5-13(b) are 49.9, 54.2 and 68.6, with the standard deviation 0.98, 1.55 and 1.80 *kJ/m*^{2}, respectively. Fig. 5-13(b) also indicates that with the exclusion of the area after point D in Fig. 5-12, the w_f values become relatively independent of the ligament length, which is consistent with the prediction by Eq. (5.5). The results in Fig. 5-13 suggest that the above approach for extraction of energy consumption for mode II fracture meets the third criterion given in Section 2.4.

Supporting evidence for mode II fracture was obtained by examining plastic deformation in the grooved specimens. All of the specimens for Fig. 5-13 show constrained plastic deformation that is limited to regions around the ligament section, with no indication of any size change (d in Fig. 5-4) with the variation of the ligament length. However, w_f value varies with the change of groove thickness, as shown in Fig. 5-13(b), possibly due to the deformation energy induced by the generation of the first pair of cracks. Process to minimise this part of energy will be discussed later in this section.

Further investigation of the generation of the first pair of cracks was conducted through microscopy. A typical SEM micrograph of fracture surface from specimens for Fig. 5-13 is shown in Fig. 5-14(a). The half-elliptical shape on the right side of the micrograph that shows crack growing into the fracture surface represents the first pair of cracks generated in the Iosipescu test. The remaining part of the fracture surface is relatively flat, containing fibrils that fractured in the last stage of the test, i.e. after point D in Fig. 5-12. The half-elliptical shape in Fig. 5-14(a) was possibly caused by the toughness variation due to the change of the deformation conditions, that is, from plane-stress-biased deformation in regions close to the edge towards the plane-strain-biased in the centre. As known in the classical mechanics [36], material deformation in a plane-stress condition yields higher toughness than that in a plane-strain condition [37]. Therefore, the growth of the first crack is deepest in the centre (along A-A in Fig. 5-14(a)) due to the apparent low toughness in the region, and the depth is gradually reduced towards the edges due to the increase in toughness, which leads to the formation of an elliptical contour of the fracture surface.

To examine the fracture surface topography, some of the specimens were cut along the centre line (A-A in Fig. 5-14(a)) and viewed using a Mitutoyo profile projector, as shown in Figs. 5-14(b) and 5-14(c) for groove thickness of 4 and 2 mm, respectively. The two photographs clearly suggest that the decrease of groove thickness from 4 to 2 *mm* has significantly reduced the growth depth of the first crack, labelled d_h in Fig. 5-14(b). This can also be understood from the viewpoint of transition from plane-strain to plane-stress conditions, that is, by decreasing the groove thickness, deformation in the central region is increasingly dominated by the plane-stress condition, hence raising the toughness and reducing the depth of penetration by the crack growth.

Further support to the above concept is shown in Fig. 5-15 in which variation of the penetration depth (d_h in Fig. 5-14(b)) is plotted as a function of ligament length (Fig. 5-15(a)) and groove thickness (Fig. 5-15(b)). The penetration depth in Fig. 5-15(a) is almost constant with the average at 0.76 *mm* and the standard deviation of 0.03 *mm*, while it increases with groove thickness in Fig. 5-15(b). The figures clearly show that the penetration depth is independent of the ligament length, but dependent on the groove thickness in an almost linear fashion. Therefore, by extrapolating the groove thickness to zero, plane-stress condition should prevail and penetration depth by the growth of the first pair of cracks should be minimised. Through this minimization process, it can be postulated that the energy consumption caused by the first pair of cracks becomes negligible for the calculation of w_f.

It may be wondered why the increase of w_f with the increase of the groove thickness (Fig. 5-13(b)) is much larger than the corresponding increase of the fracture energy for the generation of the first pair of cracks (area O-A-B-O' in Fig. 5-12). This can be understood through the components that contribute to the fracture displacement, Δ_f, defined as the displacement at point D of Fig. 5-12. Fig. 5-16 shows Δ_f as a linear function of the groove thickness. We believe that Δ_f comes from 3 components:

$$\Delta_f = \Delta_{FPZ} + \Delta_f^p + \Delta_f^e \qquad (5.8)$$

where Δ_{FPZ} is the displacement responsible for the formation of the FPZ, Δ_f^p for the plastic deformation zone and Δ^e_f for the corresponding elastic deformation. Values of Δ_{FPZ} is expected to be constant, independent of the grove thickness. Value of Δ^e_f is expected to be very small, of which variation with the change of groove thickness should be negligible. Therefore, the only component that dominates the change of Δ_f with groove thickness is Δ^P_f. With the assumption of uniform distribution of the strain inside the plastic deformation zone, the critical fracture strain in the zone (γ_f) can be expressed as the ratio of Δ^P_f to the width of the plastic deformation zone (d_P):

$$\gamma_f = \Delta^P_f / d_P \tag{5.9}$$

Since γ_f is expected to be constant in the range of thickness studied here, value of d_P is expected to increase with the increase of Δ^P_f. As a result, the linear increase of Δ_f (thus Δ^P_f) with the increase of the groove thickness, as shown in Fig. 5-16, suggests that the width of the plastic deformation zone, d_P, is proportional to the groove thickness. In other words, the role of groove thickness in the specific work of fracture in mode II (w^{II}_f) is similar to the role of the ligament length in mode I (Eq. (5.2)).

By excluding the energy consumed after point D in Fig. 5-12 as well as by extrapolating the corresponding specific work of fracture w_f to a value for zero groove thickness, in order to minimize the energy consumption contributed from the generation of the first pair of cracks and that from the plastic deformation zone, the specific essential work of fracture w_e should be for the generation of shear crack, thus representing w^{II}_e, i.e. the essential work of fracture in mode II.

Fig. 5-17 presents the plot using the above approach, from specimens of the same ligament length (5 *mm*), machined by a cutter with cutting angle of 60° and thickness of 25 *mm*. Linear extrapolation of the data to zero groove thickness yields w_e^{II} value of 32.3 kJ/m^2. It should be noted that deformation of these specimens met all 3 criteria defined in Section 2.4 for mode II fracture. Compared to the w_e^{I} value of 13.1 kJ/m^2 (Fig. 5-7), fracture toughness of ABS in mode II is about 2.5 times of that in mode I.

Following the report by the TC4 Committee of the European Structural Integrity Society (ESIS) [25] that the w_e^{I} value might be affected by the notch shape, additional specimens were prepared for the Iosipescu tests using a cutter of 45° in angle and 20 *mm* in thickness. Ligament length for these specimens was the same as that for Fig. 5-17, i.e. 5 *mm*. Results from the new set of specimens are presented in Fig. 5-18, with w_e^{II} value of 31.2 kJ/m^2 that is very close to that given in Fig. 5-17. Although further investigation may be needed before drawing a firm conclusion on the methodology for the w_e^{II} measurement, the two sets of data indicate that the change of groove angle and notch angle, both from 60° to 45°, did not have any noticeable effect on the deduced w_e^{II} value. It should be noted that although the same groove thickness and ligament length were used, the two sets of specimens for Figs. 5-17 and 5-18 showed different deflection stiffness. As a result, the data should not be grouped together to determine the value of w_e^{II}.

Some additional DEN specimens were prepared using a cutter of 90° in angle and 25 *mm* in thickness. But these specimens showed additional tensile cracks that were generated on the face of the notch, causing the increase of the energy consumption for the mode I fracture, thus could not be used to determine w_e^{II}.

5.4.4 Discussion

Shear fracture process

As shown in Figs. 5-14(d) and 5-8(d), the fracture surface of Iosipescu specimen with grooves shows similar features as those without grooves, but the former are slanted more closely in parallel to the fracture surface. Based on the observation of fracture development (Fig. 5-11) and surface topography (Fig. 5-14), the fracture process for the grooved DEN specimens in shear loading is proposed as follows. Firstly, an array of voids are formed along the grooves, each growing in a direction perpendicular to the maximum principal stresses, as shown in Fig. 5-19(a). As the deformation increases, the voids rotate and become almost parallel to the direction of cross-head movement (horizontal in Fig. 5-19). The cracks then emanate from the tips of the voids as shown in Fig. 5-19(b). Because of the geometric constraint by the grooves, the deformation occurs in a narrow region with the final fracture aligned with the grooves, as depicted in Fig. 5-19(c) that shows half of a fractured specimen. The similarity of Figs. 5-19(c) and 5-14(a) demonstrates the plausibility of using the proposed fracture process to explain the orientation of the slanted feature that is nearly parallel to the fracture surface.

EWF in Mode II

Based on the above results, we propose a modification of Eq. (5.5) using the same concept for Eq. (5.2), to account for the dependence of w_f^{II} on the groove thickness:

$$w_f^{II} = w_e^{II} + \beta_4 w_p^{II} t_0 \qquad (5.10)$$

where β_4 is a shape factor, t_0 the groove thickness and w_p^{II} the average plastic work density in mode II fracture. The above expression satisfies the requirement of the 3rd criterion for mode II fracture, i.e. the specific work of fracture being independent of the ligament length. Both Eqs. (5.2) and (5.10) show the thickness effect, but on different mechanisms. The change of specimen thickness in Eq. (5.2) affects the energy consumption for necking; while that in Eq. (5.10) affects the energy consumption for plastic deformation. Eq. (5.10) suggests that groove thickness is the main factor that affects the measured w_f^{II} value in the Iosipescu test, similar to the effect of ligament length L_0 in the DEN tensile test.

Value of w_e^{II} for mode II fracture of ABS was found to be around 32.3 *kJ/m*^{2} that is about 2.5 times of the w_e^I value for mode I fracture. Such significant difference of toughness between the two fracture modes is believed to be the driving force for mode I dominating the fracture in products made of ABS.

5.5 Conclusions

A series of double-edge-notched Iosipescu tests were conducted to search for a means to determine the essential work of fracture in mode II, w_e^{II}. Three criteria based on physical shear deformation of polymers are proposed to identify the mode II fracture, and a test methodology based on Iosipescu device using DEN specimens with side grooves is proposed to quantify w_e^{II}.

The new test methodology yields w_e^{II} value of 32.3 *kJ/m*^{2} for ABS, which is about 2.5 times of the corresponding value for mode I fracture, w_e^I, of 13.1 *kJ/m*^{2}. The significant difference of toughness is believed to be the driving force for the mode I fracture to dominate the deformation in ABS products.

In contrast to the specific work of fracture in mode I, w_f^I, the mode II counterpart, w_f^{II}, was found to be independent of the ligament length, but showed a linear relationship with the change of the groove thickness. Based on the results, we propose an expression to correlate the essential work of fracture (w_e^{II}) with the specific work of fracture (w_f^{II}), the average plastic work density (w_p^{II}), and groove thickness (defined as the specimen thickness in the grooved cross section).

Further studies will be conducted to validate the new test methodology on the measurement of mode II fracture toughness using polymers of very different deformation characteristics. We believe that the proposed test methodology can also be applied to metallic or ceramic-based materials for the measurement of their fracture toughness in mode II. In addition to the toughness measurement, these studies will elucidate the micro-deformation mechanisms involved in the fracture process that yield significantly different toughness in the two modes of fracture.

Figures

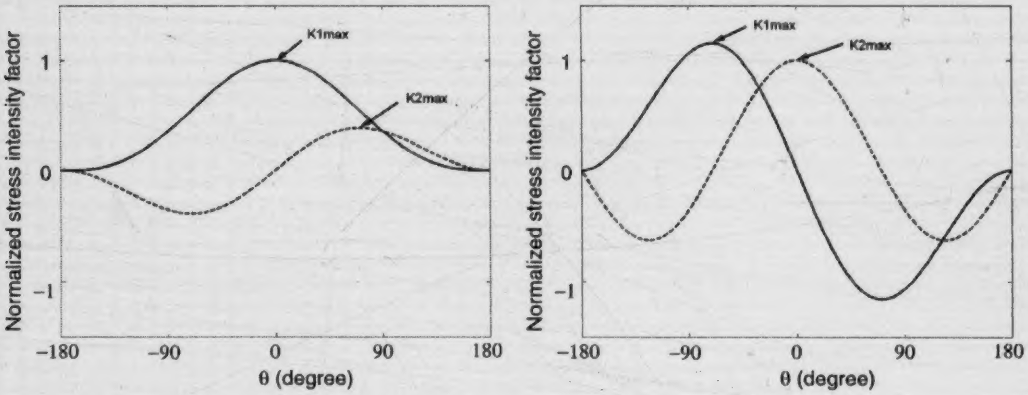

(a) (b)

Fig. 5-1 Normalized variation of $K_1(\theta)$ (———) and $K_2(\theta)$ (- - -) with respect to θ: (a) under mode I (tensile) loading, and (b) under mode II (shear) loading.

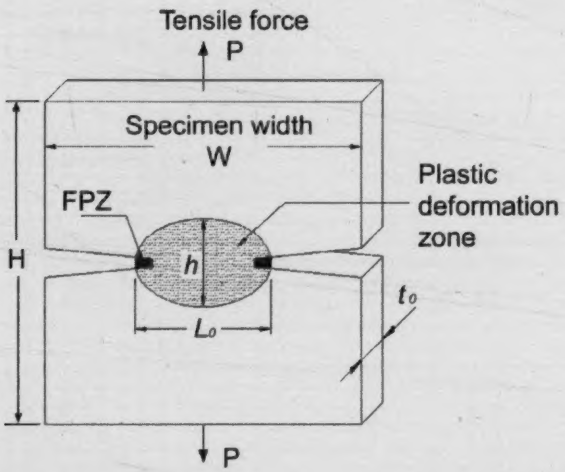
Tensile force
P
Specimen width
W
FPZ
Plastic deformation zone
H
h
t_o
L_o
P

Fig. 5-2 Double-edge-notched (DEN) tensile specimen for mode I fracture.

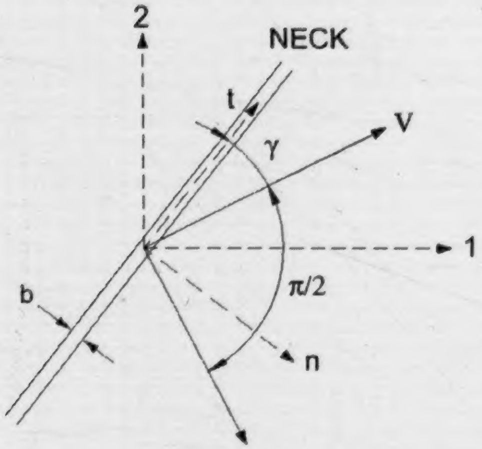
2
NECK
t
V
γ
1
b
π/2
n

Fig. 5-3 Velocity discontinuity.

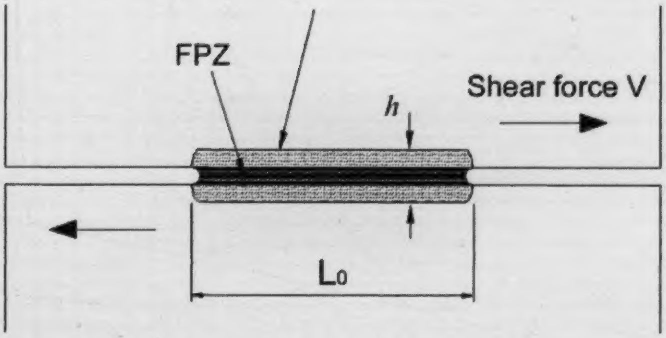
FPZ
Shear force V
h
L0

Fig. 5-4 Double-edge-notched (DEN) shear specimen for mode II fracture.

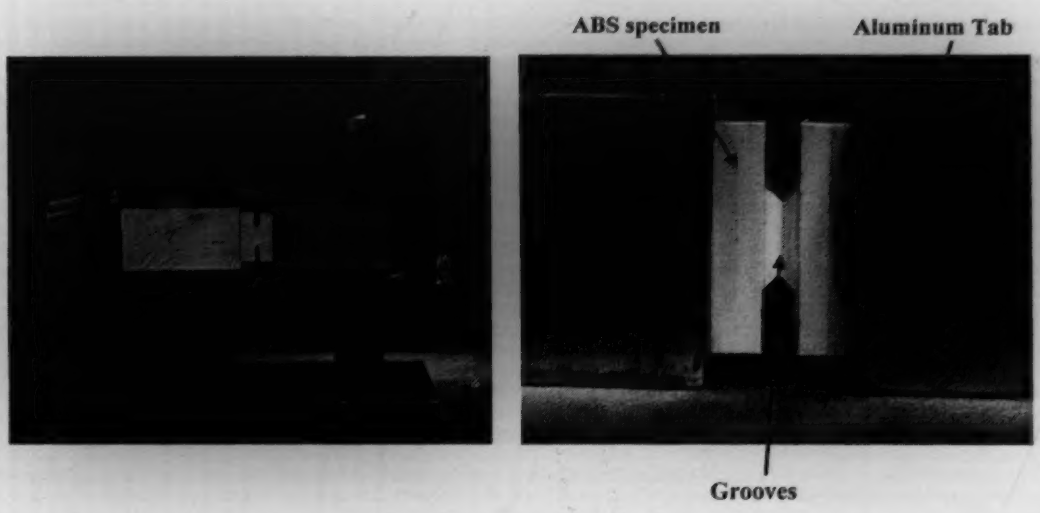
ABS specimen
Aluminum Tab
Grooves

(a) (b)

Fig. 5-5 Test set-up and specimens used in this study: (a) Iosipescu device and the specimen without grooves, and (b) the specimen with grooves.

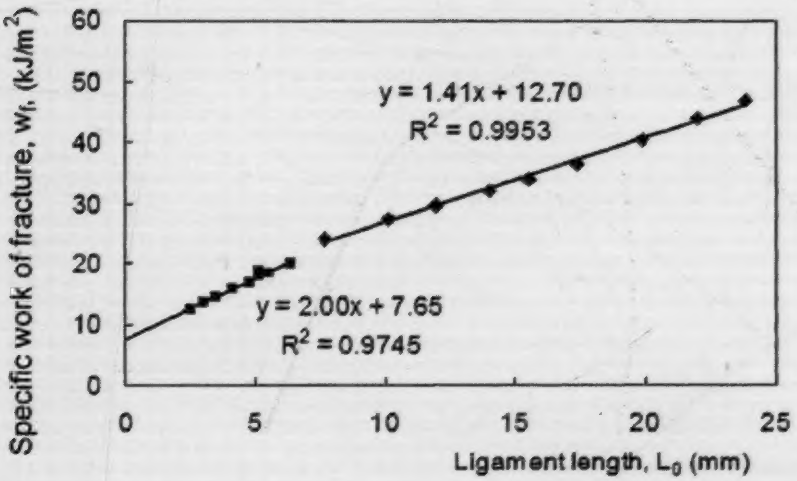

Fig. 5-6 Plot of specific work of fracture in mode I (w_f^I) as a function of ligament length.

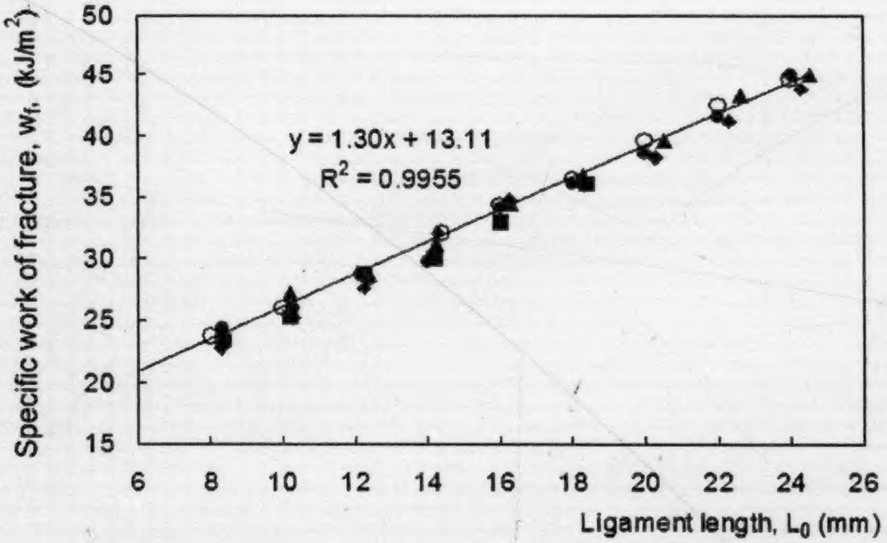

Fig. 5-7 Plot of specific work of fracture in mode I (w_f) as a function of ligament length with different thickness: ○, 6mm; ✸, 5mm; ▲, 4mm; ■, 3mm; ◆, 2mm.

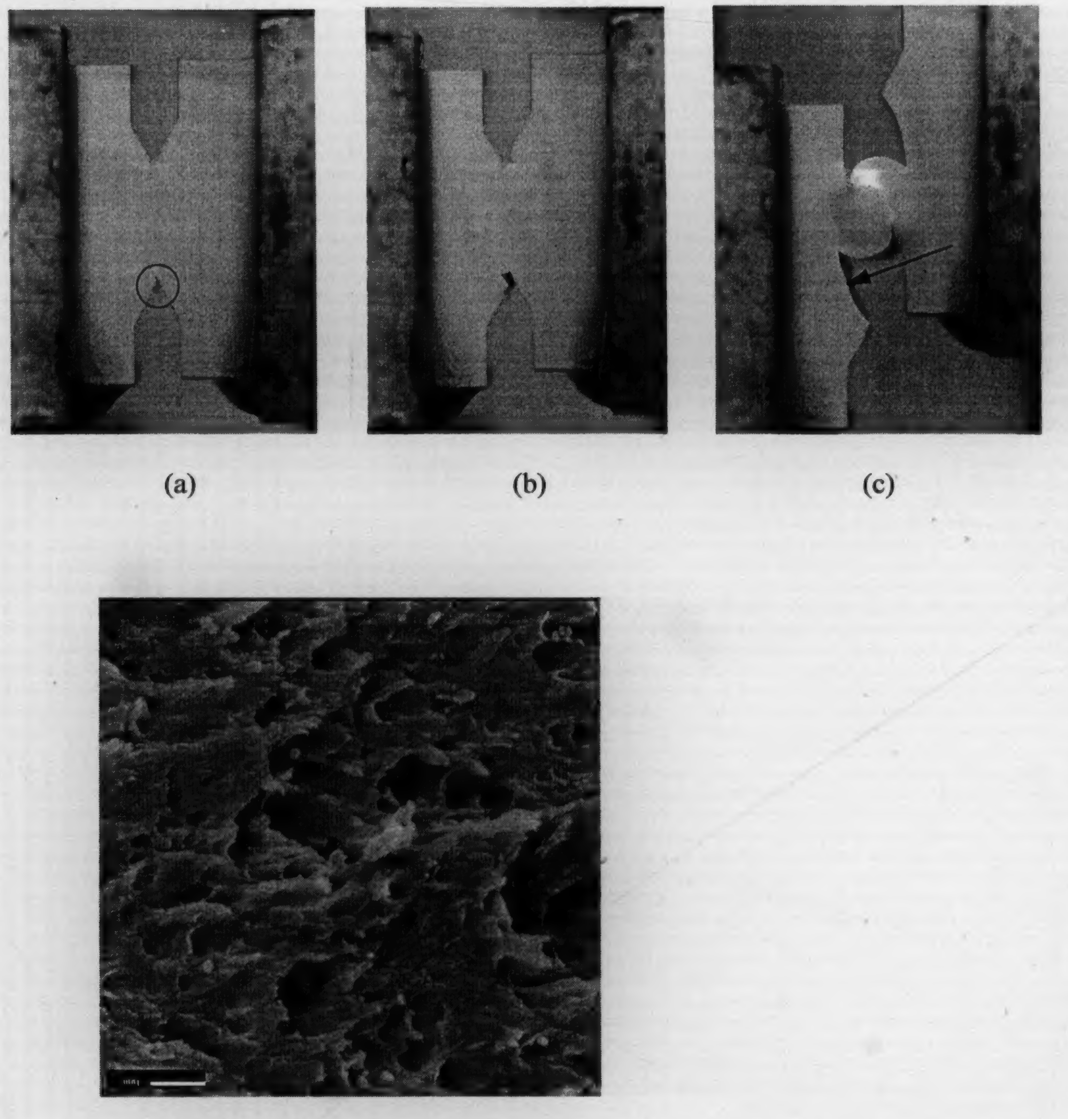

(a)

(b)

(c)

(d)

Fig. 5-8 Crack propagation during the Iosipescu test on specimens without the grooves: (a) first crack generation, (b) second crack generation, (c) formation of a cylinder during the crack growth, and (d) SEM micrograph taken from the fracture surface indicated by an arrow in (c).

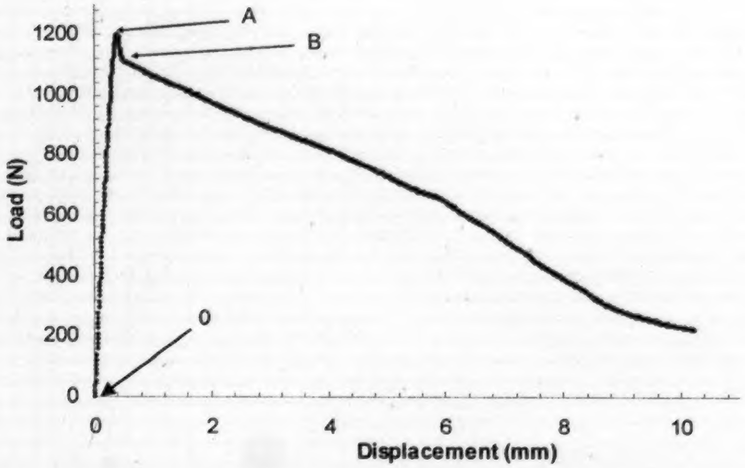

Fig. 5-9 Typical load-displacement curve from the Iosipescu test of ABS specimens without grooves.

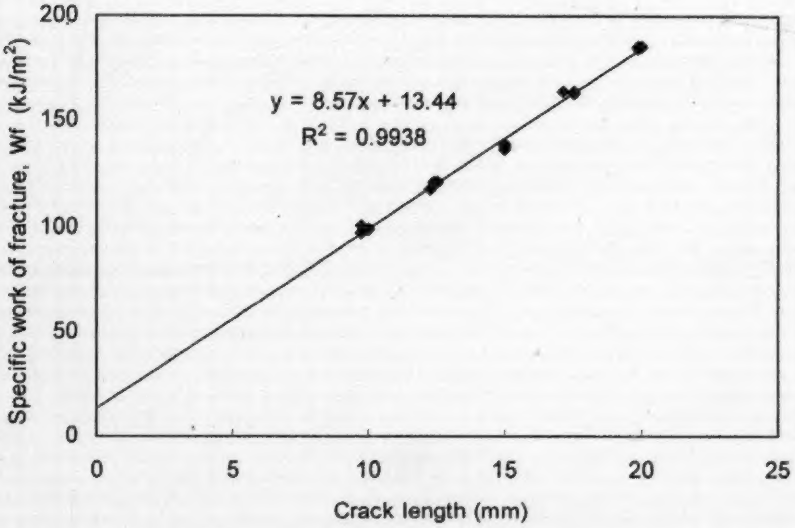

Fig. 5-10 Plot of specific work of fracture from Iosipescu test specimens without grooves.

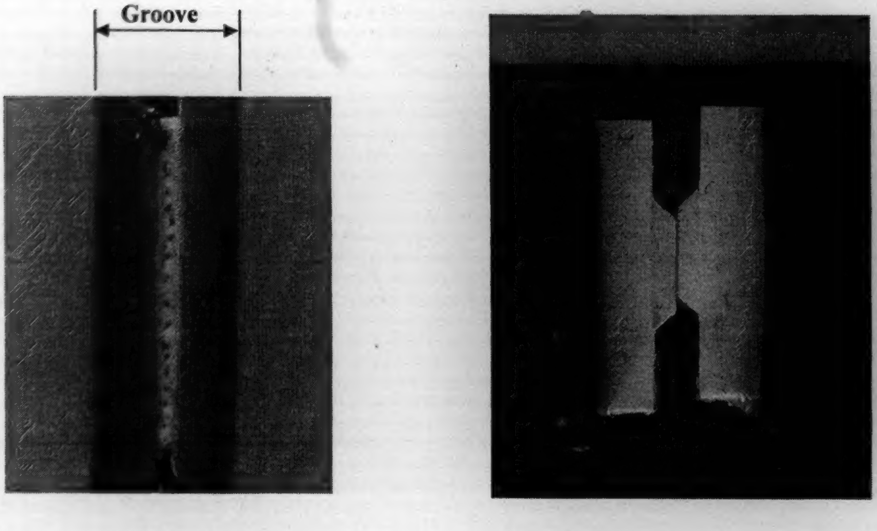

(a) (b)

Fig. 5-11 Iosipescu test on the grooved specimens, showing (a) an array of cracks generated in the whole ligament section, and (b) the velocity discontinuity along the groove.

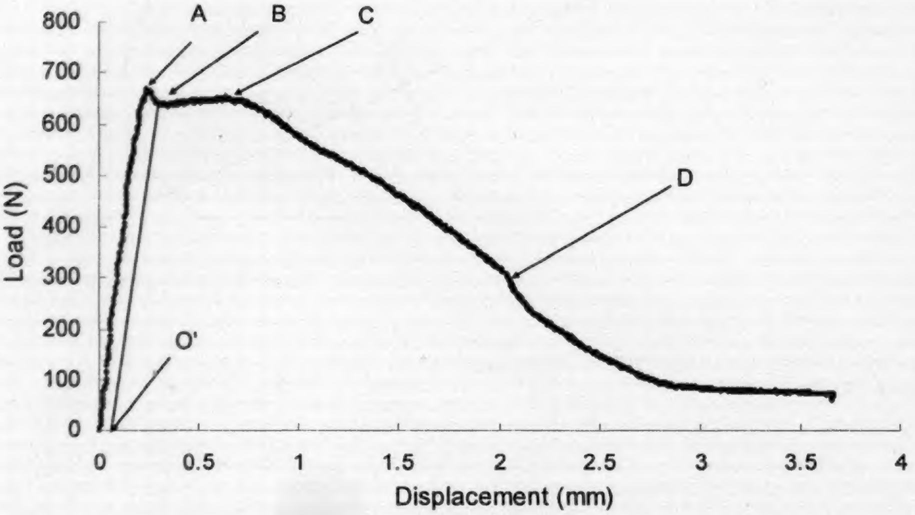

Fig. 5-12 A typical load-displacement curve from the Iosipescu test of the grooved specimens.

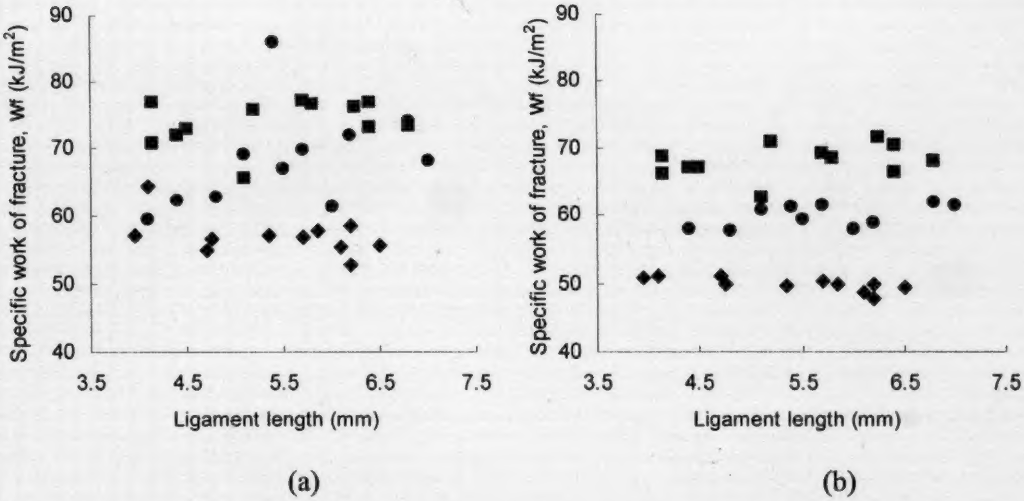

Fig. 5-13 Plots of the specific work of fracture (w_f) against ligament length: (a) from the total area under the curve, (b) by excluding the area covered by the curve after point D in Fig. 5-12. Groove thickness is 4 mm (■), 3 mm (●), and 2 mm (◆).

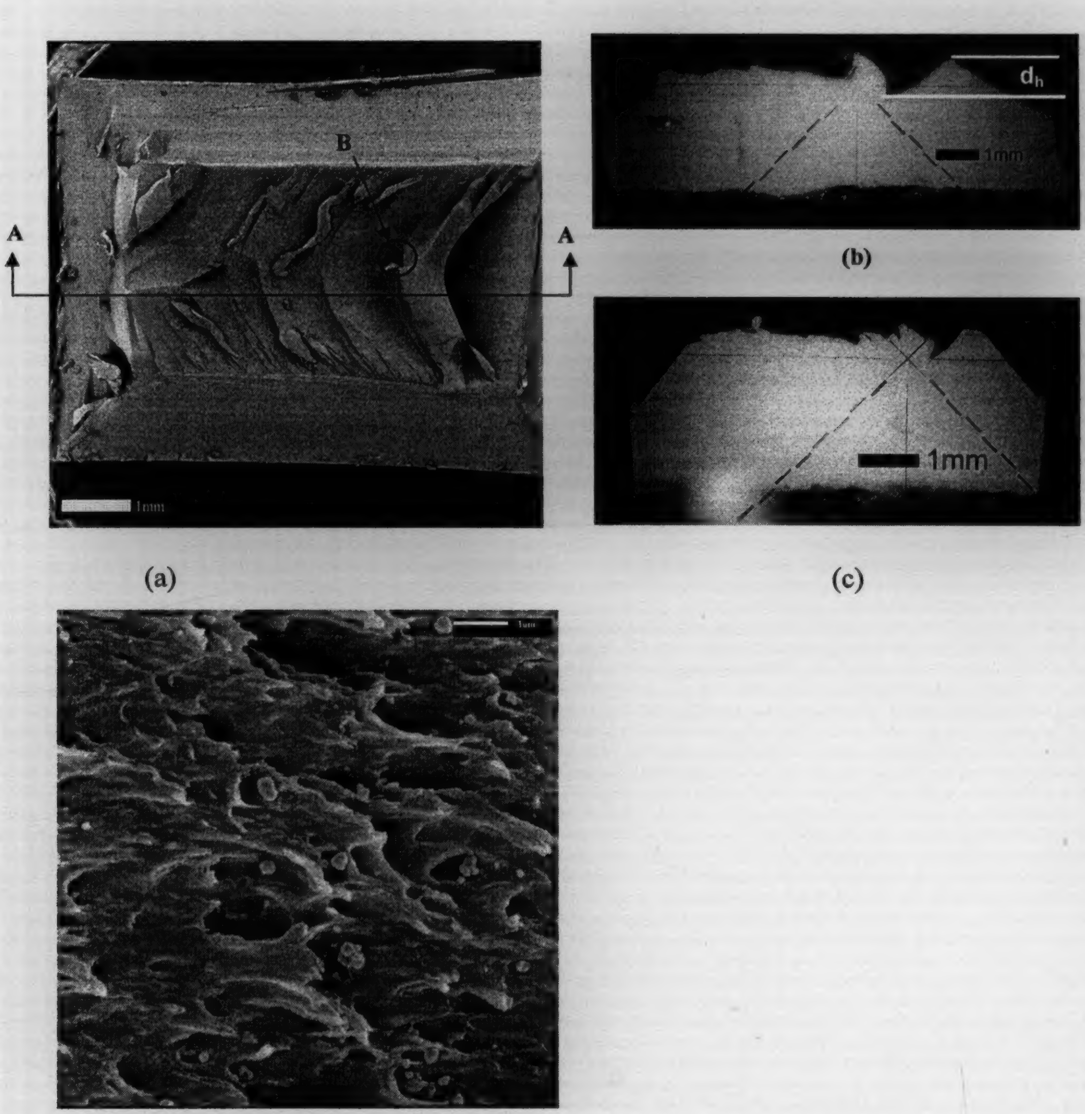

(b)

(a)

(c)

(d)

Fig. 5-14 (a) SEM micrograph of fractured surface from a specimen with groove thickness of 4 mm, (b) cross-sectional view along A-A in (a) for a specimen with groove thickness of 4 mm, (c) cross-sectional view for a specimen with groove thickness of 2 mm, and (d) magnified image from the circle B in (a).

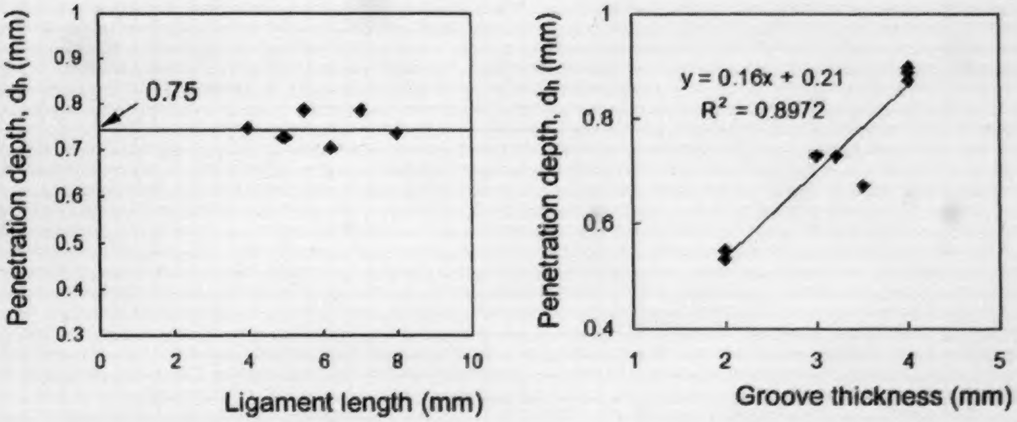

(a) (b)

Fig. 5-15 Penetration depth of each of the first pair of cracks against (a) ligament length, and (b) groove thickness.

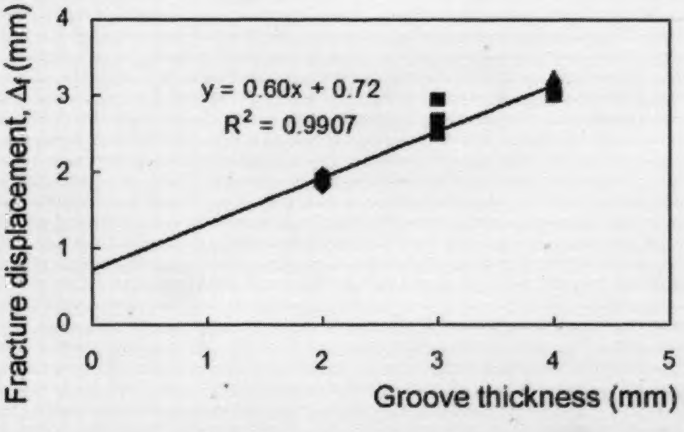

Fig. 5-16 Plot of the fracture displacement (Δ_f) as a function of groove thickness, using specimens of the same ligament length (5 mm), with the grooves and notches machined by a cutter of 60° in angle and 25 mm in thickness.

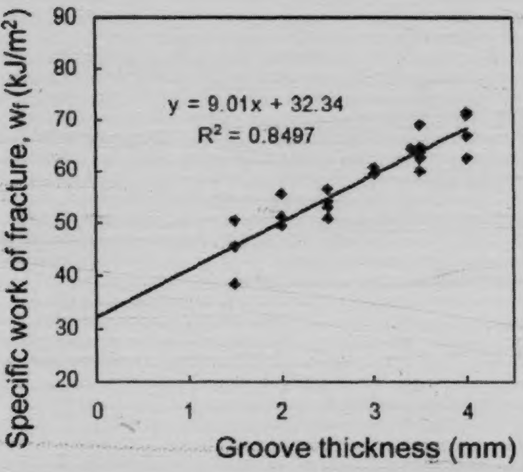

Fig. 5-17 Plot of the specific work of fracture (w_f) as a function of groove thickness, using specimens of the same ligament length (5 mm), with the grooves and notches machined by a cutter of 60° in angle and 25 mm in thickness.

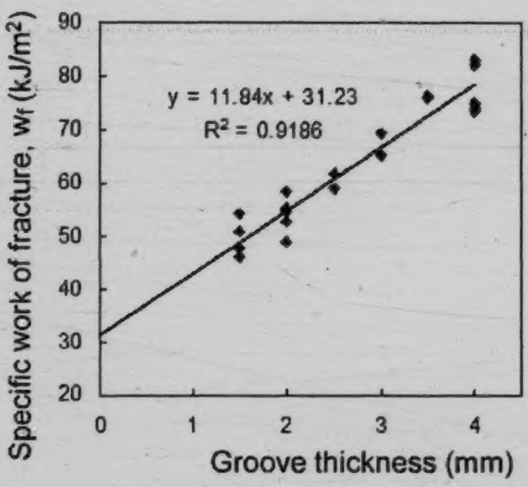

Fig. 5-18 Plot of the specific work of fracture (w_f) as a function of the groove thickness, using specimens of the same ligament length (5 mm) with the grooves and notches machined by a cutter of 45° in angle and 20 mm in thickness

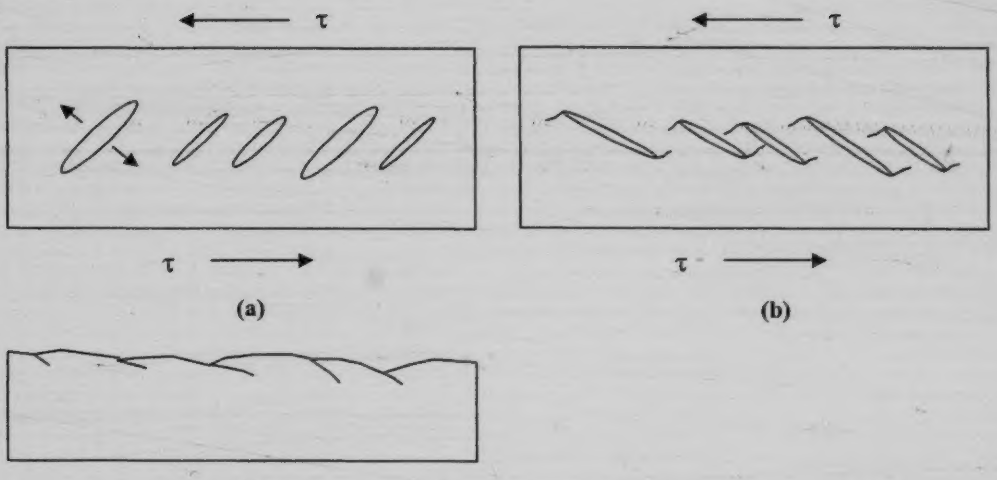

(a)

(b)

(c)

Fig. 5-19 Schematic representation of shear fracture process of ABS: (a) voids formation, (b) void rotation and crack emanation, and (c) side view of the surface topology.

References

1. Williams JG. Fracture Mechanics of Polymers, Chichester, England: Ellis Horwood Limited, 1984. pp. 45, 75.
2. Husaini K, Kishimoto K, Notomi M, Shibuya T. Fatigue Fract Engng Mater Struct 2001;24:895-903.
3. Li J, Zhang X-B, Recho N. Engng Fract Mech. 2004;71:329-343.
4. Cotterell B, Reddel JK. Int J Fract 1977;13:267–277.
5. Broberg KB. Int J Fract Mech 1968;4:11.
6. Broberg KB. J Mech Phys Solids 1971;19:407-418.
7. Cotterell B, Pardoen T, Atkins AG. Engng Fract Mech 2005;72(6):827-848.
8. Pardoen T, Hachez F, Marchioni B, Blyth PH, Atkins AG. J Mech Phys Solids 2004;52:423-452.
9. Wong JSS, Ferrer-Balas D, Li RKY, Mai YW, Maspoch ML, Sue HJ. Acta Materialia 2003; 51: 4929-4938 .
10. Iosipescu N. J Mater 1967;2(3):537-66.
11. Sullivan JL, Kao BG, Van Oene H. Exp Mech 1984:223-32.
12. Erdogan F, Shi GC. J Basic Engng 1963;85(4): 519-27.

13. Palaniswamy K, Knauss WG. Int J Fract Mech 1972; 8: 114-7.

14. Sih GC. Int J Fract 1974;10:305-21.

15. Rao Q, Sun Z, Stephansson O, Li C, Btillborg B. Rock Mech and Mining Sci 2003;40:355-375.

16. Todo M, Jar P-YB, Takahashi K. Compos Sci and Tech 2000;60:263-272.

17. Chao YJ, Liu S. Int J Fract 1997;87:201-223.

18. Pardoen T, Marchal Y, Delannay F. Engng Fract Mech 2004;69:617–631.

19. Mai YW. Int J Mech Sci 1993;35(12):995-1005.

20. Lauwerier HA, Koiter WT. Foundations of the theory of plasticity, Amsterdam: North-Holland Publishing Co, 1971. pp. 272-277.

21. Hill RJ. Mech Phys Solids 1952;1:19-25.

22. O'Brien TK. Compos 1998; 29B:57-62.

23. Broberg KB. J Mech Phys Solids 1971;19:407-418.

24. Mai YW, Cotterell B, Horlyck R, Vigna G. Polym Eng and Sci 1987;27(11):804-809.

25. Clutton EQ. Fracture of polymers, composites and adhesives, Amsterdam: Elsevier 1999, ESIS publication 27, pp. 187.

26. Edward M, Rodney LT. J Composite Materials 1968;2(4):523-6.

27. Yen SC, Craddock JN, Tech KT. Experimental Techniques 1988:22-5

28. Iosipescu N. J of Mater 1967;2(3):537-66.

29. Hawong JS, Shin DC, Baek UC. Eng Fract Mech 2004;71:233-243

30. Pindera Ma, Choksi G, Hidde JS, Herakovich CT. J compos Mater 1987;21:1164-85.

31. Adams DF, Walrath DE. J compos Mater 1987;21:494-507.

32. Tohgo K, Ishii H. Engng Fract Mech 1992;41(4):529-540.

33. Mai YW, Cotterell B. Int J Fract 1986;32:105-125.

34. Ching Emma CY, Li Robert KY, Mai YW. Polym Engng Sci 2000;40(2):310-319.

35. Sutton MA, Zhao W, Boone ML, Reynolds AP, Dawicke DS. Int J Fract 1997;83:275-290.

36. Williams JG. Fracture Mechanics of Polymers, Chichester, England: Ellis Horwood Limited, 1984. pp. 98-99.

37. Hertzberg RW. Deformation and fracture mechanics of engineering materials, 4th ed. New York: John Wiley & Sons, Inc., 1996. pp. 342-345.

Chapter 6

Toughness of High-Density Polyethylene in Shear Fracture

6.1 Introduction

A new test methodology was reported in our previous paper (Kwon et al. 2005) for measuring essential work of fracture (EWF) of polymers in shear mode (mode II). The study concludes that side grooves along the ligament of double-edge-notched (DEN) specimens facilitate the alignment of the shear band in the loading direction, thus encouraging specimen fracture in mode II. Through linear regression of the specific work of fracture to zero ligament thickness, shear fracture toughness for poly(acrylonitrile-butadiene-styrene) (ABS) was determined. It showed that mode II fracture toughness of ABS is about 2.5 times larger than its mode I counterpart.

Following the above study, this paper examines applicability of the new test method to measuring mode II EWF value of high-density polyethylene (HDPE) that is known for its excellent ductility in the plane-stress condition. HDPE was chosen because

** A version of this chapter has been accepted. International Journal of Fracture (Aug. 2007).

of its contrasting deformation behaviour from ABS. Excellent ductility and significant work-hardening of HDPE has enabled the development of stable necking during the plastic deformation (G'sell et al. 1979; Hutchinson et al. 1983). This is different from ABS that does not show any work hardening behaviour, with its neck formation quickly leading to the final fracture. Due to the large deformation involved in the HDPE fracture, its toughness is often impossible to measure using the conventional approaches such as J-integral method (Atkins et al. 1985). Hence, a study has been conducted to investigate possibility of using the EWF concept to quantify the HDPE toughness.

This paper presents an approach for measuring mode II fracture toughness of HDPE. The paper provides a brief review of relevant literature, and compares mode II fracture toughness of HDPE with its mode I counterpart.

6.2 Literature Review

Literature relevant to fracture mode prediction and toughness evaluation is reviewed in this section. The review is not meant to be comprehensive, but focusing on the work that has been considered during the course of the study.

Traditional Approaches for Fracture Mode Prediction

The traditional approach to predict the fracture mode is limited to the fracture initiation stage. In the framework of linear elastic fracture mechanics (LEFM), mode for crack development is often predicted based on the values of tensile strength (σ_C) and shear strength (τ_C) (Theocaris 1989). Ritchie et al. (1973) proposed the use of σ_C/τ_C to predict the crack growth mode, which is known as RKR criterion. The criterion suggests that if the ratio of the maximum tensile stress ($\sigma_{\max}$) to the maximum shear stress ($\tau_{\max}$), i.e. $\sigma_{\max}/\tau_{\max}$, for a given loading condition is higher than σ_C/τ_C the crack growth should be in mode I, and conversely in mode II. In other words, the criterion suggests that the following condition should be satisfied for mode I fracture to occur:

$$\frac{\sigma_{\max}}{\tau_{\max}} > \frac{\sigma_C}{\tau_C} \tag{6.1}$$

but for mode II fracture:

$$\frac{\sigma_{\max}}{\tau_{\max}} < \frac{\sigma_C}{\tau_C} \tag{6.2}$$

Note that σ_C/τ_C for extremely brittle materials is very close to 1; for very ductile materials close to 2; and in between for other materials.

Sih et al. (Sih et al. 1961) showed that under mode I loading σ_{max}/τ_{max} is 2.6 that is higher than σ_C/τ_C for all materials. Thus, the RKR criterion suggests that mode I loading always generates mode I fracture, which has been widely supported from experimental studies.

Under mode II loading, on the other hand, σ_{max}/τ_{max} is 1.15. Although this value is greater than σ_C/τ_C for brittle materials, it is small enough to allow mode II fracture to occur in materials with some ductility. Therefore, in the current study Iosipescu loading (Iosipescu 1967) was selected to apply the shear force, in hope to generate mode II fracture in HDPE that often occurs in a very ductile manner.

The RKR criterion, however, is only applicable to the crack development at an early stage. The subsequent crack growth in ductile fracture can occur in a different mode. This is supported by experimental studies (Li et al. 2004), showing that mode II crack growth in ductile polymers can be initiated by mode II loading, but the subsequent crack growth may be switched to mode I. To our knowledge, no test method is currently available to generate mode II crack growth in the whole fracture process. Therefore, some indirect data deduction method is needed to quantify the mode II fracture toughness.

Essential Work of Fracture (EWF)

The essential work of fracture is a relatively new concept for determining the energy consumption that is directly relevant to the fracture surface formation in the crack growth process (Cotterell et al. 1977; Mai et al. 1986; Karger-Kocsis et al. 1998). Several test methods have been designed based on the concept, to separate the energy consumed in the fracture process zone (FPZ) from the other forms of energy consumption during the crack growth, including that for the global plastic deformation in ductile fracture (Kwon et al. 2006a). Currently, double-edge-notched tensile test (DENT test) is the most popular method based on the EWF concept, and has been successfully used to quantify toughness for ductile fracture in mode I, commonly known as specific essential work of fracture (w_e^I). Value of w_e^I represents the energy consumed in the FPZ for unit area of crack growth, provided that necking in the FPZ is unstable (Broberg 1968). However, the test method has also been applied to crack growth that involves stable necking, such as that occurring in HDPE, (Mai et al. 1991; Saleemi et al. 1990; Mai et al. 1987). Some groups suggest that the traditional EWF method should be modified to be applicable to HDPE (Kwon et al. 2006a; Karger-Kocsis et al. 2003); but at this stage, none of the proposed modifications has been fully validated.

The data analysis widely adopted for the DENT test is to use the following relationship for the energy consumption to quantify the material toughness, represented by the specific essential work of fracture (w_e^I):

$$w_f^I = w_e^I + \beta_p^I w_p^I L_0 \tag{6.3}$$

where the superscript *I* represents mode I deformation, w_f^I the specific work of fracture, w_p^I the average plastic work density, β_p^I the shape factor for the plastic deformation zone, and L_0 the original ligament length. The expression suggests that w_f^I value is a combination of w_e^I that is directly related to the fracture surface formation and w_p^I for the plastic deformation in the ligament region. The above expression also suggests that the w_e^I value can be determined by linear regression of w_f^I values to zero ligament length. Pardoen et al. (Pardoen et al. 2004) proposed that w_e^I is a combination of the real specific work of fracture that is independent of specimen thickness and the specific necking energy that is proportional to the specimen thickness. Therefore, a generalized expression of Eq. (6.3) is

$$w_f^I(L_0,t_0) = \Gamma_0^I + \beta_n^I w_n^I t_0 + \beta_p^I w_p^I L_0 \tag{6.4}$$

where Γ_0^I is the mode I EWF that is independent of the thickness and w_n^I the average work density for the neck formation.

For double-edge-notched specimens subjected to mode II loading, such as that in Iosipescu test, expression for the specific work of fracture, w_f^{II}, has been suggested to be (Kwon et al. 2005):

$$w_f^{II} = w_e^{II} + \beta_p^{II} w_p^{II} t_0 \tag{6.5}$$

where the superscript *II* represents the mode II deformation, w_e^{II} the specific essential work of fracture, w_p^{II} the average plastic work density, β_p^{II} the shape factor, and t_0 the ligament thickness in regions where the crack growth occurs. The above expression suggests that w_f^{II} is dependent on t_0 only, not L_0 for non-work-hardening materials (Hill 1952). However, it is not clear whether the expression is also applicable to polymers with stable necking like HDPE. This is because unlike ABS, significant work hardening can be involved in HDPE during the plastic deformation, thus showing ligament-length dependence of the fracture energy.

Therefore, in general, for crack development in mode II loading, the deformation occurs in both mode I and mode II mode, for which w_f can be expressed by combining Eqs. (6.11) and (6.12). That is,

$$w_f(L_0,t_0) = \Gamma_0^I + \Gamma_0^{II} + (\beta_n^I w_n^I + \beta_p^{II} w_p^{II})t_0 + \beta_p^I w_p^I L_0 \qquad (6.6)$$

Note that Γ_0^{II} represents the energy consumption term for mode II that is independent of t_0, like Γ_0^I in Eq. (6.4). If Eq. (6.6) is indeed the expression for w_f in the mixed mode of deformation, the non-essential terms, i.e. the terms on the right-hand side that vary with L_0 and t_0, can be removed by double extrapolation of w_f values to zero ligament length and zero ligament thickness.

6.3 Experimental Details

Similar to our previous study, the Iosipescu test was used to apply shear loading to the DEN specimens. As depicted in Fig. 6-1, aluminium tabs of 4 *mm* length (L_1 in Fig. 6-1) were glued to both sides of the specimen to enhance their bending stiffness. The specimens were machined from commercial-grade, extruded high-density polyethylene

(HDPE) plates of 6.25 *mm* thick, provided by McMaster-Carr in USA, to have dimensions 17 *mm* wide (W in Fig. 6-1) and 90 *mm* long (L in Fig. 6-1). Density of the HDPE was 0.96 g/cm^3. Variation in ligament length was from 2 to 7 *mm*. The specimen/aluminium tab assembly was placed in the Iosipescu rig, and loaded using an Instron universal testing machine at a cross-head speed of 2.5 *mm/min*. Fracture behaviour was recorded using a digital video camera with a micro-zoom lens. Most specimens have side grooves introduced along the ligament length, to encourage the crack growth along that direction. Specimens without the side grooves were also used in the study, for comparison of the deformation behaviour.

The side grooves were V-shaped and lay between the notch tips, as shown in Fig. 6-1. The notches and the side grooves for most specimens were machined using a mill cutter of 60°. To examine the effect of the groove tip angle, a mill cutter of 90° was also used to machine the notches and side grooves for some specimens. Both cutters generated the notch tip radius of 30 μm. Based on results from the previous study (Kwon et al. 2005), the side grooves were expected to enhance the velocity discontinuity along the ligament length direction, thus encouraging the mode II fracture (Hill 1952). In this paper, specimen thickness between the tips of the side grooves is referred to as the ligament thickness (t_0).

6.4 Results

Typical results from the Iosipescu tests of HDPE are presented here, and compared with the results from ABS that were reported previously (Kwon et al. 2005).

Deformation and Fracture Behaviour

Deformation behaviour of the DEN specimens without the side grooves is presented in Fig. 6-2. Fig. 6-2(a) was taken at an early stage of the Iosipescu test, while Fig. 6-2(b) at a later stage in which a stretched segment was formed in the ligament section. Note that apart from the stretched segment, the specimen has been separated into two halves at this stage. The formation of a stretched segment shown in Fig. 6-2(b) indicates that tensile deformation was involved in the fracture process. The behaviour is very different from that observed in ABS with similar specimen geometry, also without the side grooves (Kwon et al. 2005). The ABS specimens showed a course of crack development that after the crack initiation from the notch tip, deviated significantly from the loading direction; while the crack growth in the HDPE specimens maintained very close to the loading direction throughout the test. We believe that even without the side grooves, the HDPE specimens have mode II deformation dominate the fracture process.

Introducing side grooves in the HDPE specimens did not seem to alter the fracture behaviour significantly. As shown in Fig. 6-3, taken from a specimen with side grooves, the crack growth direction that maintained very close to the loading direction throughout the test also had a stretched segment visible at a later stage of the test (Fig. 6-3). This is contradictory to that observed in ABS wherein the side grooves changed the crack growth direction dramatically. We believe that the formation of the stretched segment was partly due to the significant work hardening of HDPE during the plastic deformation. The presence of the stretched segment also suggests that the HDPE specimens in the Iosipescu tests may have mode I deformation involved even with the presence of the side grooves.

Load-Displacement Curve

Typical load-displacement curves obtained from the testing, after the load is normalized by the original ligament area, are presented in Fig. 6-4 as a function of displacement. Fig. 6-4(a) was from a specimen without the side grooves and Fig. 6-4(b) from a specimen with the side grooves, both having the initial ligament length of 4 mm. The two curves suggest that the use of side grooves raised the initial loading rate slightly, but its effect on the load dropping rate was very significant, especially immediately after point A in Fig. 6-4 was passed. For specimens without the side grooves, Fig. 6-4(a), the load dropping rate after point A maintained relatively constant till around point B, where the load dropping rate increased and then maintained relatively constant to around point C. It should be noted that the photograph in Fig. 6-2(b) was taken at a stage around point C where except the stretched segment the specimen has separated into two halves. The stretched segment fractured at the last stage of the test, that is, after point D in Fig. 6-4(a).

For specimens with side grooves, Fig. 6-4(b), the load did not drop immediately after point A. Instead, it maintained relatively constant to form a plateau section. This phenomenon is similar to that observed in ABS (Kwon et al. 2005), indicating that the side grooves did enhance mode II deformation in the HDPE specimens. Fig. 6-4(b) shows that at the end of the plateau section, the load dropping rate resumed and was nearly constant till around point B, where the load dropping rate increased but again maintained relatively constant to around point C, similar to that shown in Fig. 6-4(a). However, the specimens with the side grooves did not generate a consistent trend of the load-displacement relationship for further loading from point C. Some specimens showed a gradual decrease of the load dropping rate, as indicated in Fig. 6-4(b); but the others had the load dropping rate maintain constant till the end of the test. We believe that variation of the load dropping rate at this stage was caused by the inconsistent size of the stretched segment, for which the causes are not clear and require further investigation.

Although both HDPE and ABS specimens with side grooves showed a plateau section on the load-displacement curve, the deformation mechanisms involved in the fracture process were different. By introducing side grooves to the ABS specimens, an array of micro-cracks was developed in the plateau section, which later coalesced to form the fracture surface (Kwon et al. 2005). On the other hand, crack growth in the HDPE specimens with side grooves was found to advance progressively from the notch tips, which bears strong similarity to that shown by the specimens without the side grooves.

Therefore, we believe that the plateau section shown in Fig. 6-4(b) was due to the balance of the stress rise from the work-hardening and the reduction of the ligament length from the crack growth. The presence of the side grooves prolonged the balance of the two mechanisms (work hardening vs. crack growth) by enhancing the localisation of the plastic deformation around the groove tips. Eventually, the crack growth prevailed and resulted in the load drop shown at a later stage of the test.

Plot of Specific Work of Fracture

Typical $w_f - L_0$ plots from Iosipescu test of HDPE specimens are shown in Fig. 6-5. Specimens used for Fig. 6-5(a) had the original thickness of 6.25 *mm*, and those for Fig. 6-5(b) had the ligament thickness 3 *mm*. Both plots in Fig. 6-5 show that w_f is linearly proportional to the ligament length, down to the ligament length of 3 mm, conforming to the expression of Eq. (6.3). The curve fitting in Fig. 6-5 did not include data for ligament length of 2 *mm*. This is because a transition of the trend line occurred when the ligament length became shorter than the ligament thickness, as to be discussed at the end of the next section under the heading "Discussion".

The main difference between the two plots in Fig. 6-5 is the dependence of w_f on the change of the ligament length. With the side grooves, Fig. 6-5(b), w_f becomes less sensitive to the change of the ligament length. This is consistent with that observed in ABS (Kwon et al. 2005), though for ABS the presence of the side grooves completely eliminated the dependence of w_f on the ligament length. We believe that the reduced dependence on the ligament length for HDPE is an indication of the presence of the side grooves increasing the involvement of mode II deformation in the fracture process.

6.5 Deduction of Mode II Fracture Toughness

In the study of ABS (Kwon et al. 2005), the specific essential work for mode II fracture (w_e^{II}) was determined solely by linear regression of w_f values to zero ligament thickness, as the w_f values were independent from the ligament length. This approach, however, cannot be directly applied to the HDPE specimens, because their w_f values still show the dependence on the ligament length. Therefore, the data deduction scheme needs to be modified to include a linear regression process of w_f variation on the ligament length. The modification will be justified by elucidating the mechanisms involved in the fracture process, as to be discussed in the following sections.

Dependence on the Ligament Length

Hill (Hill 1952) suggested that orientation of sliding discontinuity can be used to define the fracture mode. This, however, is only applicable to non-work-hardening materials. For HDPE, the possible severe work-hardening during the plastic deformation raises the question on whether the sliding discontinuity can be used to define the mode of the fracture process. We speculate that the severe work hardening may also be responsible for the dependence of the plastic zone size on the ligament length, resulting in the variation of w_f with the change of the ligament length in the mode II fracture.

Nevertheless, pure mode II fracture in the Iosipescu test should have the crack growth along the ligament length, with no rotation of the two halves of the specimen during the test. In order to reinforce the two halves of the DEN specimen of HDPE, aluminium tabs were bonded to the two halves, as shown in Fig. 6-1, in hope that the right half of the specimen could move strictly upwards during the test while the left half remained stationary. This, however, could not be fully achieved because of a central gap between the two sets of the aluminium tabs. The central gap was necessary to avoid adhesive covering the surface in the ligament region, but resulted in the exposed central section being much softer than the rest of the specimen, which created a bending motion during the test, as depicted in Fig. 6-6(b) with some exaggeration on the deformation level. We believe that this bending motion led to the formation of the stretched segment between the two halves, as shown in Figs. 6-2(b) and 6-3(c). Since the amount of the bending motion is expected to be proportional to the applied force, the extent of its occurrence depends on the ligament length, which can be eliminated by reducing the ligament area to zero, that is, by extrapolating the w_f values to zero ligament length.

Dependence on the Ligament Thickness

Similar to that suggested in our previous work on ABS (Kwon 2005), we believe that the plastic deformation size generated in the Iosipescu tests is proportional to the ligament thickness. Therefore, extrapolating the w_f values at the zero ligament length to zero ligament thickness can eliminate the involvement of the plastic deformation in the energy consumption, yielding the w_e^{II} value that is independent of the ligament length and the ligament thickness.

Discussion

The above data deduction process is designed to remove the energy consumption due to the ligament rotation and the plastic deformation, by applying the linear regression process to the measured w_f values twice, first to zero ligament length and then to zero ligament thickness. The extrapolation to zero ligament length is to reduce the maximum force for fracture to zero, thus eliminating the specific energy consumption due to the ligament rotation. The following extrapolation to zero ligament thickness is to exclude the specific energy for plastic deformation. Therefore, the process is expected to yield the specific EWF value for the mode II fracture, i.e. w_e^{II}.

Justification

Validity of the above data deduction process was investigated by examining values of the "further displacement" in the test, defined as the remaining displacement to fracture after the displacement reached the value of the original ligament length, which in Fig. 6-4(b) is the difference between the displacement of 4 *mm* (equivalent to the original ligament length) and that at point F. It is believed that for an ideal mode II fracture in the Iosipescu test, the total displacement at fracture should be equivalent to the original ligament length. That is, the "further displacement" should be zero when pure mode II fracture occurs. If the above double linear regression process can be used to determine the true w_e^{II} value, the process should yield zero for the value of the "further displacement".

Linear regression of the "further displacement" to zero ligament length was conducted for specimens with the original ligament length longer than 2 *mm*, and the results are shown in Fig. 6-7(a). The values at zero ligament length are then plotted as a function of the ligament thickness in Fig. 6-7(b). Fig. 6-7(b) yields a value around 0.02 *mm* at zero ligament thickness, which is less than 1% of the total displacement generated in the tests. Therefore, it is believed that the double linear regression process can indeed be used to determine the w_e^{II} value.

Essential Work of Fracture for Mode II

Fig. 6-8 presents the double linear regression process, in which Fig. 6-8(a) is the plot of w_f versus L_0 for specimens of different ligament thickness. The values at zero ligament length are then plotted as a function of the ligament thickness in Fig. 6-8(b). This process yields a value of 12.4 kJ/m^2, which represents w_e^{II} for the HDPE.

Note that only w_f values for L_0 longer that 3.5 *mm* were used in the linear regression process, as all w_f values for specimens with ligament lengths shorter than 3.5 mm collapsed together. As to be discussed in a later section, this phenomenon turns out to be related to the ligament thickness. That is, when the ligament length was equal to or shorter than the ligament thickness the data trend changed, as shown in Fig. 6-5(b). However, data for specimens with short ligament lengths could be used to provide a rough estimate of the w_e^{II} value, which will be demonstrated in the section "Simplified Iosipescu test for specific mode II EWF".

Groove Tip Angle

The effect of the groove tip angle on w_e^{II} value was examined by changing the angle of the mill cutter teeth from 60° to 90°. The results are shown in Fig. 6-9. The corresponding w_e^{II} value is 12.75 KJ/m^2 that is very close to the value given in Fig. 6-8, determined from specimens with the groove tip angle of 60°. In addition, Fig. 6-8(b) and Fig. 6-9(b) have very similar slope, suggesting that the w_e^{II} value is relatively insensitive to the groove tip angle. This is consistent with the conclusion from the previous study on ABS (Kwon et al. 2005).

Modified Expression for Specific Work of Fracture

The above results suggest that w_e^{II} for HDPE can be determined through a double linear regression approach, i.e. to zero ligament length and zero ligament thickness. The results also suggest that Eq. (6.6) should be modified for HDPE, to include a term of specific energy that is proportional to L_0:

$$w_f = w_e^{II} + \beta_{p,L}^{II} w_{p,L}^{II} L_0 + \beta_{p,t}^{II} w_{p,t}^{II} t_0 \tag{6.7}$$

where $\beta_{p,L}^{II}$ is the shape factor for the dependence of w_f on the ligament length, and $w_{p,L}^{II}$ the associated average plastic work density. However, both $\beta_{p,L}^{II}$ and $\beta_{p,t}^{II}$ are unknown at this stage. Therefore, it is not clear whether values of $w^{II}_{p,L}$ and $w^{II}_{p,t}$ are independent from each other.

Simplified Iosipescu Test for Specific Mode II EWF

As mentioned earlier, Fig. 6-8(a) suggests that the trend line for w_f versus L_0 changes when the ligament length is shorter than the ligament thickness. For example, data for specimens with ligament thickness 4 *mm* show the transition of the trend line occurring at the ligament length around 4 *mm*. As a result of the transition of the trend lines, all w_f values from specimens with ligament length shorter than 3.5 *mm* collapse together, suggesting that a critical ligament length exists, below which the w_f values are no longer dependent on the ligament thickness.

By using all w_f values from specimens with ligament lengths shorter than 3.5 *mm* for the linear regression process, the value at zero ligament length is estimated to be between 10 and 16 kJ/m^2, as shown in Fig. 6-8(a), which is consistent with the value determined from the above double linear regression approach (12.4 kJ/m^2). Therefore, we believe that the use of specimens with ligament lengths shorter than the ligament thickness could be a simpler alternative to obtain a rough estimate of the w^{II}_e value. This approach, however, has limited accuracy due to the small number of data that can be obtained for different ligament lengths from 6.25-*mm*-thick specimens. Nevertheless, additional study is needed to verify the validity of this approach.

A question to which the study cannot provide an answer is whether energy consumption for mode I deformation is still involved in the w^{II}_e value. As mentioned earlier, Hill (Hill 1952) suggested that pure mode II fracture can never be achieved in work-hardening materials, and the mode I deformation should always be involved in the fracture process. Based on this suggestion, and if work-hardening has occurred in HDPE in the Iosipescu test, the w_e^{II} value determined in this study may still contain energy consumption for the mode I deformation, and perhaps the linear regression process in Fig. 6-8 yields a value that is a combination of Γ_0^I and Γ_0^{II}, as suggested by Eq. (6.6).

Nevertheless, by comparing w_e^{II} value reported here with the w_e^I values reported previously for the same HDPE (Kwon et al. 2006b), it seems that the mode II EWF value is about twice of its mode I plane-strain counterpart, but much smaller than its plane-stress w_e^I value. This is because in the latter case significant plastic deformation is involved in the fracture process.

6.6 Conclusions

Mode II fracture toughness of HDPE was determined using a double linear regression process based on the EWF concept. This methodology was verified by examining the "further displacement" (defined as the difference between the displacement at fracture in the Iosipescu test and the original ligament length), which turned out to be nearly zero through the double linear regression process. The study shows that mode II fracture toughness of HDPE is about twice of its mode I counterpart, provided that only limited plastic deformation is involved in the fracture process. The study also shows that by using specimens with ligament length shorter than the ligament thickness, single extrapolation of w_f to zero ligament length could provide a rough estimate of the w_e^{II} value.

Figures

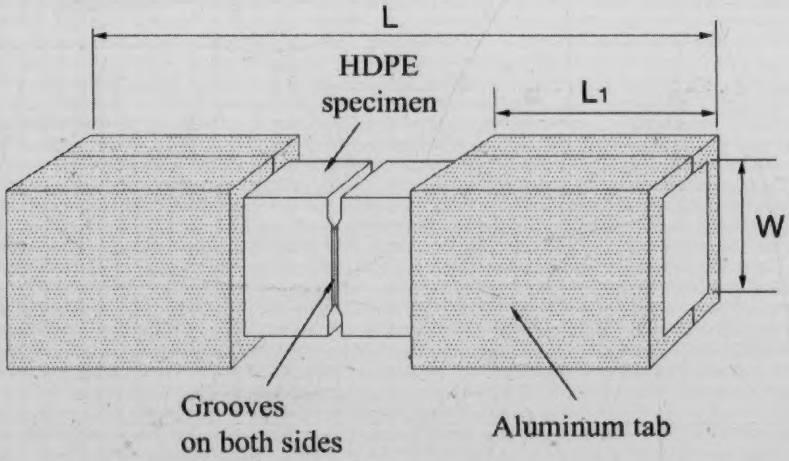
L
HDPE specimen
L1
W
Grooves on both sides
Aluminum tab

Fig. 6-1 Description of the DEN specimens used in the study.

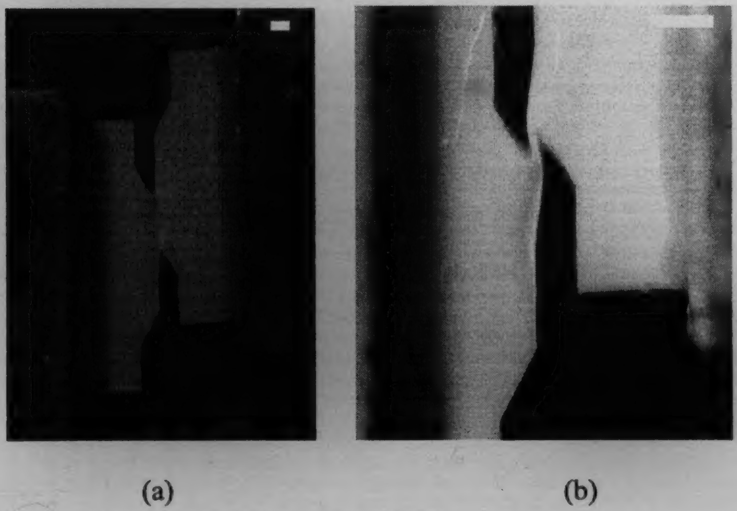
(a) (b)

Fig. 6-2 Crack propagation during the Iosipescu test, for a HDPE specimen without side grooves. Length of the white bar corresponds to 1mm.

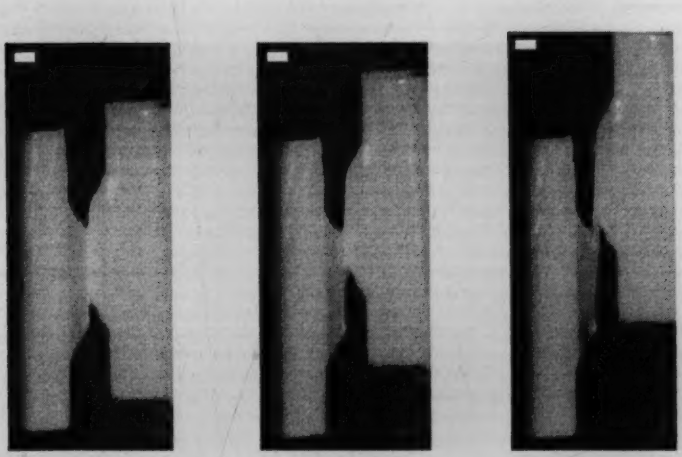

(a) (b) (c)

Fig. 6-3 Crack propagation during the Iosipescu test, for a HDPE specimen with side grooves. Length of the white bar corresponds to 1mm.

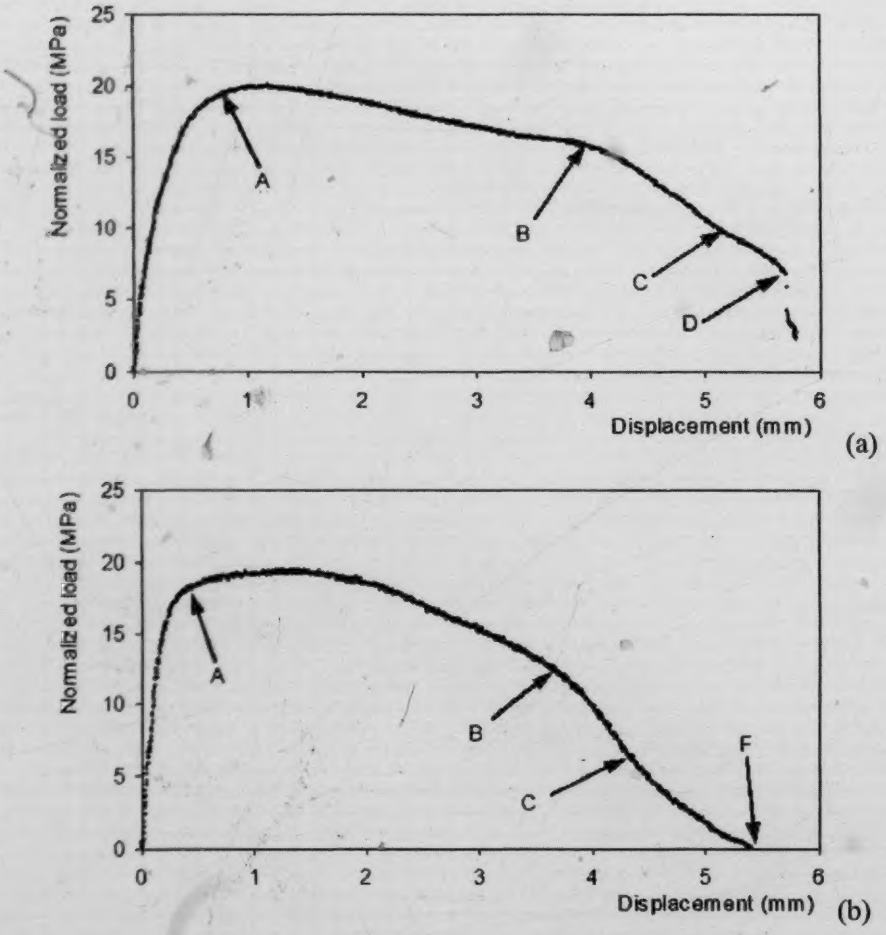

Fig. 6-4 Typical plots of normalized load versus displacement from the Iosipescu tests of HDPE specimens: (a) without the side grooves (having the original thickness of 6.25 *mm*), and (b) with the side grooves and ligament thickness of 4 *mm*.

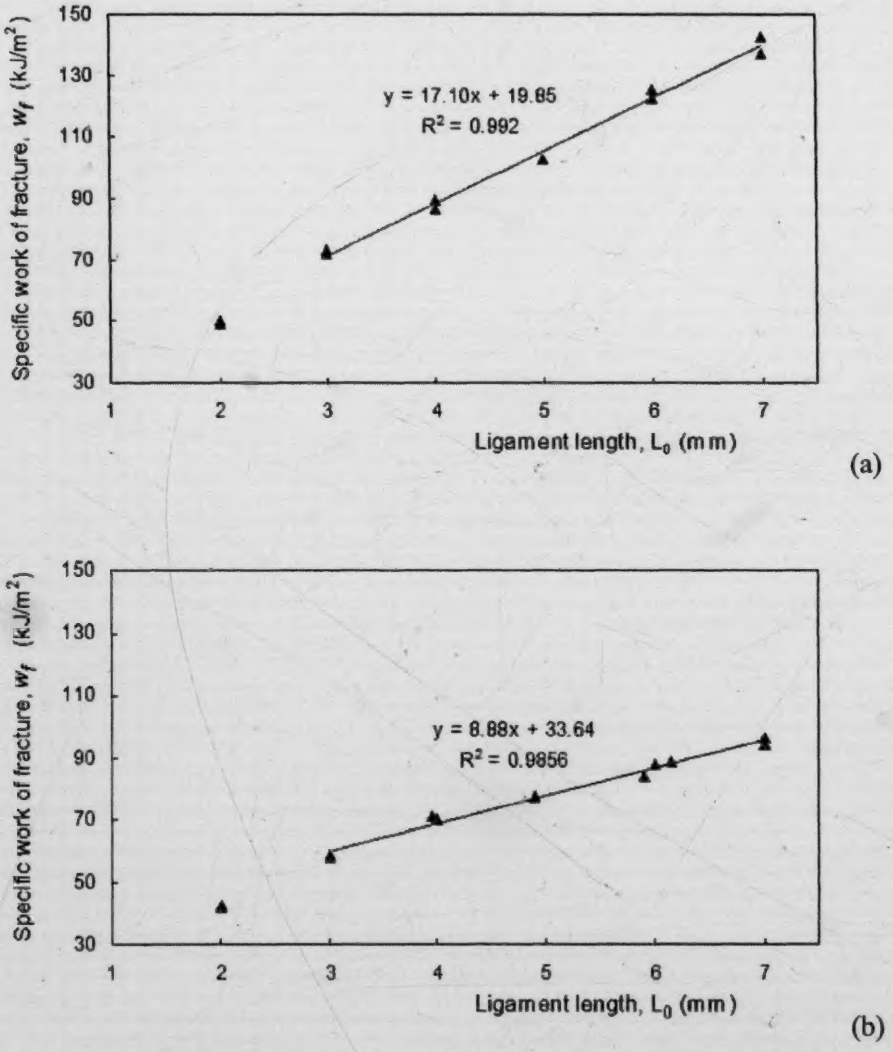

Fig. 6-5 Specific work of fracture as a function of ligament length: (a) from specimens without the side grooves (having the original thickness of 6.25 *mm*), and (b) from specimens with the side grooves and ligament thickness of 3 *mm*.

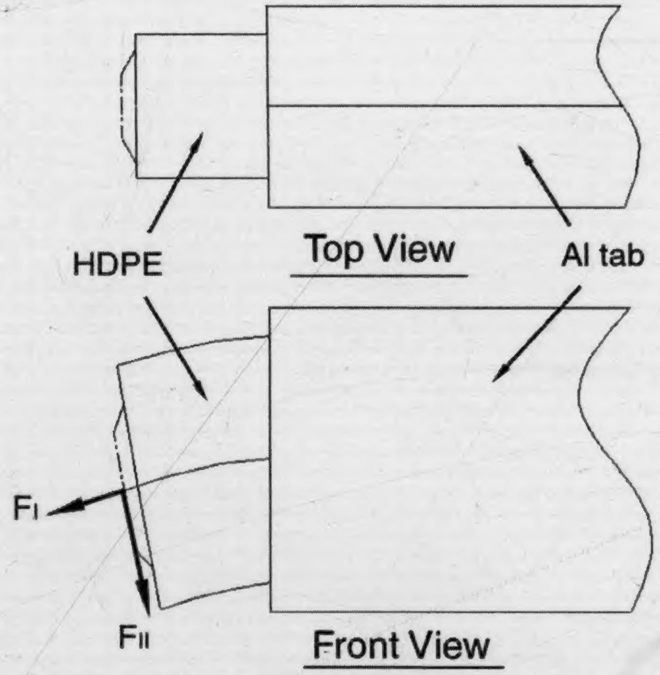
HDPE
Top View
Al tab
F$_I$
F$_{II}$
Front View

Fig. 6-6 Depiction of the bending motion of the right half of the DEN specimen during the Iosipescu test.

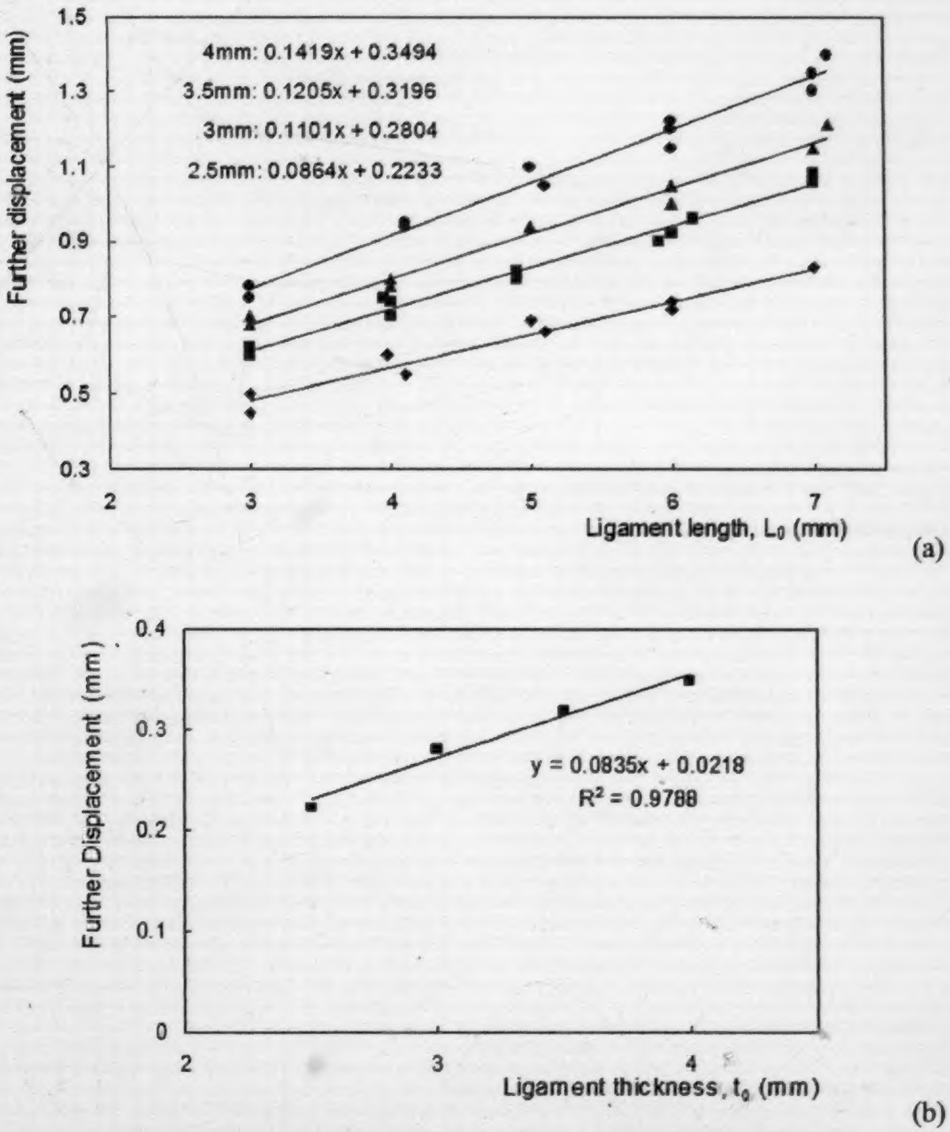

Fig. 6-7 Plots of the “further displacement”: (a) experimentally measured values versus the ligament length for specimens of different ligament thickness (ligament thicknesses: 4 *mm* (●), 3.5 *mm* (▲), 3 *mm* (■), and 2.5 *mm* (◆)), and (b) the extrapolated values from (a) at zero ligament length versus ligament thickness.

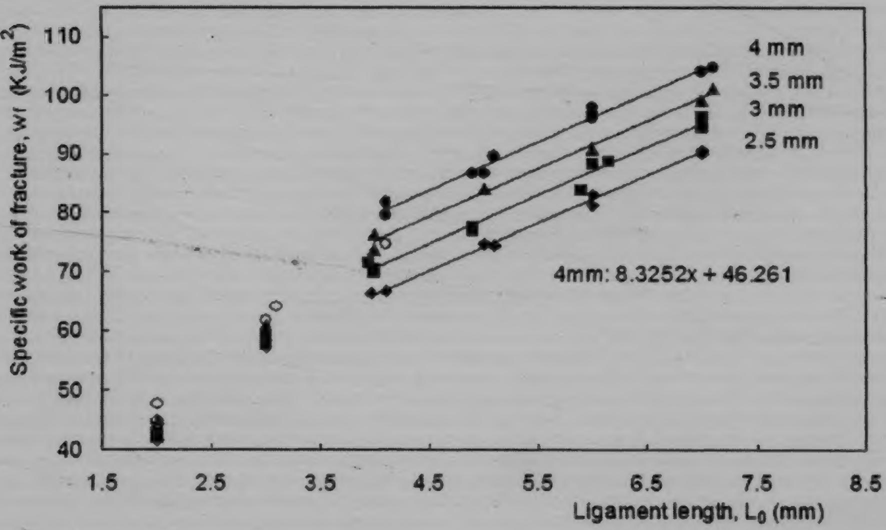

(a)

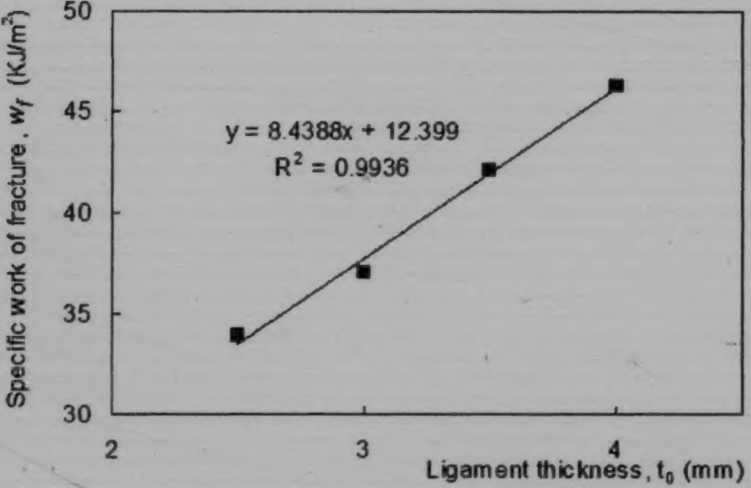

(b)

Fig. 6-8 Plots of the specific work of fracture (w_f) from specimens machined using a mill cutter of 60°: (a) experimentally measured values versus ligament length based on the total energy consumption (ligament thicknesses: 4 *mm* (●), 3.5 *mm* (▲), 3 *mm* (■), and 2.5 *mm* (◆)), and (b) the extrapolated values from (a) at zero ligament length versus ligament thickness.

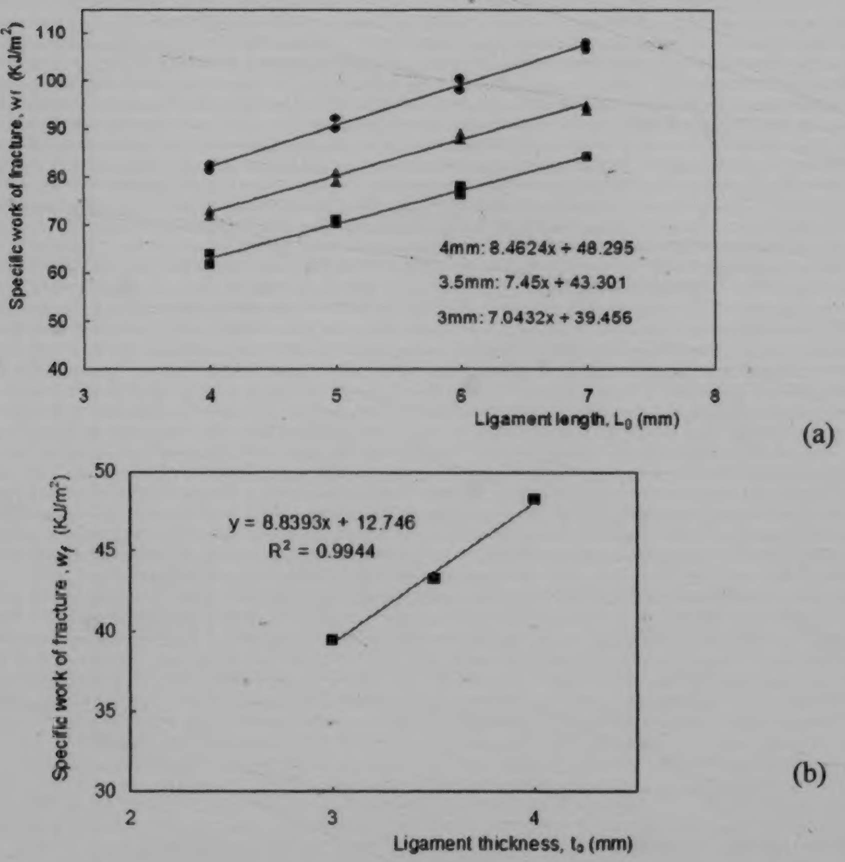

Fig. 6-9 Plots of the specific work of fracture (w_f) from specimens machined using a mill cutter of 90°: (a) experimentally measured values versus ligament length based on the total energy consumption (ligament thicknesses: 4 *mm* (●), 3.5 *mm* (▲), and 3 *mm* (■)), and (b) the extrapolated values at zero ligament length from (a) versus ligament thickness.

References

Atkins AG, Mai Y (1985) Elastic and Plastic Fracture. Ellis Horwood Limited, Chichester, UK

Broberg KB (1968) Critical Review of Some Theories in Fracture Mechanics. Int J Fract Mech 4: 11-17

Cotterell B, Reddel JK (1977) The essential work of plane stress ductile fracture. Int J Fract 13(3): 267-277

G'sell C, Jonas JJ (1979) Determination of the plastic behaviour of solid polymers at constant true strain rate. J Mater Sci 14(3): 583-591

Hill R (1952) On discontinuous plastic states, with special reference to localized necking in thin sheets. J Mech Phy Solids 1: 19-30

Hutchinson JW, Neale KW (1983) Neck propagation. J Mech Phys Solids 31(5): 405-426

Iosipescu N (1967) New accurate procedure for single shear testing of metals. J Met 2(3): 537-566

Karger-Kocsis J, Czigany T et al (1998) Deformation rate dependence of the essential and non-essential work of fracture parameters in an amorphous copolyester. Polymer 39(17): 3939-3944

Karger-Kocsis J, Barany T et al (2003) Plane stress fracture toughness of physically aged plasticized PETG as assessed by the essential work of fracture (EWF) method. Polymer 44(19): 5691-5699

Kwon HJ, Jar P-B (2006a) On the Application of Essential Work of Fracture Concept to Toughness Characterization of High-Density Polyethylene. Polym Eng Sci (Submitted)

Kwon HJ, Jar P-B (2006b) Toughness of High-Density Polyethylene in Plane-Strain Fracture. Polym Eng Sci 46(10): 1428-1432

Kwon HJ, Jar P-B (2005) Fracture toughness of polymers in shear mode. Polymer 46(26): 12480-12492

Li J, Zhang X et al (2004) J-M^p based criteria for bifurcation assessment of a crack in elastic-plastic materials under mixed mode I-II loading. Eng Fract Mech 71(3): 329-343

Mai Y, Powell P (1991) Essential work of fracture and J-integral measurements for ductile polymers. J Polym Sci 29(7): 785-793

Mai Y, Cotterell B (1987) The Essential Work of Plane Stress Ductile Fracture of Linear Polyethylenes. Polym Eng Sci 27(11): 804-809

Mai Y, Cotterell B (1986) On The Essential Work of Ductile Fracture in Polymers. Int J Fract 32(2): 105-125

Pardoen T, Hachez F et al (2004) Mode I Fracture of Sheet Metal. J Mech Phys Solids 52(2): 423-452

Ritchie RO, Knott JF et al (1973) On The Relationship Between Critical Tensile Stress and Fracture Toughness in Mild Steel. J Mech Phys Solids 21(6): 395-410

Saleemi AS, Nairn JA (1990) The plane-strain essential work of fracture as a measure of the fracture toughness of ductile polymers. Polym Eng Sci 30(4): 211-218

Sih GC, Paris PC et al (1961) Crack-tip, stress-intensity factors for plane extension and plate bending problems. In: ASME Meeting APMW-29, 28-30 Aug 1961

Theocaris PS (1989) Variations on the theme of fracture criteria. Eng Fract Mech 33(2): 205-214

Chapter 7

On the Application of FEM to the Deformation of High-Density Polyethylene

7.1 Introduction

It is well known that yield criterion for the plastic deformation can be expressed as:

$$f(\sigma_{ij}) = Y \tag{7.1}$$

where f represents the yield surface that is a function of stresses and Y the yield stress. The yield function f is mainly affected by the second principal stress invariant J_2. The following yield function has been applied to isotropic materials:

$$f(J_2) = \sqrt{3J_2} \tag{7.2}$$

Once the correct yield stress Y is known, the above equation can be used to determine the stress states for yielding. Value of Y is usually determined using uni-axial tensile test, with

---

** A version of this chapter has been submitted. International Journal of Solids and Structures (Aug. 2007).

the assumption that the stress state in the gauge section is uni-axial, thus the true axial stress is equivalent to the effective stress. This paper will show that this assumption is not applicable to large deformation that involves work hardening, because its *Y* may not show isotropic increase with different stress components.

Deformation studied in this paper is for high-density polyethylene (HDPE) that often involves stable necking when subjected to tensile stress. Stable necking in HDPE has been commonly observed in uni-axial tensile (UT) test (G'Sell and Jonas, 1979; Kwon and Jar, In Press; Neale and Tugcu, 1985), which is an indication of sufficient compensation for cross section reduction by the work-hardening-induced strength increase. The behaviour has been extensively studied at both microscopic and macroscopic levels (Buckley and Costas, 2004; Coates and Ward, 1978; Coates and Ward, 1980; G'Sell and Jonas, 1979; G'Sell et al., 1983; G'Sell et al., 1992; Gaucher-Miri et al., 1996; Ginzburg, 2005; Haward and Thackray, 1968; Haward, 1987; Haward, 1993; Hiss et al., 1999; Hutchinson and Neale, 1983; Marquez-Lucero et al., 1989; Mimaroglu, 1995; Neale and Tugcu, 1985; Peterlin, 1971; Peterlin, 1987; Seguela and Darras, 1994; Tugcu and Neale, 1987a; Tugcu and Neale, 1987b; Tugcu and Neale, 1988; Van Dommelen et al., 2003; Van Dommelen et al., 2004). The true axial stress-strain curve for the stable necking is usually determined using curve-fitting techniques, such as Gaussian (Haward and Thackray, 1968; Haward, 1987; Haward, 1993) or exponential functions (G'Sell and Jonas, 1979; G'Sell et al., 1983; G'Sell et al., 1992), and has been used as the input for finite element method (FEM) to simulate the ductile deformation process (G'Sell et al., 1992; Marquez-Lucero et al., 1989; Neale and Tugcu, 1985; Tugcu and Neale, 1987a; Tugcu and Neale, 1987b; Tugcu and Neale, 1988). However, necking often generates a tri-axial stress state (G'Sell et al., 1983; Neale and Tugcu, 1985), with the possibility that stress along the loading direction being very different from the effective stress. As a result, FEM simulation based on the conventional approach in which the axial stress is treated as an approximation of the effective stress, cannot reproduce the observed deformation behaviour. This paper will show that the axial yield stress determined from the UT test should not be used as an approximation for *Y* in the FEM simulation.

In addition to the above problem, this paper will point out that in order to simulate large deformation behaviour of HDPE, the isotropic yield function given in Eq. (7.2) should be modified. The modification is to distinguish the roles of normal and shear stresses on the work-hardening behaviour, and is based on the concept that the expansion of yield surface by work hardening in the shear stress direction is less significant than that in the normal stress direction.

First part of this paper is to describe the approach we proposed to determine *Y*, in order to reconcile the difference between simulation and experimental results. Review of literature on relevant studies will be provided, followed by a case study that compares FEM simulation of HDPE deformation with the experimental observation from the UT test, to point out the source of inconsistency generated by the conventional approach. That is, axial yield stress is used as the approximation for the effective yield stress in the FEM simulation. A simple iterative process will be described to accurately determine the effective yield stress for the FEM simulation of the UT test.

The second part of the paper will propose an approach to determine the anisotropic expansion of the yield surface in the necking process. The approach will be verified by simulating deformation behaviour of HDPE in double-edge-notched tensile (DENT) test, in which necking is accompanied by crack propagation. The verification will be based on previous experimental results, and show that the proposed modification of using anisotropic yield function can successfully simulate the load-displacement curve and the deformation behaviour observed in the experiment.

It should be noted that simulation of the DENT test has been attempted before, but using a 2-dimensional model (Chen et al., 1999). Since nature of the necking process involves inhomogeneous variation in the 3rd dimension, the 2-D model could never mimic the necking process.

7.2 Literature Review

7.2.1 Large deformation of materials and its constitutive equations

Mechanisms for large deformation of semi-crystalline polymers like HDPE have been studied extensively in the past. Peterlin (1971) proposed a three-stage deformation process that involves plastic deformation of the original spherulitic structure, transformation of the spherulites to fibril structures by micro-necking, and plastic deformation of the fibril structure; but all three stages may contribute to the global necking phenomenon. Hiss et al. (1999) studied the true stress-strain behaviour of various polyethylenes and related copolymers, and found that deformation at small strain mainly occurred in the amorphous inter-crystalline layers through inter-lamellar shear slips. Deformation at large strains, on the other hand, is attributed to crystallite fragmentation and chain disentanglement. Increase of work-hardening was observed with the increase of the strain rates, crystallinity and network density.

With an appropriate combination of temperature and strain rate the neck development can become a stable process, that is, it propagates to the neighboring region in a steady fashion. This process is also known as "cold drawing" (Carothers and Hill, 1932) as the intrinsic deformation behaviour is the basis of film and fibre processing industries. Howard and Thackray (1968) proposed a micro-mechanical model to represent the large deformation of glassy thermoplastic polymers. Based on this model, Argon (1973) proposed a relationship between true stress and extension ratio in the large deformation:

$$\sigma = Y_0 + G_p(\lambda^2 - 1/\lambda) \tag{7.3}$$

where Y_0 is the initial tensile yield stress, λ the extension ratio defined as the ratio of deformed length to the original length, and G_p the strain hardening modulus. The same equation was also derived by Cross and Haward (1978), and showed good agreement with the experimental results for several thermoplastic polymers (Haward, 1987; Haward, 1993; Haward, 1995).

In a slightly different approach, G'Sell and Jonas (1979) proposed an empirical constitutive equation that separates the effect of strain hardening from that of viscosity when deformation occurs at a constant strain rate. The equation was later modified by Hutchinson and Neale (1983), in which the part relevant to the strain hardening can be expressed as:

$$\sigma = \begin{cases} \alpha k \varepsilon^{N} & \textit{for} \quad \varepsilon \le \varepsilon_0 \qquad \text{(7.4a)} \\ k \exp(M\varepsilon^{\beta}) & \quad\quad\;\; \varepsilon \ge \varepsilon_0 \qquad \text{(7.4b)} \end{cases}$$

where k, ε_0 and M are material constants. Value of β is suggested to be 2 for HDPE at a constant strain rate, and values of N and α determined by imposing stress continuity at

ε_0. Based on the above equations, true stress-strain curves have been reported for several thermoplastic polymers, including polyethylene of different grades (Buckley and Costas, 2004; G'Sell et al., 1983; G'Sell et al., 1992; Marquez-Lucero et al., 1989; Tugcu and Neale, 1987a; Tugcu and Neale, 1987b; Tugcu and Neale, 1988). It should be noted that all expressions in Eqs. (7.3-4) are based on strain measurement using the change of cross section where neck initiation occurs.

7.2.2 Numerical simulation on cold drawing of semi-crystalline polymers

Simulation of large deformation in polymers has been attempted by many researchers in the past. Neale and Tugcu (1985) carried out FEM analysis for neck initiation and steady-state neck propagation in a cylindrical tensile specimen. The stress-strain relationship given in Eq. (7.4) was adopted for the study, with the addition of a relationship between stress and strain in the elastic region. Isotropic-hardening J_2 flow theory was employed, with the assumption that elastic-plastic deformation is independent of the strain rate. The study presented a relationship between the loading curve and the change of specimen profile, but the computed load was not compared with the experimental data.

Fager and Bassni (1986) performed a similar study for a plane-strain condition based on the J_2 flow theory, assuming isotropic, rate-independent plastic deformation. They presented the load-elongation curve, deformation shape and tri-axial stress distribution generated by the FEM model. Again, the load was not compared with the experimental values, only stating that they are qualitatively in close agreement.

Since then, many FEM studies have been carried out for axi-symmetric (Tomita et al., 1990) and plane-strain neck propagation (Tugcu and Neale, 1987b). Strain rate sensitivity (Tugcu and Neale, 1987a; Tugcu and Neale, 1987b; Tugcu and Neale, 1988) and kinematic hardening (Tugcu and Neale, 1987b) were also investigated. In addition, Tugcu (1995) considered the effect of heat conduction during the cold drawing process on the deformation behaviour of elastic-thermo-visco-plastic materials. Unfortunately, none of these studies showed a clear consistency in the load-elongation curve between the simulation and the experiment. As to be discussed later in detail, source for the inconsistency is that the studies ignored the tri-axial stress state in the necked region and assumed isotropic yielding during the neck development.

A well known micromechanical model, originally proposed by Boyce et al. (1988), was often adopted in FEM analysis to predict the true stress-strain relationship in glassy polymers. The results were found to be in good agreement with experimental data (Arruda and Boyce, 1993; Wu and Giessen, E., 1993). Based on this model, Wu and Giessen (1995) studied neck initiation and propagation of glassy polymers in tensile deformation. Unfortunately, the simulated load-elongation curve was not evaluated by comparing with the experimental data.

Very recently, Masud (2005) used a 3-D FEM model to simulate neck propagation in ductile deformation of polymers. The study compared the strain variation with the simulation results published in refs. (Neale and Tugcu, 1985; Tomita and Hayashi, 1993), but again not with any experimental data.

The above review clearly shows that little work has been done to validate the FEM work using the experimental data, though such validation is critical for applications that rely on FEM for the deformation analysis. Two case studies presented in this paper will compare the simulation results with the experimental data, to show that material input parameters used in the past should be modified to reconcile the difference of results between the simulation and the experiment.

7.3 Uni-axial Tensile Test

Experimental method used in this study to determine the true stress-strain curve is the same as that used before (Kwon and Jar, In Press), i.e. through measuring the change of axial load and specimen width at the neck initiation section. Test details are described in Appendix A. A typical engineering stress-elongation curve from the UT test is presented in Fig. 7-1(a). The peak load at which neck is initiated corresponds to 25 MPa (point A) and the stable load for neck propagation to 16.3 MPa (point B). Since many papers are available in the literature to describe the neck development process in relation to the load-elongation curve (G'Sell and Jonas, 1979; G'Sell et al., 1983; Kwon and Jar, In Press; Marquez-Lucero et al., 1989), its details for HDPE are omitted here.

7.3.1 Determination of yield stress based on the traditional approach

Most studies in the past assume that gauge section of a UT specimen is subjected to a uni-axial stress state and that stress and strain distributions are uniform on the cross section. Therefore, the true axial stress that is determined based on the change of the cross section is regarded as equivalent to the von Mises stress (also known as the effective stress which has been widely used as a criterion for yielding of ductile materials (Hill, 1952)). Traditionally, functions that fit the true stress-strain curve so determined, such as that shown in Fig. 7-1(b), are used as the input yield stress, $Y(\varepsilon)$, for the FEM analysis. This paper will show that such a yield stress does not represent the true yield stress for HDPE when necking occurs. In this section, we applied the traditional approach to our own UT test data for HDPE, to demonstrate the discrepancy it causes between simulation results and experimental data.

Following the traditional approach, stress and strain in Eqs. (7.2a and 7.2b) are used to fit the part of the curve in Fig. 7-1(b) after neck is initiated. For the section of the curve before the neck initiation, the Hookean equation is used for the linear region (Neale and Tugcu, 1985; Tugcu and Neale, 1987a; Neale and Tugcu, 1988) and a slightly modified version of Ogden's equation (Ogden, 1972) for the following non-linear section but before the neck initiation. Those equations are combined as the strain function of the yield stress, $Y(\varepsilon)$, for the input to the FEM model. That is,

$$Y(\varepsilon) = \begin{cases} E\varepsilon & (\varepsilon \le \varepsilon_y) \\ d[a(\varepsilon+b)^{(c-1)} - (a(\varepsilon+b)^{-c}] + e & (\varepsilon_y \le \varepsilon \le \varepsilon_n) \\ \alpha k \varepsilon^N & (\varepsilon_n \le \varepsilon \le \varepsilon_t) \\ k\exp(M\varepsilon^n) & (\varepsilon \ge \varepsilon_t) \end{cases} \tag{7.5}$$

where the constants for HDPE used here are presented in Tables 1 and 2.

Although n value in Eq. (7.5) was suggested to be 2 by G'Sell and Jonas (1979), it was found to be 1.8 for HDPE used here, in order to provide the best-fit to the test data, especially with strain larger than 1.0. Fig. 7-1(b) also suggests that when the axial strain in the neck, determined from the change of the cross-sectional width, reaches around 1.8, neck propagation to its neighboring regions starts. At this stage, the necked section became very rigid due to the formation of fibrils in the loading direction. The final fracture occurred in a brittle manner after the neck has been developed in the whole gauge length, but often at a section that was not where the neck was initiated.

7.3.2 Numerical simulation based on the traditional approach

Using a 3-D FEM model (ABAQUS 6.5 Standard), neck initiation and propagation was simulated as a rate-independent deformation process, following the traditional approach as the input of material properties. The model is shown on the left of Fig. 7-2(a), consisting of 2660 20-node brick elements, in which Cartesian coordinates are used with 1-, 2- and 3-axes in the directions of width, length and thickness, respectively. Incremental J_2 plasticity theory was employed, assuming that plastic deformation was isotropic. The yield stress $Y(\varepsilon)$ followed the expressions given by Eq. (7.5), with the constants determined by fitting to the axial stress-strain curve from the UT test. Details of FEM simulation are to be found in Appendix B.

Necking was initiated in the FEM model by reducing cross-sectional area at the middle of the gauge section (bottom of Fig. 7-2(a)) by 0.04%, as suggested by Neale and Tugcu (1985). Because of the geometrical symmetry, the model only corresponds to half length of a specimen with a quarter of the cross section. The overall deformed shape, as shown on the right of Fig. 7-2(a) that was taken at elongation of 50 mm, is very close to the deformation behaviour observed experimentally.

The nominal stresses determined from the tensile test and that generated by the FEM simulation are plotted as functions of elongation in Fig. 7-2(b). The section in the curve that corresponds to the neck initiation is very similar to the experimental data, particularly in terms of the peak load and the trend of load drop during the initial neck formation. However, the loading level during the neck propagation is around 18 MPa from the FEM model which is about 10% higher than the experimental value, 16.3 MPa. By setting n value in Eq. (7.5) to be 2, as suggested by G'Sell and Jonas (1979), the computed steady load raised to 19.25 MPa, moving further away from the experimental data.

To reconcile the above difference in loading level, possibility of the rate-dependent deformation process was considered, but later ruled out because previous studies had shown that this factor could not lower the steady loading level (Tugcu and Neale, 1987b; Tugcu and Neale, 1988). Possibility of the influence from visco-plasticity was also considered. However, this has already been factored into $Y(\varepsilon)$, as the timeframes for the simulation and the experiment were similar. Therefore, this should not be a major factor for the above discrepancy, either.

It is worth noting that the above discrepancy is common in the literature. For convenience in the discussion, load drop ratio (DR), defined as the ratio of the steady load for neck propagation to the peak load, is used here to compare results in the literature. The DR value from our experimental data, Fig. 7-2(b), is 65%, and 72% from the FEM simulation. Values of DR from the literature are summarised in Tables 3 and 4, from FEM and experimental studies, respectively. The two tables clearly show that DR values from the FEM simulation, ranging from 72 to 90% (Fager and Bassani, 1986; Neale and Tugcu, 1985; Tomita and Hayashi, 1993; Tugcu and Neale, 1987a; Tugcu and Neale, 1987b), are generally higher than those from the experiments, from 66 to 78% (G'Sell and Jonas, 1979; G'Sell et al., 1983; Hiss et al., 1999; Marquez-Lucero et al., 1989). Note that the highest experimental DR value in Table 4 (78%) corresponds to a load-displacement curve determined at a constant strain rate. If the test were conducted at constant cross-head speed, the DR value would have been lower.

It should also be noted that the FEM studies in refs. (Neale and Tugcu, 1985;

Tugcu and Neale, 1987a; Tugcu and Neale, 1987b) referred to the same experimental data provided in ref. (G'Sell and Jonas, 1979). Therefore, the FEM studies would have generated a DR value similar to that determined from the experiment if a correct FEM model was used. Since the DR values between Tables 3 and 4 are clearly different, the comparison suggests that the above FEM simulations had some misconception.

The potential misconception in the previous simulation work was investigated by constructing the axial (true) stress-strain curve based on load and width changes of the FEM model, in a way like a virtual UT test using FEM. Since the true stress and strain in Fig. 7-1(b) were calculated based on the variation of specimen width, the same scheme was used to determine the strain values in the deformed FEM model. The true stress-strain curve so generated is compared with experimental data in Fig. 7-2(c). The figure suggests that the two curves are quite consistent in the low strain range, up to a strain value of about 1.8 which corresponds to the width reduction of about 60%. Note that this was the maximum width reduction observed in the experiments during the neck propagation. The maximum width reduction achieved in the FEM model, on the other hand, was around 70%, corresponding to a strain nearly 2.4. The difference is also reflected by the highest axial stress generated in the neck before its propagation to the neighboring regions, which was 105 MPa from the experiments and 190 MPa from the FEM simulation. When stable neck propagation was about to occur at constant load, the axial stress in the experiment reached a value of 105 MPa at a strain value of 1.8. For the FEM model, the axial stress reached a value of about 190 MPa at a strain value of about 2.3. This significant difference is believed to be the cause of high steady load from the FEM model, which may have been originated from the assumption of a uni-axial stress state in the neck. We believe that if transverse normal and shear stresses were considered, the input of effective yield stress could be different, possibly leading to the generation of a loading curve that is consistent with the experimental data. This idea has been examined, as presented in the next section.

7.3.3 Uni-axial tensile tests

To explain the difference between the two curves in Fig. 7-2(c), and the associated width reduction and loading level for neck propagation, additional experimental UT tests were conducted with a special attention to the width change in cross sections at different distances from the neck-initiation section. Test details are described in Appendix A. Figs. 7-3(a) and 7-3(b) summarize the variation of axial strains and stresses, respectively, as functions of time based on the width change at various cross sections of the specimen. Arrow in each figure indicates the direction for increase of the distance from the neck initiation section. Combining Figs. 7-3(a) and 7-3(b) produces axial stress-strain relationships at various sections, as shown in Fig. 7-3(c). The figure suggests that all axial stress-strain curves from locations away from the neck initiation section converge into one, except the initial "hump" that represents the transition period from the neck initiation to its propagation to the cross section where the strain was measured. Fig. 7-3(c) shows that all lower curves merge with the upper curve at an axial strain around 1.5.

Strain variation similar to that shown in Fig. 7-3(a) was also reported in refs. (G'Sell et al., 1983; Peterlin, 1971) but without further discussion, except stating that the axial stress-strain relationships for sections at different distances from the neck-initiation section are not identical (Peterlin, 1971). Our explanation for the difference is presented in the following section.

7.3.4 Stress distribution inside the specimen

Validity of the assumption of uni-axial stress state is examined here using the FEM model. Since strain distribution is no longer uniform along the gauge length once the neck is initiated, stress distribution needs to be examined in the necked and un-necked sections. Fig. 7-3(a) shows that before the neck reaches a specific cross section, axial strain (based on the change of its width) at that cross section remained constant, at a value as low as 0.26. The corresponding stress distribution at this strain level in two locations (at neck initiation section and at a section of 3-mm away), as well as their stress distributions at two higher strain levels, 0.5 and 0.75, are summarized in Figs. 7.4-7.6. The following stress components were considered in the comparison: axial stress (S2), effective stress (Se), transverse normal stress (S1 in the width direction and S3 in the thickness direction), and shear stress (S12 and S23), according to the coordinates defined in Fig. 7-2(a).

Variation of the above stresses at the strain of 0.26 at the neck initiation section and 3 mm away is presented in Fig. 7-4(a) and 4(b) respectively, as functions of the distance from the centre of the cross section in the thickness (axis 3) and width (axis 1) directions. Fig. 7-4(a) shows that the stress distribution at the neck initiation is close to the assumption of uni-axial stress state. Values of S1 and S3 are very small, which result in Se being only slightly lower than S2. However, at 3 mm away, due to the presence of negative S1 and S3, Se becomes much higher than S2. It is the lower value of S2 than Se that caused the generation of lower curves in Fig. 7-3(c) at sections away from the neck initiation. The corresponding effective stresses at different cross sections, however, should follow the same relationship with the strain increase. Fig. 7-4 clearly shows that even at a low strain level of 0.26, the stress distribution on a cross section may not be uniform, with the possibility of significant stress variation from the centre towards the edges. This is consistent with that reported by G'Sell et al. (1983) about the variation of stress triaxiality on a cross section.

At the axial strain of 0.5, Fig. 7-5(a) shows that the difference between S2 and Se at the neck initiation section increased slightly, compared to that at the axial strain of 0.26, Fig. 7-4(a). However, at 3 mm away, Fig. 7-5(b), the trend of Se > S2 no longer exists. The data in Fig. 7-5 also suggest that the average S2 for a given cross section is higher than Se. This clearly illustrates the invalidity of the assumption that uni-axial stress state can still be applied when the neck is developed. Therefore, in the simulation of the neck formation process S2 cannot represent Se as the input to the FEM model. The use of S2 as Se is expected to result in overestimate of the work hardening involved in the deformation. We believe that this is why the two curves in Fig. 7-2(c) are very different in the high strain range.

It is worth mentioning that the general trend of S2 decreasing from centre to the edges on the cross section is reversed in Fig. 7-5(b) at about 3.7 mm along the width direction. This is possibly because the neck growth front at this stage is very close to the 3-mm-away section. As the drawing process involved in the neck formation could stretch the surface layer more than the core, the large deformation in the surface layer may have raised the S2 value so much to reverse the trend there.

Stress distribution by further deformation to an axial strain of 0.75 is presented in Fig. 7-6. At this stage the neck growth front has passed by the 3-mm-away section, resulting in its stress distribution getting closer to that at the neck initiation section. The results support the phenomenon shown in Fig. 7-3(c) that the lower curves eventually merge with the upper curve after the neck growth front passes through that section.

The above FEM analysis clearly suggests that when necking occurs, the stress state is no longer uni-axial, but in a complex tri-axial condition with the stress values varying significantly in the necking process. Therefore, the effective yield stress for the plastic deformation that involves the neck formation cannot be approximated by the axial stress. In the following section, a method is proposed to determine the effective yield stress using iterative FEM analysis.

7.3.5 Determining effective yield stress-strain curve

The proposed remedy for the inconsistency between simulation and experimental results in Fig. 7-2 is through an iterative correction method that determines the new yield stresses as the input for the i^{th} correction ($Se_{(i)}$) based on a correction factor that is the ratio of the average effective stress, $\overline{Se}_{(i-1)}$, to the average $S2$, $\overline{S2}_{(i-1)}$, in the $(i\text{-}1)^{th}$ correction. That is,

$$Se_{(i)} = Se_{(i-1)} \frac{\overline{Se}_{(i-1)}}{\overline{S2}_{(i-1)}} \qquad (6)$$

where $Se_{(i-1)}$ is the effective yield stress input for the $(i\text{-}1)^{th}$ correction. More information on the proposed scheme is given in Appendix B.

It is worth mentioning that the current study only required the correction process once to have the S2 value from the FEM (■) coincide with that determined experimentally (solid line), as shown in Fig. 7-7. The plot of *Se* versus strain in Fig. 7-7 (O) is the new effective yield stress that should be used as input to the FEM model. It should be pointed out that such an iteration procedure is needed only if the FEM model is to simulate large deformation in the necking process, as values of *S2* and *Se* are nearly identical in the small strain range, i.e. below a strain of 0.25.

The nominal stress-elongation curve from the FEM simulation, based on the genuine effective yield stress, is compared with the experimental curve in Fig. 7-8(a), with the corresponding change of axial strain versus elongation in Fig. 7-8(b). The figures suggest that results from the FEM simulation agree with the experimental data very well, especially in the neck-forming process.

7.4 Double-Edge-Notched Tensile Test

As mentioned in Introduction, FEM simulation of DENT test was used to investigate the anisotropic expansion of yield surface in the necking process. In contrast to most simulation work in the past that used isotropic yield functions such as Eq. (7.2), a simple anisotropic yield function was proposed for the FEM simulation, as to be presented in this section. To validate this function, a deformation process that involved both normal and shear stresses was needed, and was chosen to be DENT test which has been shown in the previous study on HDPE (Kwon and Jar, 2006; Kwon and Jar, In Press) that it generates significant necking in the ligament section before the fracture.

The necking process in the DENT test occurs in two stages. The first stage was for the neck inception in which the neck grew from the two notch tips through the whole ligament length. At the end of this stage, height of the neck between the two crack tips was relatively constant. The second stage was for the growth of the neck in the loading direction till the two crack tips met at the mid-point of the ligament. Note that crack growth maintained relatively constant through the whole fracture process (Kwon and Jar, In Press). As a result of simultaneous growth of neck and crack at the second stage, a deformation zone of triangular shape was formed which should also be generated by the FEM model if a correct yield function was used for the simulation.

7.4.1 Numerical simulation of the DENT specimen

There are only a few papers in the literature concerning FEM simulation of DENT test. Knockaert et al. (1996) used a 3-D FEM model of DENT test, based on classical J_2 plasticity theory with isotropic work hardening, to investigate the deformation behaviour of low carbon steel. Due to the limited ductility of the steel, the simulation was conducted only up to the peak load without any involvement of crack initiation or growth. As mentioned earlier, Chen et al. (1999) also attempted to simulate deformation of HDPE in the DENT test, with the consideration of crack growth based on crack tip opening angle (CTOA) criterion. A two-dimensional, plane-stress 2-D model was used to generate load-displacement curves of various ligament lengths. However, as pointed out by Knockaert et al. (1996), the 2-D model could not take into account the significant variation of through-thickness stress near the crack tip. In addition, the 2-D model could not generate the necking behaviour. Therefore, a 3-D model should be used.

The FEM model used in this study represents quarter of a full-sized DENT specimen with half thickness, i.e. width (W) of 45 mm, length (B) 130 mm, and thickness (t) 3.125 mm. Full ligament length (L_0) considered was in the range of 16 to 24 mm. These were shown to be the dimensions for plane-stress fracture of HDPE (Kwon and Jar, 2006). Loading was applied in a similar manner to that in the experiment, that is, uniform tensile displacement along the width in the specimen length direction, at a speed of 5 mm/min. The FEM model was developed using ABAQUS 6.5 Standard, as shown in Fig. 7-9, consisting of 1056 20-node brick elements. In the first attempt, the genuine effective yield stress developed in the previous section was adopted as the input to the FEM model, with the use of isotropic yield function J_2.

Crack growth in the FEM model was set at a constant speed starting at the maximum load, following the experimental observation (Kwon and Jar, In Press). Since the half ligament length in the model was divided into 10 sections, as shown in Fig. 7-9, crack growth was simulated by freeing the boundary condition of each section gradually from the notch tip to generate an average crack growth speed that was consistent with the experimental observation. Details of FEM simulation are given in Appendix B. Fig. 7-10 shows an example of the deformed DENT specimen after the crack has grown a distance of 40% of the ligament length.

Fig. 7-11 compares the experimental data (solid line) with the normalized load-displacement curve generated by the above FEM model (◊), based on the genuine effective yield stress determined in the previous section. Although the 10 divisions in the half ligament length might be insufficient to generate smooth crack growth and stress contours, the resulting load-displacement curve shows an acceptable level of smoothness. In the figure, Δ_y and Δ_f represent the displacements at the commencement of crack growth from the notch tip and that at the final fracture, respectively. Note that value of Δ_y was initially determined from the experimental data, but was later assigned as the displacement when the load drop occurred in the FEM model. This was because the two choices of Δ_y generated the same load-displacement curve.

Although the FEM-generated load-displacement curve in Fig. 7-11 shows a transition from the first to the second stage of the neck development, the transition occurs earlier than that observed in the experiment. In addition, the FEM model overestimated the loading level in the 2nd stage of neck growth in which the neck propagation was in the loading direction. Note that the computed loading level was even higher if the axial yield stress determined from the UT test was used. The inconsistency was possibly due to the resistance to deformation in the FEM model being higher than that occurred in the experiment. This speculation prompted the idea that normal and shear stresses may have had different roles on the work hardening. That is, the expansion of yield surface along normal and shear stress coordinates should be different. As to be discussed in section 4-2, a parameter is proposed to differentiate the roles of normal and shear stresses on the expansion of yield surface due to work hardening. Value of the parameter was varied in the study to fit the FEM-generated load-displacement curve to the experimental data.

7.4.2 Yield Function

In the case of isotropic work hardening, the yield criterion based on the J_2 plasticity theory (Neale and Tugcu, 1985; Tugcu and Neale, 1987a; Tugcu and Neale, 1987b; Tugcu and Neale, 1988) can be expressed in terms of normal and shear stresses as:

$$\frac{1}{\sqrt{2}}\left[(\sigma_{11}-\sigma_{22})^2+(\sigma_{22}-\sigma_{33})^2+(\sigma_{33}-\sigma_{11})^2+6(\sigma_{12}^2+\sigma_{23}^2+\sigma_{31}^2)\right]^{1/2}=Y \quad (7)$$

where Y is the effective yield stress. However, for semi-crystalline polymers such as HDPE, large deformation may introduce a different level of work hardening in the direction of normal and shear stresses. Therefore, Eq. (7.7) should be modified to reflect the anisotropic work-hardening.

A general form of anisotropic yield function is (Hill, 1950):

$$f = \left[F(\sigma_{22}-\sigma_{33})^2 + G(\sigma_{33}-\sigma_{11})^2 + H(\sigma_{11}-\sigma_{22})^2 + 2(L\sigma_{23}^2 + M\sigma_{31}^2 + N\sigma_{12}^2)\right]^{1/2} \quad (8)$$

where F, G, H, L, M, and N are parameters to characterize the state of anisotropy. These parameters can be expressed in terms of yield stress ratio R_{ij}, defined as the ratio of the non-zero stress component at non-isotropic yielding, $\overline{\sigma}_{ij}$, to the equivalent stress component in the case of isotropic yielding. For example, for simple tensile loading, $R_{11} = \overline{\sigma}_{11} / Y$ and for pure shear loading $R_{12} = \overline{\sigma}_{12} / \tau_Y = \sqrt{3}\dfrac{\overline{\sigma}_{12}}{Y}$, where Y is the normal stress and τ_Y the shear stress for isotropic yielding. In principle, those yield stress ratios can be obtained by mechanical testing of materials at different directions, but extremely difficult for large deformation. In this study, a simplified version of the above approach was adopted, which had all normal stresses act equal roles to the yield function, hence $F = G = H$ in Eq. (7.8). The same assumption was applied to the shear stresses, i.e. $L = M = N$. Furthermore, value of 1/2 was assigned to F, G, and H, and set L, M, and N to be functions of a single parameter R_s:

$$L = M = N = \frac{3}{2R_s^2} \quad (9)$$

The corresponding yield function is:

$$f = \frac{1}{\sqrt{2}}\left[(\sigma_{11}-\sigma_{22})^2 + (\sigma_{22}-\sigma_{33})^2 + (\sigma_{33}-\sigma_{11})^2 + \frac{6}{R_s^2}(\sigma_{12}^2 + \sigma_{23}^2 + \sigma_{31}^2)\right]^{1/2} = Y \quad (10)$$

R_s is an adjustable parameter of which value was varied to fit the FEM-generated load-displacement curve to the experimental data. Using Y determined from the UT test and $R_s < 1$, Eq. (7.10) implies that work hardening in the shear stress direction should be less significant than that in the normal stress direction.

A series of load-displacement curves from a FEM model of DENT specimen with ligament length equal to 20 mm, but different R_s values, are compared with the experimental curve (solid line) in Fig. 7-12. The comparison suggests that the best R_s value to fit the experimental curve in the neck propagation stage is about 0.67. Note that since the FEM simulation assumed anisotropic yielding in the whole range of displacement, instead of a more realistic, progressive transition from isotropic to anisotropic yielding with the increase of the displacement, the load in the neck inception stage varied in an opposite trend to that in the neck propagation stage. That is, while the simulated load in the neck propagation stage approached the experimental values when R_s reduced from 1 to 0.67, difference of the load in the neck inception stage increased. This could be fixed by decreasing the R_s value gradually from 1 with the increase of the displacement. However, dependence of R_s on the extent of deformation is not clear at this stage.

7.4.3 Simulation scheme for DENT test

Because of the above problem, a simple simulation scheme was developed, as described here, to take into account the change of R_s during the test. In this scheme, R_s was assigned to be 1 before the maximum load was reached, after which the R_s value was changed to 0.67. Note that no additional experiment was carried out to determine Δ_y and Δ_f values for the FEM simulation. This was because load drop in the FEM simulation was found to be caused by the neck initiation at the notch tip, less dependent on the onset of the crack growth. Also, Δ_f value for a given ligament length could be determined by linear regression using previous experimental data, as its value showed a linear relationship with the initial ligament length (Kwon and Jar, In Press).

In the proposed simulation scheme, the displacement at the load drop was assigned to be Δ_y and crack was set to grow from the notch tip at this point, at a constant speed that allowed the crack growth to reach the centre of the specimen at the displacement Δ_f. More information on the proposed scheme is given in Appendix B.

Load-displacement curves generated by the above simulation scheme for ligament lengths of 16, 20 and 24 mm are presented in Fig. 7-13. The curves are compared with the corresponding experimental curves obtained previously (Kwon and Jar, 2006; Kwon and Jar, In Press). All curves show relatively good agreement with the experimental data.

Fig. 7-14 presents a deformed FEM model with half ligament length of 10 mm, after Δ_f is reached. The deformation behavior is very similar to that observed experimentally (Kwon and Jar, In Press), with a distinct triangular shape formed by simultaneous growth of neck and crack during the test.

The above approach of using different R_s values for deformation before and after the maximum load was reached, enabled us to simulate the deformation behaviour of HDPE in the DENT test. Further studies will be conducted to explore possibilities of simulating large deformation of HDPE in complex loading conditions, which may require the replacement of R_s by the yield stress ratios R_{ij}.

7.5 Conclusions

FEM simulation of large deformation of HDPE in UT and DENT tests has been conducted. The study showed that the conventional approach based on data from the UT test overestimated the stress and strain required for the neck propagation. The study proposes a simple iterative process to determine the effective yield stress for the FEM simulation. The study shows that by using this effective yield stress, the flow stress required for neck propagation can be predicted accurately.

The study also showed that the isotropic yield function based on J_2 plasticity deformation theory cannot be used to simulate large deformation involved in HDPE during the DENT test. A simple anisotropic yield function is proposed that distinguishes difference of normal and shear stresses in the work hardening process. The new function contains an adjustable parameter R_s of which value can be determined through curve-fitting to the experimental data. Based on the experimentally observed constant crack growth speed and the new anisotropic yield function, the study showed that large deformation in the DENT test can be simulated by the FEM model. The study successfully demonstrated the use of correct effective yield stress and yield function for FEM simulation of large deformation in HDPE, in both UT and DENT tests. The technique will be further investigated, which may lead to development of fracture criterion for HDPE in large deformation.

Figures

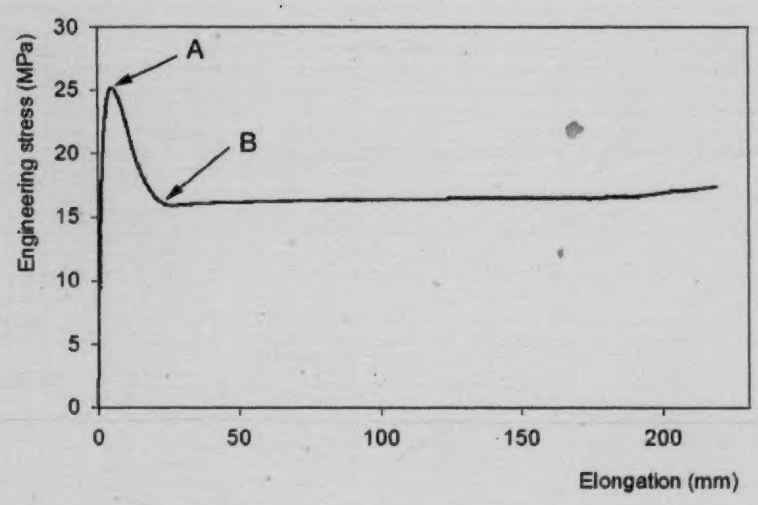

(a)

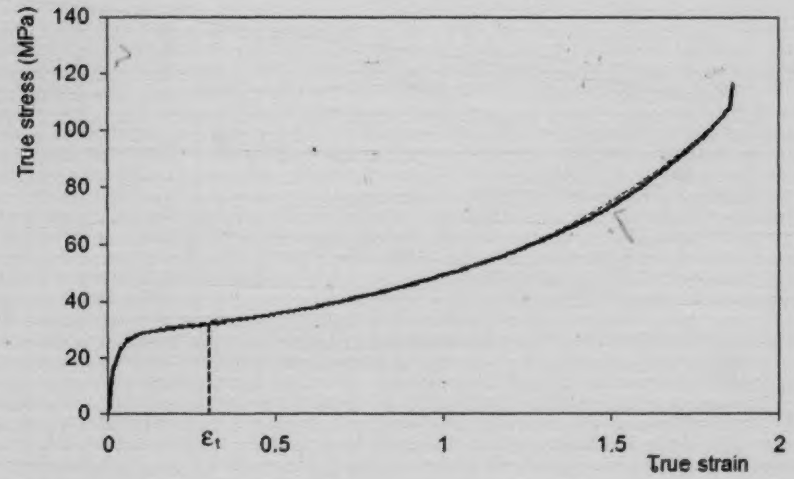

(b)

Fig. 7-1 Typical UT test results for HDPE: (a) Nominal stress-elongation curve, and (b) true stress-strain curve: test data (______) and trend curve from Eq. (7.2) with $n = 1.8$ (_ _ _).

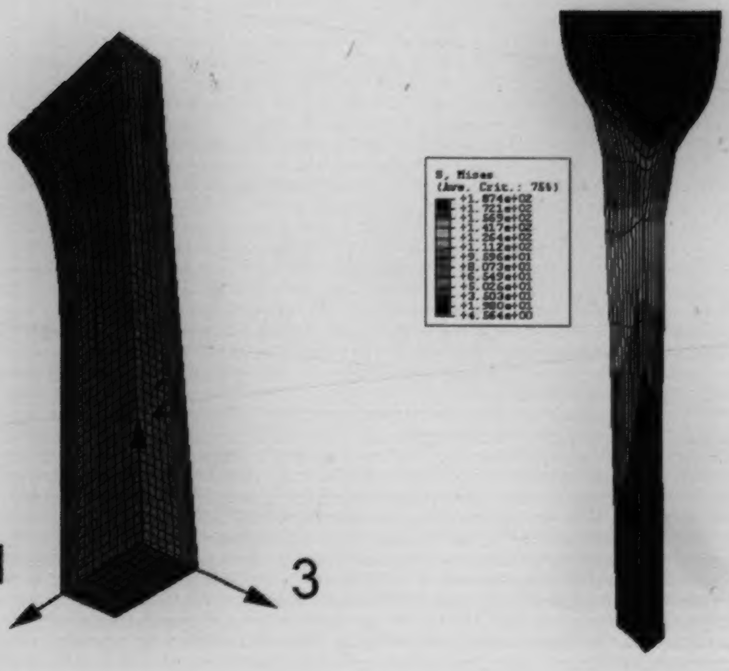
S, Mises
(Ave. Crit.: 75%)
+1.874e+02
+1.721e+02
+1.569e+02
+1.417e+02
+1.264e+02
+1.112e+02
+9.596e+01
+8.073e+01
+6.549e+01
+5.026e+01
+3.503e+01
+1.980e+01
+4.564e+00
1
2
3

(a)

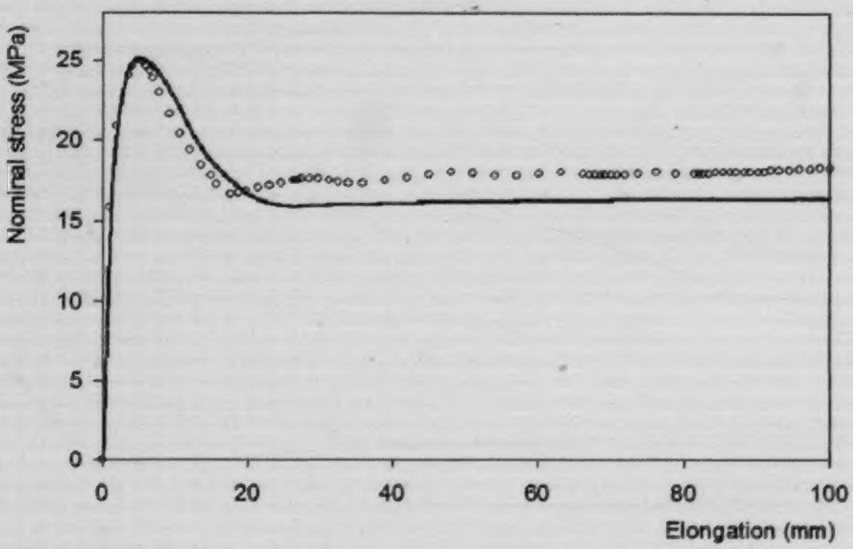
Nominal stress (MPa)
0
5
10
15
20
25
0
20
40
60
80
100
Elongation (mm)

(b)

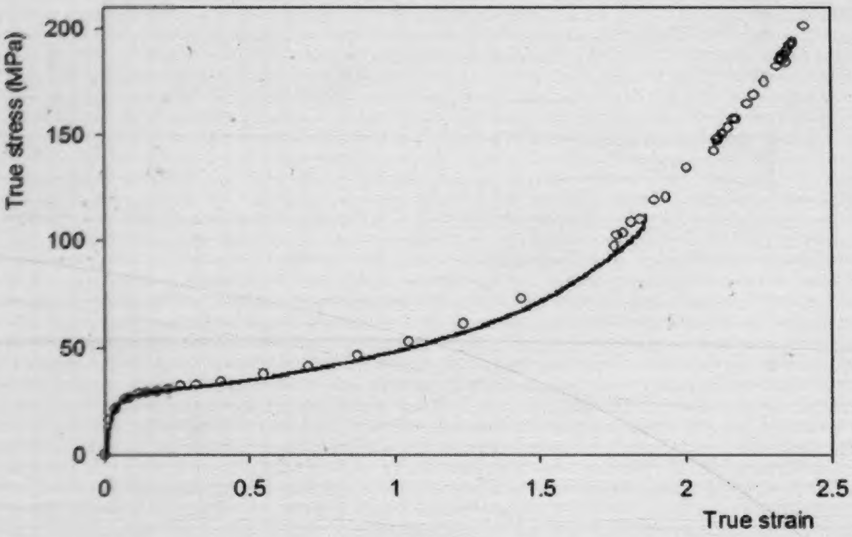

(c)

Fig. 7-2 Results of the FEM numerical simulation of UT test: (a) the un-deformed model and deformed model at elongation of 50 mm, (b) load-elongation curve, and (c) true stress-strain curve: solid line (——) from test data and “O” from the FEM simulation with $n = 1.8$.

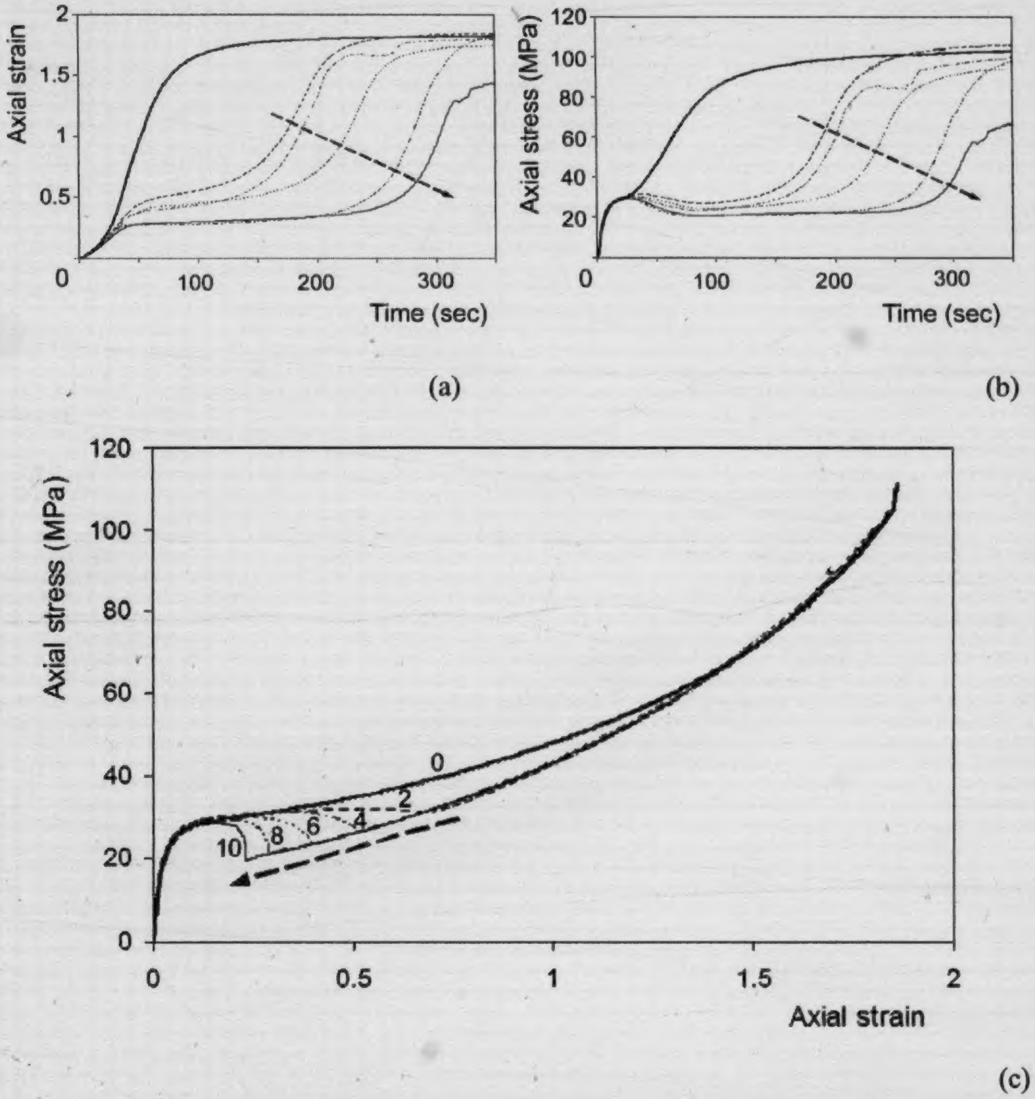

(a)

(b)

(c)

Fig. 7-3 UT test results: the plots of (a) axial strain, (b) axial stress and (c) stress-strain curves at the distance of 2 mm (_ _ _), 4 mm (_._.), 6 mm (----), 8 mm (_.._) and 10 mm (_____) from the neck initiation section. The arrows in the plots indicate the direction of the increase of the distance from the neck initiation section

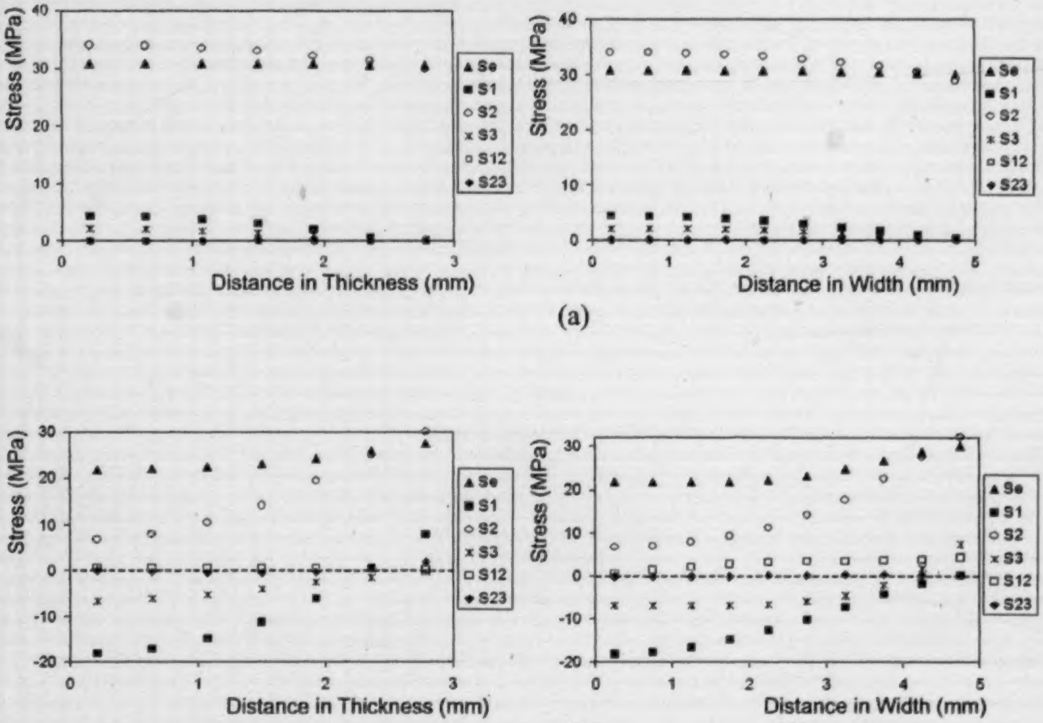

(a)

(b)

Fig. 7-4 Stress distribution at (a) axial strain of 0.26: at the neck initiation section; and (b) at 3mm away, in the thickness and width directions.

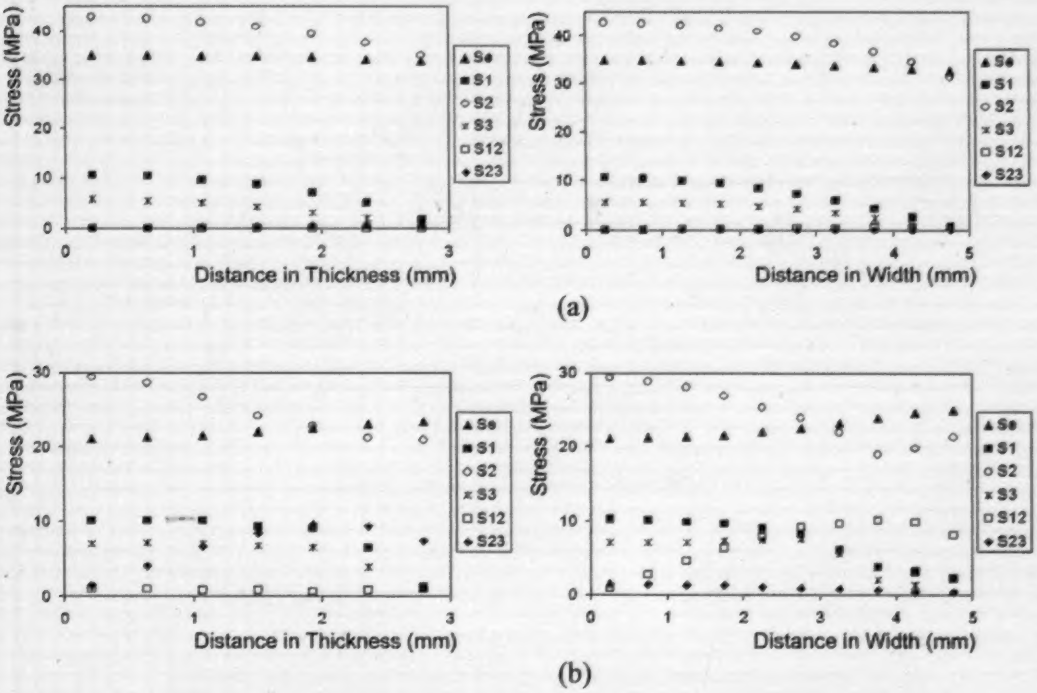

Fig. 7-5 Stress distribution at (a) axial strain of 0.5: at the neck initiation section; and (b) at 3mm away, in the thickness and width directions.

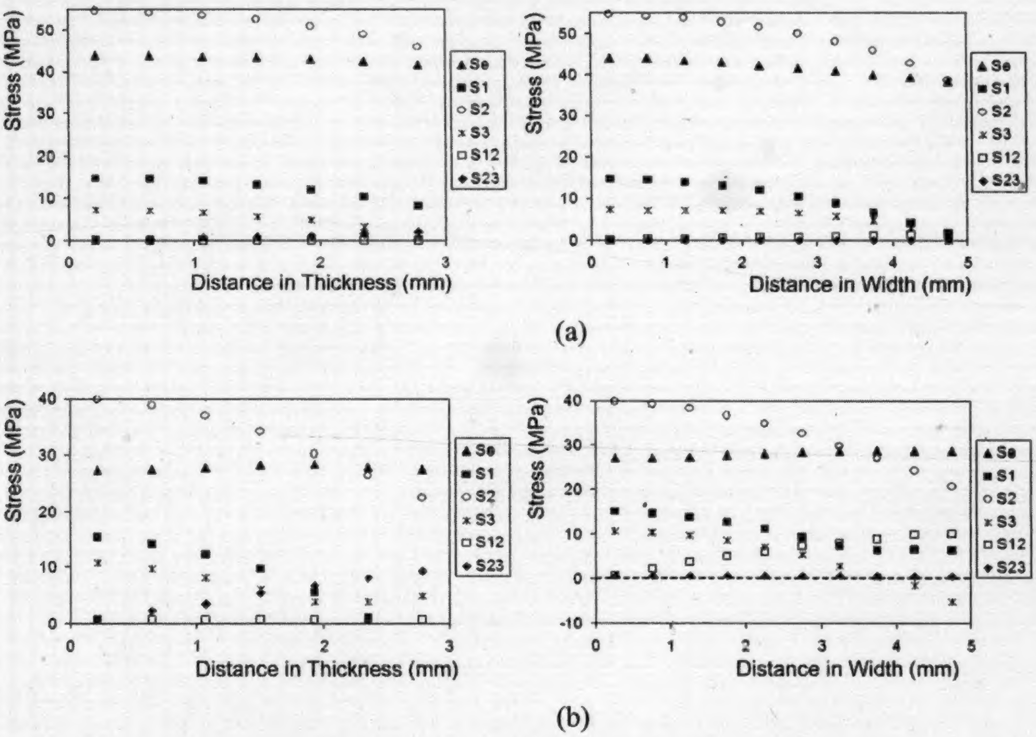

Fig. 7-6 Stress distribution at (a) axial strain of 0.75: at the neck initiation section; and (b) at 3mm away, in the thickness and width directions.

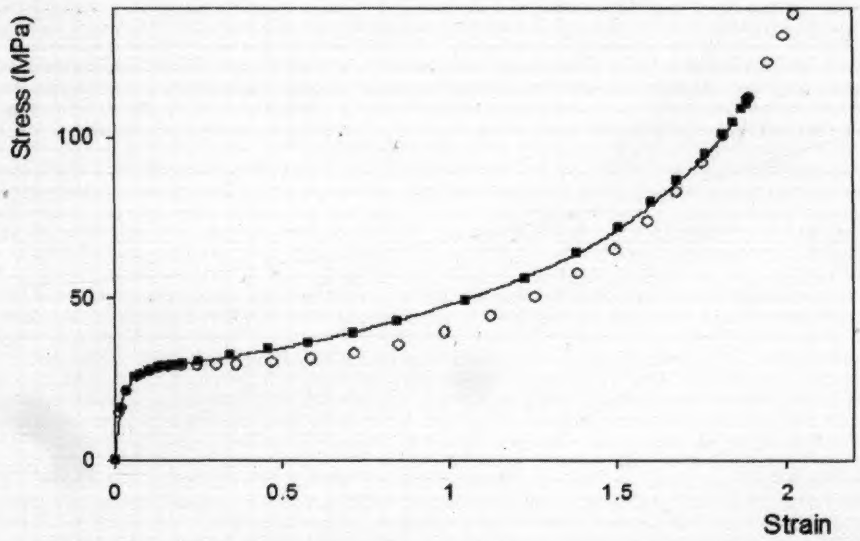

Fig. 7-7 S2 stress determined experimentally (———) and by FEM simulation (■) after one iteration. Data presented by (○) represent the effective yield stress function as input to the FEM model to determine S2 (■).

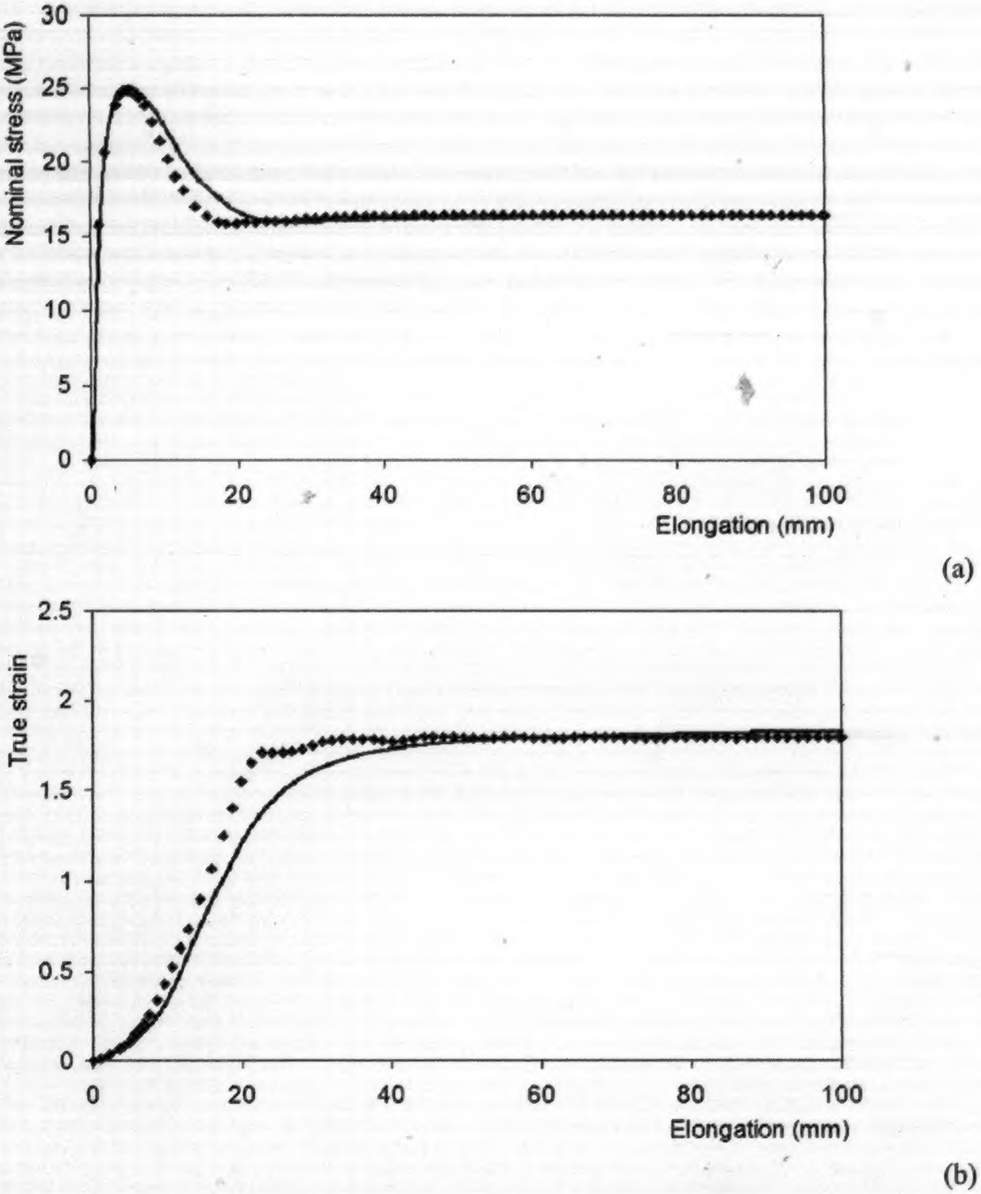

Fig. 7-8 (a) Load - elongation and (b) axial strain - elongation curves, from the experiment (____), and the FEM simulation after one iteration (◆).

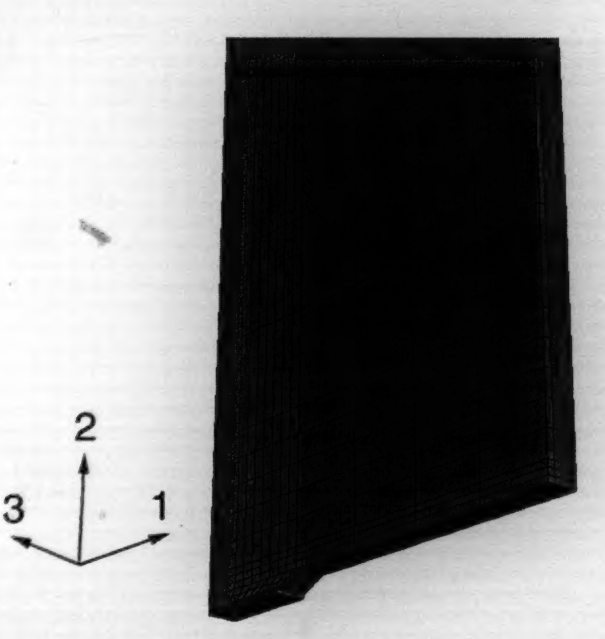

Fig. 7-9 The FEM model of DENT specimen with $L_0 = 20\ mm$.

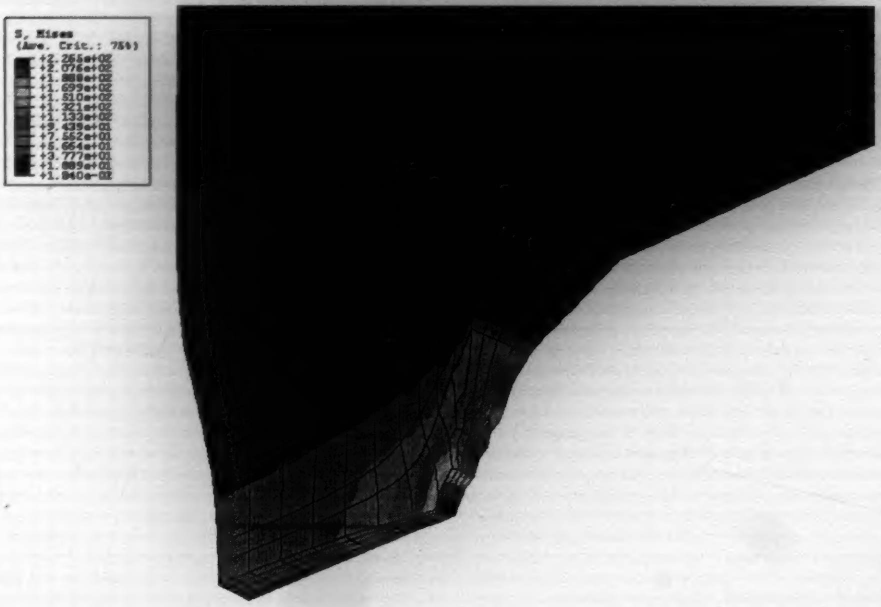
S, Mises
(Ave. Crit.: 75%)
+2.265e+02
+2.076e+02
+1.888e+02
+1.699e+02
+1.510e+02
+1.321e+02
+1.133e+02
+9.439e+01
+7.552e+01
+5.664e+01
+3.777e+01
+1.889e+01
+1.840e-02

Fig. 7-10 The deformation behaviour of DENT specimen after 40% of the half ligament length was debonded.

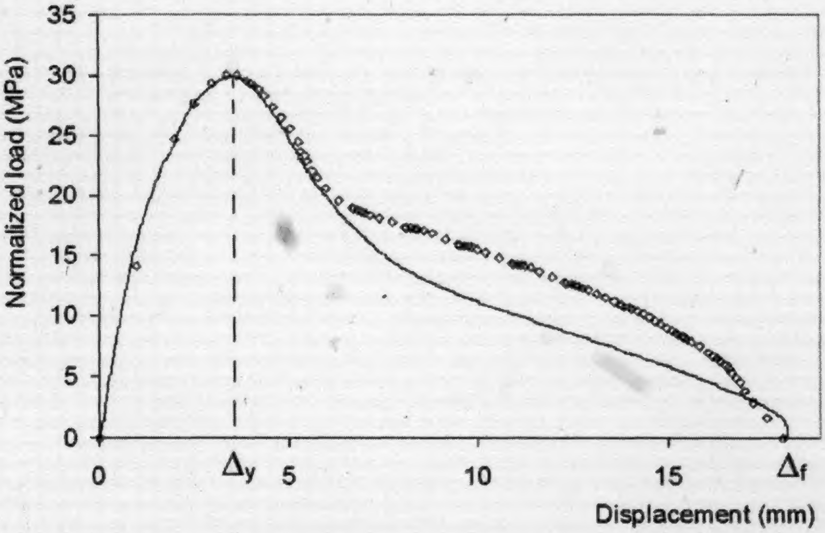

Fig. 7-11 Load-displacement curve for the DENT specimen with $L_0 = 20\ mm$, from the test (———) and FEM simulation (◊).

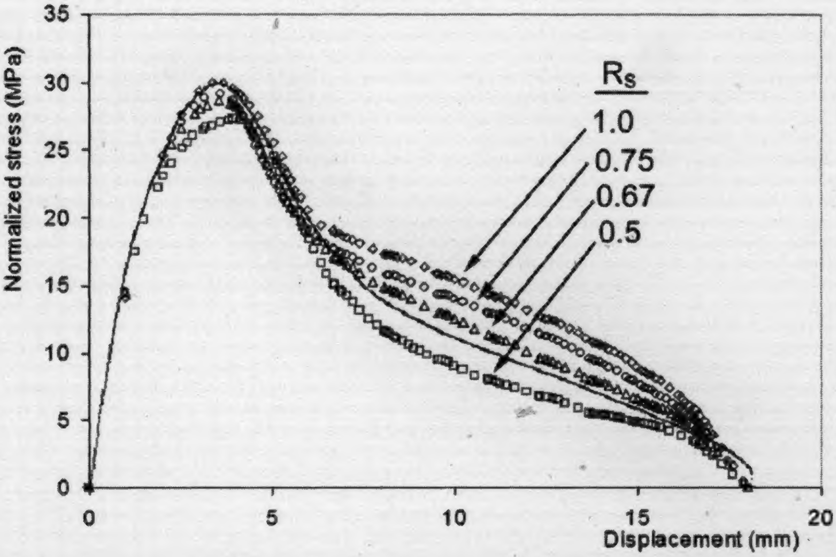

Fig. 7-12 Comparison of experimental curve of normalized load vs. displacement (solid line) with those determined from the FEM simulations with various R_s values.

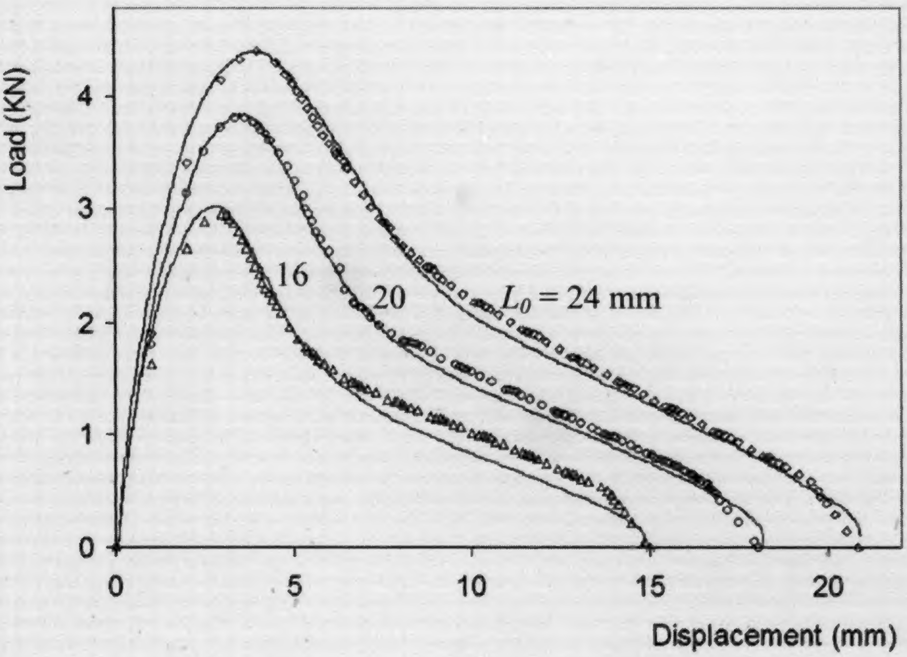

Fig. 7-13 Comparison of experimental curves (solid lines) with the FEM simulation for DENT tests with different ligament lengths (L_0):, $24\,mm$ (◊), $20\,mm$ (○), and $16\,mm$ (□).

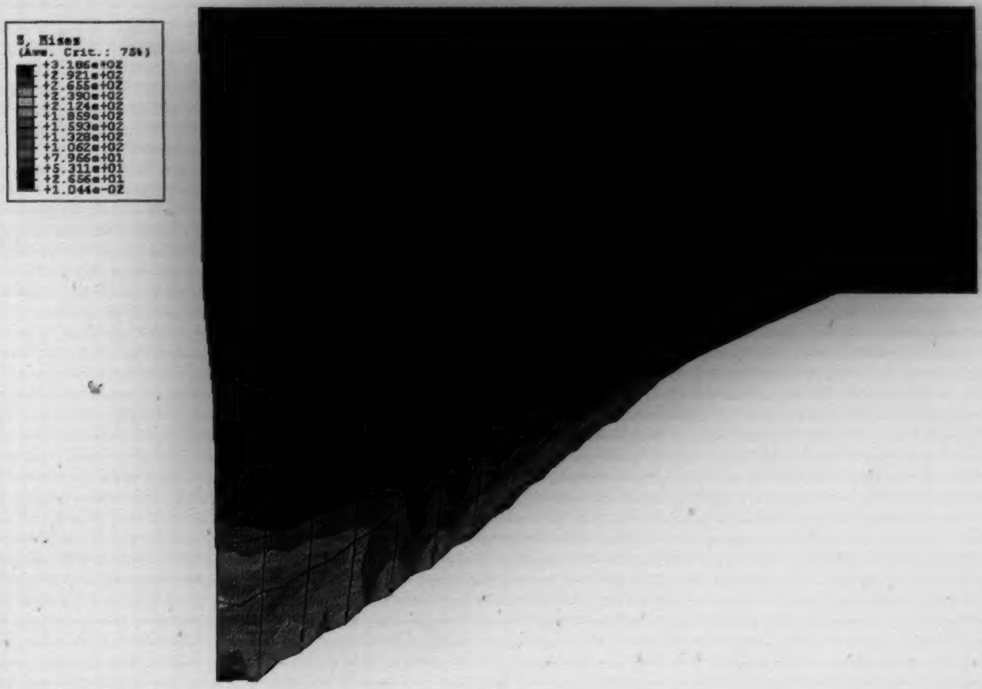
S, Mises
(Ave. Crit.: 75%)
+3.106e+02
+2.921e+02
+2.655e+02
+2.390e+02
+2.124e+02
+1.859e+02
+1.593e+02
+1.328e+02
+1.062e+02
+7.966e+01
+5.311e+01
+2.656e+01
+1.044e-02

Fig. 7-14 FEM model of DENT specimen after fracture (simulated using $R_s = 0.67$). The original half ligament length = 10 mm.

Tables

Table 7-1. Constants in Eq. (7.3) before necking.

Constant	E (*MPa*)	ε_y	ε_n	ε_t	*a*	*b*	*c*	*d* (*MPa*)	*e* (*MPa*)
Value	0.015	0.015	0.09	0.32	40.053	0.01	-0.156	-12.506	14.5

Table 7-2. Constants in Eq. (7.3) after necking.

Constant	αk	*N*	*k* (*MPa*)	*M*	*n*
Value	35	0.1	29.525	0.427	1.8

Table 7-3. Load drop ratio (DR) from the simulation.

Literature	DR	Condition
This study	72,77%	Rate independent (b=1.8, 2.0)
Neale & Tugcu, [3]	86%	Rate independent
Fager & Bassani [31]	82%	Rate independent, Plane strain
Tugcu & Neale [8]	90%	Rate independent, Plane strain
Tugcu & Neale [9]	83-86%	Plane strain visco-plasticity
Tomita,Y.; Hayashi,K. [41]	80%	thermo-elastic-viscoplastic

Table 7-4. Load drop ratio (DR) from the experiment.

Literature	DR	Condition
Experiment in this study	65%	Constant cross-head speed
G'Sell & Jonas [2]	66%	Constant strain rate
G'Sell, Aly-Helal & Jonas [7]	72%	Constant strain rate
Marquez-Lucero et al. [11]	68%	Constant cross-head speed
Hiss et al. [22]	78%	Constant strain rate

References

Argon, A.S., 1973. Physical basis of distortional and dilational plastic flow in glassy polymers. Journal of Macromolecular Science, Part B 8 (3 & 4) 573-596.

Arruda, E.M., Boyce, M.C., 1993. Three-dimensional constitutive model for the large stretch behavior of rubber elastic materials. Journal of the Mechanics and Physics of Solids 41 389.

Boyce, M.C., Parks, D.M., Argon, A.S., 1988. Large inelastic deformation of glassy polymers. I. Rate dependent constitutive model. Mechanics of Materials 7 (1) 15-33.

Buckley, C., Costas, M., 2004. Neck propagation in polyethylene. Journal of Polymer Science, Part B: Polymer Physics 42 (11 SPEC ISS) 2081-2091.

Carothers, W.H., Hill, J.W., 1932. Studies of polymerization and ring formation. XV. Artificial Fibers from Synthetic Linear Condensation Superpolymers. Journal of the American Chemical Society 54 1579-1596.

Chen, X.-H., Y.-W. Mai, L.-C. Zhang, , 1999. Numerical simulation of the essential fracture work method. In: Fracture of Polymers, Composites and Adhesives, ESIS Publication 27. Elsevier, Amsterdam, pp. 175-186.

Coates, P.D., Ward, I.M., 1980. Neck profiles in drawn linear polyethylene. Journal of Materials Science 15 (11) 2897-2914.

Coates, P.D., Ward, I.M., 1978. The plastic deformation behaviour of linear polyethylene and polyoxymethylene. Journal of Materials Science 13 (9) 1957-70.

Cross, A., N., H., R., 1978. Orientation hardening of PVC. Polymer 19 (6) 677-682.

Fager, L.O., Bassani, J.L., 1986. Plane strain neck propagation. International Journal of Solids and Structures 22 (11) 1243-1257.

Gaucher-Miri, V., Francois, P., Seguela, R., 1996. On the mechanisms of initiation and propagation of plastic instability in polyethylene under tensile drawing. Journal of Polymer Science, Part B: Polymer Physics 34 (6) 1113.

Ginzburg, B.M., 2005. On the "cold drawing" of semicrystalline polymers. Journal of Macromolecular Science - Physics B44 (2) 217-23.

G'Sell, C., Aly-Helal, N.A., Jonas, J.J., 1983. Effect of stress triaxiality on neck propagation during the tensile strectching of solid polymers. Journal of Materials Science 18 (6) 1731-1742.

G'Sell, C., Hiver, J.M., Dahoun, A., Souahi, A., 1992. Video-controlled tensile testing of polymers and metals beyond the necking point. Journal of Materials Science 27 (18) 5031-9.

G'Sell, C., Jonas, J.J., 1979. Determination of the plastic behaviour of solid polymers at constant true strain rate. Journal of Materials Science 14 (3) 583-591.

Haward, R.N., 1987. The application of a simplified model for the stress-strain curves of polymers. Polymer 28 (9) 1485-8.

Haward, R.N., 1993. Strain hardening of thermoplastics. Macromolecules 26 (22) 5860-5869.

Haward, R.N., 1995. The application of a Gauss-Eyring model to predict the behavior of thermoplastics in tensile experiments. Journal of Polymer Science, Part B (Polymer Physics) 33 (10) 1481-94.

Haward, R.N., Thackray, R., 1968. The use of a mathematical model to describe isothermal stress-strain curves in glassy thermoplastics. Proceedings of the Royal Society of London, Series A (Mathematical and Physical Sciences) 302 453-472.

Hill, R, 1950. The mathematical theory of plasticity. Oxford University Press, Oxford.

Hill, R., 1952. On discontinuous plastic states, with special reference to localized necking in thin sheets. Journal of the Mechanics and Physics of Solids 1 19-30.

Hiss, R., Hobeika, S., Lynn, C., Strobl, G., 1999. Network stretching, slip processes, and fragmentation of crystallites during uniaxial drawing of polyethylene and related copolymers. A comparative study. Macromolecules 32 (13) 4390-4403.

Hutchinson, J.W., Neale, K.W., 1983. Neck propagation. Journal of the Mechanics and Physics of Solids 31 (5) 405-426.

Kwon, H.J., Jar, P.-Y.B., 2006. Toughness of High-Density Polyethylene in Plane-Strain Fracture. Polymer Engineering and Science, 46 (10), 1428-1432.

Kwon, H.J., Jar, P.-Y.B., In Press. On the application of essential work of fracture concept to toughness characterization of High-Density Polyethylene. Polymer Engineering and Science.

Marquez-Lucero, A., G'Sell, C., Neale, K.W., 1989. Experimental investigation of neck propagation in polymers. Polymer 30 (4) 636-642.

Masud, A., 2005. A 3-D model of cold drawing in engineering thermoplastics. Mechanics of Advanced Materials and Structures 12 (6) 457-69.

Mimaroglu, A., 1995. Influence of material properties on solid phase forming behaviour of polymers. Materials & Design 16 (2) 67-74.

Neale, K.W., Tugcu, P., 1985. Analysis of necking and neck propagation in polymeric materials. Journal of the Mechanics and Physics of Solids 33 (4) 323-337.

Neale, K.W., Tugcu, P., 1988. Appproximate methods for analysing the cold drawing of polymeric fibres and films. International Journal for Numerical Methods in Engineering 25 99-112.

Ogden, R.W., 1972. Large deformation isotropic elasticity: on the correlation of theory and experimental for compressible rubberlike solids. Proceedings of the Royal Society of London, Series A (Mathematical and Physical Sciences) 328 (157) 567-83.

Peterlin, A., 1987. Drawing and extrusion of semi-crystalline polymers. Colloid and Polymer Science 265 (5) 357-382.

Peterlin, A., 1971. Molecular model of drawing polyethylene and polypropylene. Journal of Materials Science 6 (6) 490-508.

Seguela, R., Darras, O., 1994. Phenomenological aspects of the double yield of polyethylene and related copolymers under tensile loading. Journal of Materials Science 29 (20) 5342-5352.

Tomita, Y., Hayashi, K., 1993. Thermo-elasto-viscoplastic deformation of polymeric bars under tension. International Journal of Solids and Structures 30 (2) 225-35.

Tomita, Y., Takahashi, T., Shindo, A., 1990. Neck and bulge propagation in polymeric cylinders under internal pressure. International Journal of Mechanical Sciences 32 (4) 335-343.

Tugcu, P., 1995. Cold drawing of elastic-thermoviscoplastic polymeric films and fibres. Rheologica Acta 34 (3) 288-297.

Tugcu, P., Neale, K.W., 1988. Analysis of neck propagation in polymeric fibres including the effects of viscoplasticity. 110 (4) 395-400.

Tugcu, P., Neale, K.W., 1987a. Analysis of plane-strain neck propagation in viscoplastic polymeric films. International Journal of Mechanical Sciences 29 (12) 793-805.

Tugcu, P., Neale, K.W., 1987b. Necking and neck propagation in polymeric materials under plane-strain tension. International Journal of Solids and Structures 23 (7) 1063-1085.

Van Dommelen, J.A.W., Parks, D.M., Boyce, M.C., Brekelmans, W.A.M., Baaijens, F.P.T., 2003. Micromechanical modeling of intraspherulitic deformation of semicrystalline polymers. Polymer 44 (19) 6089-101.

Van Dommelen, J.A.W., Schrauwen, B.A.G., Van Breemen, L.C.A., Govaert, L.E., 2004. Micromechanical modeling of the tensile behavior of oriented polyethylene. Journal of Polymer Science, Part B (Polymer Physics) 42 (16) 2983-94.

Wu, P.D., Van der Giessen, E., 1995. On neck propagation in amorphous glassy polymers under plane strain tension. International Journal of Plasticity 11 (3) 211-35.

Wu, P.D., Van der Giessen, E., 1993. On improved network models for rubber elasticity and their applications to orientation hardening in glassy polymers. Journal of the Mechanics and Physics of Solids 41 427-456.

Chapter 8

Conclusions and Recommendations

Main Conclusions

Conventionally studies on fracture have been biased by the deformation behaviour of the materials. For brittle materials, the plastic deformation preceding fracture is confined to the vicinity of the crack tip, thus their plane-strain fracture has been studied extensively in the past. For highly ductile materials, large plastic deformation is likely to be involved in the fracture process so that plane-strain fracture was rarely studied. The large deformation involved in the ductile fracture is also a huge challenge for the conventional fracture mechanics. For polymers, since their fracture and deformation behaviour is mainly dominated by mode I, their shear fracture toughness has not been well characterized. This thesis addresses these challenges that have been rarely explored. The thesis proposes new test methods for evaluating the fracture toughness in tension or shear mode that involves large plastic deformation.

The study identified transition from plane-stress to plane-strain fracture in the double-edge-notched tensile (DENT) test of high-density polyethylene (HDPE) plate. The corresponding EWF values were found to be vary more that 10 times. The conclusion was verified in Chapter 2 and 3, using 2 different approaches on specimens of different thickness. The two approaches yielded nearly identical EWF values that show little dependence on the specimen thickness.

A new work-partitioning principle was applied to the DENT test of HDPE, to determine the EWF value for each of the two stages of deformation in plane-stress condition: neck inception and neck propagation (Chapter 4.) The specific EWF values for each stage were found to be 201.5 and 44.3 kJ/m^2 for rolling direction, and 144 and 21.7 kJ/m^2 for transverse direction, respectively. Difference of the EWF values in the two stages of damage development was caused by the different speed for crack and neck growth. The results suggest that fracture toughness for materials that involve stable necking may vary during the crack growth. The value determined by the conventional EWF method only represents the mean value for the whole crack growth process.

The thesis also dealt with characterization of mode II fracture toughness of polymers (Chapter 5.) Three criteria were proposed to identify the mode II fracture, and a test methodology, based on Hill's definition of mode II fracture, was developed using Iosipescu device and double-edge-notched specimens with side grooves. The methodology was applied to poly(acrylonitrile-butadiene-styrene) (ABS), that is known to develop unstable necking in the deformation process. The study shows that its mode II EWF value is 32.3 kJ/m^2, about 2.5 times of the corresponding mode I fracture toughness. The significant difference between toughness of different modes causes the mode I fracture to dominate the deformation process in ABS.

The above study on mode II fracture was then extended to HDPE (Chapter 6.) Because of the strain hardening phenomenon, pure mode II fracture cannot be achieved for HDPE. Through the double linear regression process with respect to ligament length and the groove thickness, quasi-mode II fracture toughness of HDPE could be determined to be 12.4 kJ/m^2.

The study also found that conventional yield stress and yield function cannot be applied to deformation of polymers with stable necking. A simple scheme was developed to determine the effective yield stress. By adopting the effective yield stress in the FEM model, the variations of computed load and strain with elongation are very close to the experimental results.

The FEM study concludes that the isotropic yield function should be modified. In this study, the shear stress ratio was adopted to reflect the anisotropy between normal and shear stresses in work-hardening. Using new anisotropic yield function, the study successfully generated a load-displacement curve from FEM model of DENT specimen that was very close to the experimental results, by setting the shear yield stress ratio to be 0.65. The procedure was examined using DENT specimens of different ligament lengths, all of which were in plane-stress condition. The results suggested that the anisotropic work-hardening occurred after the necking was developed, thus should be considered in the FEM simulation.

Overall, the thesis has studied a variety of subjects that have not been explored in the past using conventional fracture mechanics approaches. Outcomes from the study are expected to be a stepping stone for deeper understanding of these subjects.

Recommendations

Most of the measures that quantify fracture toughness are based on the rate of energy dissipation for crack growth. Compared to linear elastic fracture mechanics (LEFM), or elastic plastic fracture mechanics (EPFM) which assumes that the energy dissipation during quasi-static crack growth occurs only in the vicinity of the crack tip, essential work of fracture (EWF) concept allows the occurrence of plastic energy dissipation in the region remote from the crack tip. The EWF concept extracts the essential work consumed for generating the crack growth, by excluding the plastic energy dissipated in the remote region from the total fracture energy. Based on the assumption that the fracture process within the FPZ remains the same during the crack growth, the essential work is usually regarded as constant which represents fracture toughness of the material.

However, the study in Chapter 4 shows that for stable necking, the essential work is not constant, but varies with the crack growth. Reasons for the variation are: i) the neck growth is much faster than crack growth, ii) the degree of necking varies with the crack growth, and iii) the size of FPZ increases with the neck growth. Therefore, for evaluating fracture toughness that involves stable necking, it is necessary to separate the energy for necking from that for creating surfaces. This has never been considered in the past, but is essential for determining the variation of fracture toughness with the crack growth.

In this study, the mode II EWF value of HDPE was evaluated through the double extrapolation to zero ligament length and thickness in Chapter 6. Even though the energy for mode I plastic deformation could be removed by the extrapolation, it is important to ensure that the specimens are designed to suppress the involvement of mode I component to the minimum level. As described in the thesis, one of the causes of mode I involvement is the central gap between the two sets of the aluminium tabs. It is important to reduce the central gap to a size as small as possible, to minimize its role on the involvement of mode I deformation.

In addition, the testing rig that was originally designed for compressive loading needs to be sufficiently high to avoid its effect on the measurement accuracy. This is because observation during the testing suggests that when the load is large, slight slanting of the Iosipescu rig occurs, which also causes the mode I deformation. Note that the compressive loading cannot be used in this study because of the need of large displacement for the ductile deformation.

Another problem that should be considered in the future is the anisotropic work-hardening that is assumed in this work to be different only between shear and normal stresses. Different levels of anisotropy are expected by different normal stress components, due to formation and alignment of fibrillar structure in the necking process. This work also assumes that the shear stress ratio, R_s, is constant during necking process. However, R_s may vary with the neck development. At present, it is not clear how to quantify the anisotropy in the deformation involving very large strains, including stable necking. The information, however, is important for simulation of the deformation behaviour under complex loading conditions.

A final subject that can extend from the current study is the fracture criterion for 3-D simulation. To my knowledge, current criterion for the simulation of large deformation, i.e. CTOA, was not derived in view of the fracture mechanisms, rather from the superficial observation of the fracture behaviour. As a result, this criterion is difficult to be implemented in 3-D simulation on structures subject to complex loading. New fracture criteria that consider large deformation and rotation are needed to correctly simulate the fracture process that involves stable necking.

Appendix A. Test Details

A-1. Uniaxial Tensile (UT) Test

1. Test Standard

All of the tensile tests performed in this study followed procedures in ASTM standard (D638-01 Standard Test Method for Tensile Properties of Plastics), unless stated otherwise.

2. Testing Conditions

All of the tensile tests were done at the ambient conditions (temperature: 23 °C, relative humidity: 60-70 %).

3. Specimens

Dog-bone specimens shown in Fig. A-1 (ASTM D638-01) were machined from the commercial polymer plates. The width and length in the gauge section of the dog-bone specimens are 10 mm and 30 mm, respectively. The neck region was made with a radius of 31.3mm that is the largest radius achievable using the existing the machining tools.

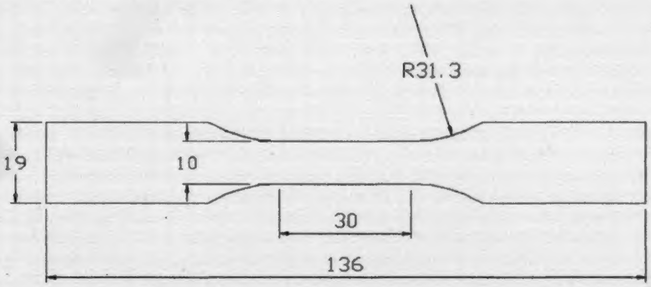

Fig. A-1 Dog-bone type tensile test specimen

4. Testing Equipment

In the test on ABS, a universal screw-driven testing frame from Instron with load capacity 250 KN was used at a ram speed of 5mm/min. In the test on HDPE, QUASAR 100 test frame from Galdavini that has a load capacity of 100 KN was used at the ram speed of 20mm/min. Both speeds conformed to the range of testing speed specified in ASTM D638.

5. Measurement

In the case of ABS, longitudinal deformation in the gauge section was measured using an extensometer with the initial gauge length of 1 inch (25.4mm), and converted to the axial true strain. In the case of HDPE, width variation was measured using a custom-built extensometer mounted across the specimen width in a section where the necking occurred. The axial nominal strain (ε_E) and the axial true strain (ε) generated in the UT tests were determined using the following equations:

$$\varepsilon_E = \left(\frac{W_0}{W}\right)^2 - 1 \qquad \textbf{(A.1)}$$

$$\varepsilon = 2\ln\left(\frac{W_0}{W}\right) \qquad \textbf{(A.2)}$$

where W_0 is the original specimen width and W the specimen width during the test.

6. Width Reduction

To ensure that deformation occurred in the gauge section where the extensometer was mounted, width around that section was reduced by 0.2mm (2% of the width, 0.1mm each side). Such width reduction is within the limit recommended in the ASTM standard for the UT test.

A-2. Double-Edge-Notched-Tensile (DENT) Test

1. Test Standard

DENT tests followed the procedures recommended by ESIS TC4 Committee (E. Clutton, *Fracture mechanics testing methods for polymers, adhesives and composites,* Elsevier, Kidlington, UK, 177 (2001)).

2. Testing Conditions

All of the DENT tests were done at the ambient conditions.

3. Specimens

DENT specimens with the dimensions of 90 mm wide (W) and 260 mm long (H) were used for the testing, as shown in Fig. A-2. Notches were firstly machined with the slitting saw and the pre-crack was generated at the notch tip by sliding a razor blazer.

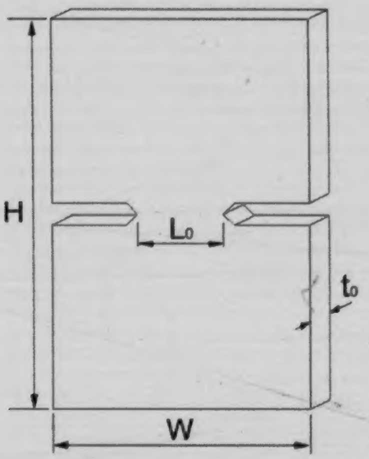

Fig. A-2 Double-Edge-Notched-Tensile (DENT) Specimen

4. Testing Equipment

A universal screw-driven testing frame from Instron that has a load capacity of 250 KN was used at the ram speed of 5mm/min.

5. Measurement

Variation of load and displacement of the ram were recorded at a sampling time of 0.03 sec. The total work of fracture (W) was calculated from the area under the load-displacement curve for the ligament length.

6. Data Analysis

At least 3 tests were carried out for each ligament length. If ΔW (deviation of the total work of fracture) from all tests were within 10% of $\overline{W}$ (average total work of fracture) they were regarded as valid data. If not, more tests were carried out until $\frac{\Delta\overline{W}}{\overline{W}}$ is less than 0.1, where $\Delta\overline{W}$ is the average deviation. If ΔW was deviated from $\overline{W}$ by more than 30%, it was regarded as an invalid data.

Appendix B. Finite Element Modeling

B-1. Simulation of UT Test

1. Modeling

UT test was simulated using a 3-D finite element model using ABAQUS 6.5 Standard. The FEM model of UT specimen (Fig. A-1) is shown in Fig. B-1 in which Cartesian coordinates are used with 1-, 2- and 3-axes in the direction of width, length and thickness, respectively.

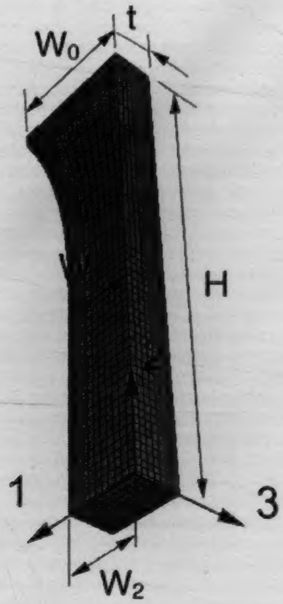

Fig. B-1. FEM model of UT specimen.

Since only a quarter of the specimen was modeled using the symmetry, W_0, W_1 and t are 9.5, 5 and 3.125 respectively. To generate the necking, width was reduced gradually to $W_2 = 4.998$ at the symmetric plane. H was set to be 32, because gripped part was excluded from this model.

2. Meshing

The model consisted of 2660 20-node brick elements. Size of the mesh in the gauge section was 0.5x0.5x0.875 mm in the width, height and thickness direction, respectively, except across the symmetric plane. In the non-gauge section, coarser mesh of the size 2.0 mm in the height direction was used. Across the symmetric plane, finer mesh (0.5x0.25x0.875 mm in the width, height and thickness direction, respectively) was used.

3. Simulation

Rate independent, incremental J2 plasticity theory was employed, with the assumption that plastic deformation was isotropic. Effective yield stress was given as a function of effective strain.

Displacement was gradually increased up to 100 mm at an initial increment of 1 mm for each step. Minimum and maximum increments are 0.005 and 5 mm. At each increment, axial load on the top plane was calculated and recorded.

4. Correcting Yield Stress

In the first simulation, the experimental yield stress ($Ye_{(0)}$) in Eq. (7.3) was employed. From the result of the first simulation, average effective stress ($\overline{Se}_{(0)}$) and average axial stress ($\overline{S2}_{(0)}$) across the symmetric plan were calculated. Then the new input yield stress in the 1st correction process was calculated as:

$$Ye_{(1)} = Ye_{(0)} \frac{\overline{Se}_{(0)}}{\overline{S2}_{(0)}} \qquad \text{(B.1)}$$

The load level and strain values from the 2nd simulation were compared with the experimental results. Since the simulation results were very close to experimental ones (difference being less than 2 %), $Ye_{(1)}$ was regarded as genuine effective yield stress.

B-2. Simulation of DENT Test

1. Modeling

DENT test was simulated using a 3-D finite element model using ABAQUS 6.5 Standard. Its FEM model, as shown in Fig. B-2, represents quarter of a full-sized DENT specimen with half of the thickness, i.e. width (W) of 45 mm, length (B) 130 mm, and thickness (t_0) 3.125 mm, with the full ligament length (L_0) of 20 mm. The ligament cross section across the symmetric ($L_0 \times t_0$) was divided into 10 sections having equal sizes that were bonded to the fixed analytical rigid plane which is not shown here.

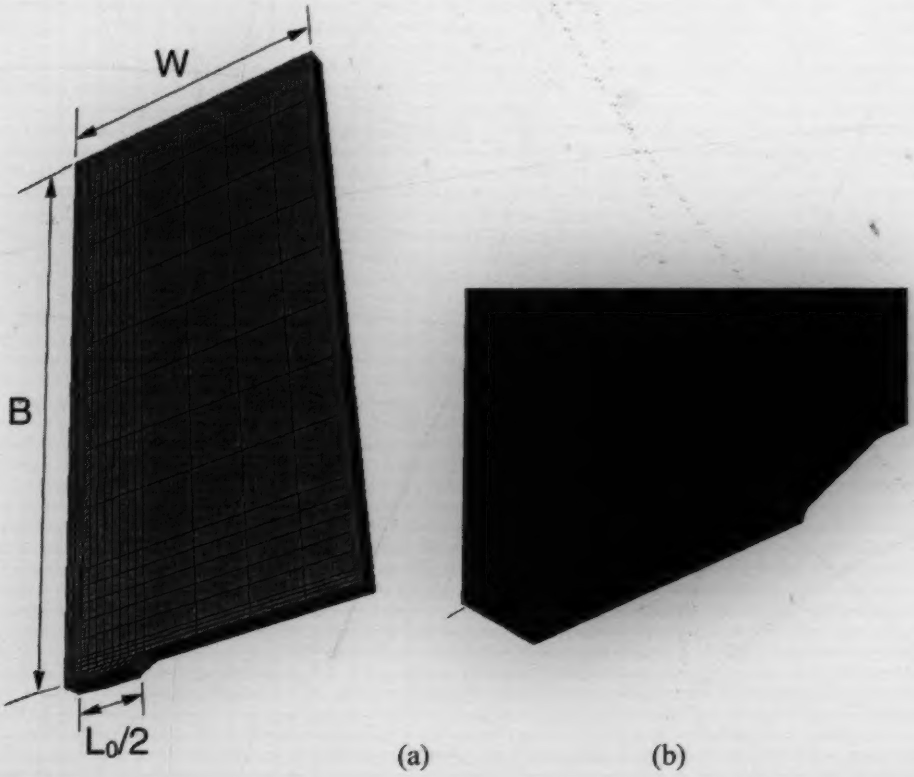

Fig. B-2. (a) FEM model of DENT specimen, and (b) ligament cross-section divided into 10 sections.

2. Meshing

The model consisted of 1056 20-node brick elements. Finest mesh was used in the ligament region across the symmetric plane. Size of the mesh in this region was 1x0.2x0.78 mm in the width, height and thickness directions, respectively.

3. Simulation based on Isotropic Work-Hardening

In the first simulation, rate independent, incremental J2 plasticity theory was employed, with the assumption that plastic deformation was isotropic. Corrected effective yield stress determined by Eq. (B.1) was employed.

Based on experimental results for the specimen with the ligament length of 20 mm, Δ_y and Δ_f were set to be 1.96 mm and 9 mm that were the half of the experimental displacements. Simulation was composed of 11 steps. In the first step (loading step), the displacement was increased by 1.96 mm without crack development. In each of the next 10 steps (crack steps), outer-most section of the ligament was debonded from the fixed analytical rigid plane from the notch tip and the displacement was increased by 0.704. Initial and minimum increments are 0.1 and 0.0001. At each increment, axial load on the top plane was calculated and recorded.

4. Simulation following the Proposed Scheme

Δ_f was determined from the empirical equation presented in Fig. B-3. Since the load drop was caused by the neck initiation, and not sensitive to the crack initiation, Δ_y could be determined by the simulation itself, i.e. the displacement at which load started to drop. Therefore, in the first step (loading step), the displacement was increased without crack development with $R_S = 1$ (isotropic yielding), until load drop was detected,.

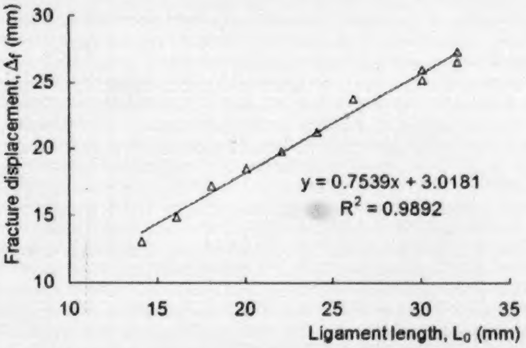

Fig. B-3. The plot of fracture displacement vs. ligament length.

When load drop was detected, the corresponding displacement was set to be Δ_y, R_S was changed to 0.67 (anisotropic yielding), and it was changed to next step (1st crack step). In each following crack steps, the displacement was increased by $(\Delta_f - \Delta_y)/10$ with debonding of one section of the ligament.

Curriculum vitae

Academic Qualifications

PhD, Mechanical Engineering, University of Alberta, 2003-2007

Research topic: Toughness of Polymers under Various Fracture Conditions.

- Plane-strain toughness of HDPE.
- Plane-stress toughness and deformation behaviour of highly ductile polymers.
- Shear fracture toughness of ABS, HDPE and FRP.
- FEM simulation of deformation behaviour and crack propagation of highly ductile materials.
- Genuine yield stress of highly ductile polymers.
- New anisotropic yield criterion of highly ductile polymers

MSc, Mechanical Engineering, University of Alberta, 2001-2003

Research topic: Damage study of ABS under biaxial fatigue loading.

- Toughness variation under uni-axial and biaxial fatigue loading.
- FEM analysis of cruciform specimen under bi-axial loading.

MSc, Production Engineering, KAIST, Korea, 1988

Research topic: FEM simulation of hydro-forming process.

BSc, Mechanical and Design Engineering, Seoul National University, Korea, 1985

Honours and Awards

- NSERC PDF Fellowships (2007-2009), Canadian Government
- Queen Elisabeth II Graduate Scholarship (May 2007), Province of Alberta.
- Andrew Stewart Memorial Graduate Prize (May 2007), University of Alberta.
- Queen Elisabeth II Graduate Scholarship (May 2006), Province of Alberta.
- Mary Louise Imrie Graduate Student Award (June 2006), University of Alberta.
- Province of Alberta Graduate Fellowship (May 2005), Province of Alberta.
- Provost Doctoral Entrance Award (Sep. 2004), University of Alberta.
- Graduate Student Scholarship (Mar. 2003), Province of Alberta.
- Mary Louise Imrie Graduate Student Award (June 2006), University of Alberta.
- Honour of Excellence (Feb. 1992), KAIST, Korea.

Work Experience

Research Assistant, Sept 2001-present. University of Alberta, Alberta, Canada. Dept. of Mechanical Engineering. Durable Materials Lab.

Teaching Assistant, Mechanical Engineering Laboratory (Winter and Fall 2002), Engineering Physics (Winter 2003), Engineering Mechanics II (Winter and Fall 2004), Pressure Vessel Design (Winter 2005), Engineering Mechanics II (Fall 2005), Manufacturing Process (Winter 2006), Mechanical Engineering Laboratory II (Fall 2006).

Engineer, May 1994-Sep. 2000. Samsung Electronics, Korea. Production Technology Laboratory. Projects included: Automation of the Inspection System for LCD Production Line, Development of Wafer-Handling System, Development of LCD Panel Robot-Handling System, Automation of Li-ion Cell Phone Battery Production Line.

Engineer, Mar. 1992-Apr. 1994. Texas Instruments, Korea. Developed DCS and SCADA application codes.

Publications

Published or accepted:

1. H. J. Kwon and P.-Y. Jar. "Fracture Toughness of High-Density Polyethylene in Shear Mode," International Journal of Fracture. Accepted.
2. H. J. Kwon and P.-Y. Jar. "On the Application of Essential Work of Fracture Concept to Toughness Characterization of High-Density Polyethylene," Polymer Engineering & Science. Accepted.
3. H. J. Kwon and P.-Y. Jar. "New Work Partitioning Approach to the Measurement of Plane-Strain Fracture Toughness of High-Density Polyethylene based on the Concept of Essential Work of Fracture," Engineering Fracture Mechanics. Accepted.
4. H. J. Kwon and P.-Y. Jar. "Toughness of High-Density Polyethylene in Plane-Strain Fracture," Polymer Engineering & Science. Vol. 66 (10), pp. 1428-1432 (Oct. 2006).

5. H. J. Kwon and P.-Y. Jar. "Fracture toughness of polymers in shear mode," Polymer, Vol. 46 (26), pp. 12480-12492 (Dec. 2005).
6. H. J. Kwon, P.-Y. Jar, and Z. Xia. "Characterization of Bi-axial Fatigue Resistance of Polymer Plates," Journal of Materials Science, Vol. 40 (4), pp. 965-972 (2005)
7. H. J. Kwon, P.-Y. Jar, and Z. Xia. "Residual Toughness of Poly(acrylonitrile-butadiene-styrene) (ABS) after Fatigue Loading – Effect of Uni-axial Fatigue Loading," Journal of Materials Science, Vol. 39 (15), pp. 4821-4828 (2004)

Submitted:

1. H. J. Kwon and P.-Y. Jar. "On the Application of FEM to Deformation of High-Density Polyethylene," International Journal of Solids and Structures. Submitted.

Conference Proceedings

1. H. J. Kwon and P.-Y. Jar. "Toughness of High-Density Polyethylene in Plane-Stress and Plane-Stress fracture," Proceedings of 15th U.S. National Congress of Theoretical and Applied Mechanics, 25-30 June 2006 Boulder, Colorado.
2. H. J. Kwon and P.-Y. Jar. "Toughness Evaluation of Ductile Polymers in Shear Fracture," Proceedings of 17th Canadian Materials Science Conference, pp. 29 (June 2005).
3. H. J. Kwon, P.-Y. Jar, and Z. Xia, "Damage Study of Polymers under Biaxial Fatigue Loading," Proceedings of 19th Canadian Congress of Applied Mechanics, Vol. I, pp. 128 (June 2003).

Computer Experience

Programming: Fortran, Matlab, C

Applications: AutoCad, ANSYS, ABAQUS 6.6

Teaching Interests

Classical mechanics: Mechanics, strength of materials, and elasticity,

Applied mechanics: Continuum mechanics and plasticity,